이학박사학위논문

Phase transitions in higher-order networks

고차 네트워크에서의 상전이

2022년 8월

서울대학교 대학원
물리·천문학부
이 용 선

이학박사학위논문

Phase transitions in higher-order networks

고차 네트워크에서의 상전이

2022년 8월

서울대학교 대학원
물리·천문학부
이 용 선

Phase transitions in higher-order networks

고차 네트워크에서의 상전이

지도교수 백 용 주

이 논문을 이학박사 학위논문으로 제출함

2022년 8월

서울대학교 대학원

물리·천문학부

이 용 선

이용선의 박사 학위논문을 인준함

2022년 7월

위 원 장: _____ (인)

부위원장: _____ (인)

위 원: _____ (인)

위 원: _____ (인)

위 원: _____ (인)

Abstract

Phase transitions in higher-order networks

Yongsun Lee
Department of Physics and Astronomy
The Graduate School
Seoul National University

A complex system is a system in which many elements interact one another in heterogeneous forms. Networks have been widely used to describe the universal charateristics of the structural properties and dynamical behavior of the system by representing each element as a vertex and their interactions as edges. However, network representation has an inherent limitation that stems from the definition. Since an edge can only express the relationship between two elements, it is difficult to express elements that do not show pairwise interaction. A higher-order network is a generalization of a network consisting of vertices and higher-order connections, which is not restricted from this limitation as it considers interactions of three or more elements.

First, in this dissertation, we analyzed the empirical data and model of a growing complex system from the perspective of a higher-order network and described the evolutionary stages of the complex system in simplicial complex representation. The stages of establishing connectivity and robustness, including the stage of the birth, were separated by the topological quantity, the Betti numbers. It was shown that loop formations in the macroscopic length scale, which is a typical characteristic of the stage where connectivity is established, can be quantified by the first Betti number.

Furthermore, the formation of locally closed surface which begins to appear as the density of the system increases, which can be interpreted as robustness enhancement, can be quantified by the second Betti number.

It has been confirmed that the Betti numbers emerge and increase successively in growing higher-order interacting systems by studying several simplicial complexes models. In particular, it was numerically confirmed that the Betti numbers defined in the growing scale-free simplicial complexes also exhibit phase transitions, homological percolation transitions. Furthermore, we analytically show that the first Betti number exhibits the same transitional behavior as the percolation phase transition in both the graph and the simplicial complex.

Second, we investigated the effect of the hub structure in higher-order interactions of complex systems on phase transitions and critical phenomena through analytical and numerical analysis of the higher-order synchronization models. Two models of globally coupled oscillators showing bistability and multistability were dealt with. It was confirmed that higher-order interactions promote a discontinuous synchronization transition with critical phenomena, a hybrid synchronization transition.

It was derived numerically and analytically that the behavior of the synchronization transition changes abruptly based on a specific value of the exponent of degree distribution ($\lambda_c = 2 + 1/(d-1)$) in the bistable model defined in a scale-free higher-order network with a heterogeneous structure. When the exponent of degree distribution is smaller than the critical value ($\lambda < \lambda_c$), unconditional synchronization occurs due to a large amount of influence of the hub. Otherwise, for $\lambda = \lambda_c$, ordinary second-order synchronization transition occurs, and for $\lambda > \lambda_c$, an explosive hybrid synchronization transition emerges.

Keywords: Phase transition, Critical phenomena, Percolation theory, Synchronization, Simplicial complex, Simplicial homology, Hypergraph

Student number: 2017-29476

Contents

List of Figures

Chapter 1

Introduction

Complex systems are composed of many elements that interact with each other in various unpredictable ways. These systems can be represented by networks, interactions among elements of a complex system are represented by a graph comprising a set of vertices (or nodes) and a set of edges (or connections) between pairs of nodes (that denote the elements) [1–6]. The network representation enables us to describe both structural and dynamical properties observed in complex systems. For example, the problems regarding structural properties could be how to determine the important elements [7], to infer missing interactions [8], and to detect community structures [9]. The dynamical processes such as the spread of diseases and synchronization among dynamical units can be explained as well [10]. We can model such systems more elaborately by including the interacting strength (weight) or direction [1], and furthermore the system-wise interactions (multiplex network) [11]. Albeit very successful to describe, there is a systematic limitation originating from the definition of network: An edge defined as a linkage of two vertices, which leads to difficulty representing a higher-order (non-pairwise) interaction. The higher-order networks can represent higher-order interaction among three or more units without loss of generality. Depending on the purpose, the higher-order network is realized either as a simplicial complex with its building block as simplex or a hypergraph with a hyperedge [12–14]. A hypergraph, which is a method for representing high-order interactions, is a generalization of a graph in which interactions involving more than two elements are represented by a hyperedge [12]. A simplicial complex, which is composed of simplexes, is a particular

form of hypergraph [13, 14]. Details on these representations are displayed subsequent sections.

Two of the most typical level-specific examples organized via higher-order interactions in real-world are as follows [15–18].

i) A macroscopic-level of example: coauthorship relations made of papers written by any number of authors,

ii) A microscopic-level of example: brain networks made of simultaneous neural stimulation.

Higher-order interacting structure is directly captured in coauthorship relations, which means every paper organized by authors represents a simultaneous interaction among those authors. In the case of the brain network, however, we can hardly see higher-order interaction due to the limitation of observation. Instead, we confirm the existence of higher-order interaction by checking if it is descriptive or not. To pose a specific example regarding this statement, one can cluster neurons to reconstruct a hierarchical structure associated with the nictation of $C.\ elegans$ by only considering motifs as the basis [17], which convincingly shows the higher-order interaction is not too much of a concern.

As it becomes more important to take the higher-order interaction into account for various kinds of problems, even for ecology [19] and evolutionary processes [20], it becomes more evident that the study on the structures and dynamical processes defined on such structures is needed [21–23]. When it comes to the study on the higher-order structures, it is much of concern studying connectivity combining topological properties based on percolation theory: inference of higher-order link [24], extension of network model [25], and topological percolation transition [26, 27]. For dynamical processes, the main object is how the higher-order interaction relates to the explosive phenomena. [28–31]

This dissertation deals with two topics. Firstly, we consider the complex system that grows in time, and explore its percolating properties inherent in the evolutionary

stages through topological analysis. Secondly, we consider the dynamical processe, especially synchronization, associated with the sympathy phenomena defined in the complex system, and investigate how the existence of the hub relates to the macroscopic behavior, phase transition and criticality. The brief introduction of percolation and synchronization is followed by the main chapters.

1.1 Percolation

It is not an exaggeration that interaction is said to be the most fundamental property that a large number of real systems possess. Any dynamical process which can be considered in the real-world is highly conditioned on the underlying topology of interactions, the structure of connections, to proceed appropriately. In other words, one can manipulate the underlying connection, i.e., topology of interaction between any pair of units, to make a dynamical process propagate properly or not, depending on the characters of the dynamical processes. For example, in a circumstance of the global spread of disease, we know that it may never end under the presence of the hub person who has many connections at a particular period of time. It is understood that the existence of the hub, say $P(k) \sim k^{-\gamma}$ with $2 < \gamma < 3$, where $P(k)$ is degree distribution, the epidemic threshold vanishes [10]. So in that situation, all we have to do is just cutting as many connections as possible to make $\gamma \gg 3$, i.e., demolishing the hub node. As the notion of connection is one of the most fundamental importance, the study related to connection has been well organized in the mathematical framework in the name of the percolation theory.

1.1.1 Overview on percolation theory

Percolation theory is organized in mathematical language so that it can reasonably provide the insight to understand how they are connected to one another or what makes the global connection occur in many other real-world systems, ranging from social

relationships to biological systems [32]. For instance, it displays many kinds of transitional behaviors concerned with global connection conditioned on any kind of parametric quantities that may require a microscopic connection. One categorizes physical systems with the transitional properties in the statistical mechanical point of view. The main object of percolation problems is the formation of the largest chunk made of connections, called the giant component. The giant component is defined as a unique set of vertices that are connected to one another both directly and indirectly and conditioned that it is of the same order compared to the system, say $G \sim O(N)$, where we denote G, N as the size of the giant component, the size of system of interset respectively. Given a set of parameters that controls the number of connections, the system undergoes phase transition between phases characterized by the giant component, G. For the simplest problem defined in Euclidean space as an example, it reveals second-order phase transition for the order parameter G, $G \sim |p - p_c|^{\beta}$, the control parameter for p, the critical exponent for β. From the fact that any kind of network is in dimension of intinity, percolation on network is understood as the percolation on Euclidean space above the critical dimension, d_c, above which the system coincides with percolation of Erdős–Rényi random graph model. There are many other diverse types of percolation transitions in complex networks, including Erdős–Rényi random graph. As for the case in Euclidean space, there are two types of percolation problems in complex networks, bond and site percolation. The site percolation concerns how the giant component emerges as one occupies each site one at a time randomly on predefined networks, whereas the bond percolation is on how the giant component emerges as one adds bonds to two nodes one at a time also in a random manner.

1.1.2 Topological viewpoint in percolation transition

It is clear enough to understand the percolation system by ”squinting” at its global form, not taking any details into account. When the spanning cluster is of a big interest, we can understand its global order by looking for the existence of long range

interactions, which makes the average distance between pairs of nodes short. In other words, the number of loops the system has is a direct indicator of percolating state. In fact, G is to do with the number of loops, which implies that the number of loops can be used to describe percolation transition of the system as well. This holds for not only the systems of pairwise interactions but also those of higher-order interactions [33,34].

1.1.3 Simplicial complex and simplicial homology

A simplicial complex, K, is a collection of some set of vertices, s_d, with the requirement that all the subsets of s_d have to be also members of K. So if we want to convert a sample from hypergraph representation to simplicial complex representation, it is required that all the downward edges of each hyperedge have to be occupied. In this representation we call s_d a d-dimensional simplex made of $d+1$ vertices, and also denote s_d as $[v_1, v_2, \ldots, v_{d+1}]$. Each subset of an d-simplex, s_d, is also a simplex which is called a face of s_d. A set of facets in K is a set of maximal faces of K. A graph is a simplicial complex made of 0-dimensional and 1-dimensional simplexes.

The d-dimensional simplicial homology help us with mathematical quantification of d-dimensional voids in a given simplicial complex. More precisely, the rank of d-dimensional homology group is exactly the same as the number of d-dimensional voids the system contains. Defining a boundary operator exerting on a chain group of each order, we can write homology group in mathematical form. For the case of $d = 1$, a 1-void refers to a closed loop made of 1-simplexes. Therefore, if the loop structure

$$\partial_k : C_k \to C_{k-1}, \tag{1.1}$$

where C_k is chain group of order k which is isomorphic to the linear sum of k-faces, k-chain. Then we can write the homology group of order k as

$$H_k(K) = \ker(\partial_k)/\mathrm{im}(\partial_{k+1}), \tag{1.2}$$

which interpreted as the number of k-cycles that are not boundaries of any faces in K. Hereafter, we only consider coefficients of all faces isomorphic to Z_2 group for the sake of simplicity.

1.2 Synchronization

Synchronization which is one of the most ubiquitous phenomena captured in many kinds of real-world systems of various scales has been mathematically described by models of coupled oscillators. From Winfree to Kuramoto, the models for coupled phase oscillators without amplitude has successfully been able to cover not only the processes of biological neural systems but also the processes of power systems composed of generators and consumers. Many efforts have been devoted to understanding of dynamics of coupled oscillators on different types of interacting substrates so far. In one hand, one of the studies, which is for the collective behavior of synchronization on small-world network, played a role of a seed for the popularization of heterogeneous substrates, the complex networks.

1.2.1 Kuramoto model

Kuramoto model is a simple model for coupled phase oscillators in which the oscillators exhibit an entrainment to one another, similar to an equilibrium phase transition of magnets. This model has its interacting term as sine function as

$$\dot{\theta}_i = \omega_i + \frac{K}{N}\sum_{j=1}^{N}\sin(\theta_j - \theta_i), \tag{1.3}$$

where K is an interacting strength between each pair of oscillators having their own phases and intricsic frequencies, θ_i's and ω_i's, placed on an all-to-all connected substrate. This simple model reveals various type of synchronization transition conditioned on both the type of diversity of intrinsic frequencies and the type of an interact-

ing substrate.

1.2.2 Synchronization transition

Given a set of intrinsic frequencies, there is a charateristic value of coupling strength, K_c, above which oscillators reveal an entrainment,

$$r \begin{cases} > 0 & \text{if } K \geq K_c \\ = 0 & \text{if } K < K_c. \end{cases} \tag{1.4}$$

where $r = \langle e^{i\theta} \rangle$ is the order parameter of the system. For instance, if a set of intrinsic frequencies is a sample of unimodal distribution, the oscillatory system undergoes a synchronization transition of second-order, i.e. $r \sim (K - K_c)^\beta$. The choice of the intrinsic frequencies and of the topology of the substrate are crucial for determining the type of synchronization transition: unimodal frequency distribution gives rise to continuous synchronization transition, bimodal distribution induces abrupt synchronization transition, and uniform distribution causes a hybrid synchronization transition [35].

1.2.3 Hybrid synchronization transition

The coupled Kuramoto oscillators exhibit their global behavior through the abruptly changing order parameter when there effects of suppression, for example, in the form of the flat distribution of intrinsic frequency, the presence of competitive interaction (frustration), or higher-order interaction. If such systems also reveal critical behavior in suprecritical regime, we call this exhibits a hybrid synchronization transition,

$$r = \begin{cases} r_c + C(K - K_c)^\beta & \text{if } K \geq K_c \\ 0 & \text{if } K < K_c, \end{cases} \tag{1.5}$$

where r_c is the amount of the abrupt change of order parameter, which indecates discontinuous synchronization transition.

Chapter 2

Homological percolations in coauthorship relations

Coauthorship relations have served as representative examples of large-scale social relationships driven by collaborations. Many studies on this subject have been published and research is still active. The main subject of this chapter is the growth of coauthorship relations in a specific scientific research field. The evolution of coauthorship relation in graph representation of several research topics, including network science, were explored as a function of time from inception [36]. The percolation transition was recognized as infinite order. Figure 2.1(b) ilustrates how the macroscopic properties of the coauthorship graph reach a mature state. The growth process is divided into three stages from the perspective of graph representation: (i) Small isolated components are created. (ii) A treelike giant component is formed by merging clusters in the early stages, followed by the connection of long-range edges. Thus, long loops are formed in the later stage. (iii) The network becomes entangled by forming intra-cluster edges. These three stages are characterized by the mean separation, $\bar{d}$, between two connected vertices averaged over different clusters. In stage (i), $\bar{d}$ remains almost constant; in stage (ii), $\bar{d}$ increases overall but with fluctuations; and in stage (iii), $\bar{d}$ decreases overall. These three stages are indicated in Figure 2.1(b). However, the classification based on $\bar{d}$ can be considered rather primitive owing to the lack of an appropriate mathematical tool in graph representation. In this chapter, we demonstrate that the evolutionary steps can be reconstructed from the perspective of simplicial complex representation as in Figure 2.2 in terms of homological percolation transitions associated with the first and second Betti numbers. The analysis is based on the homology of the sim-

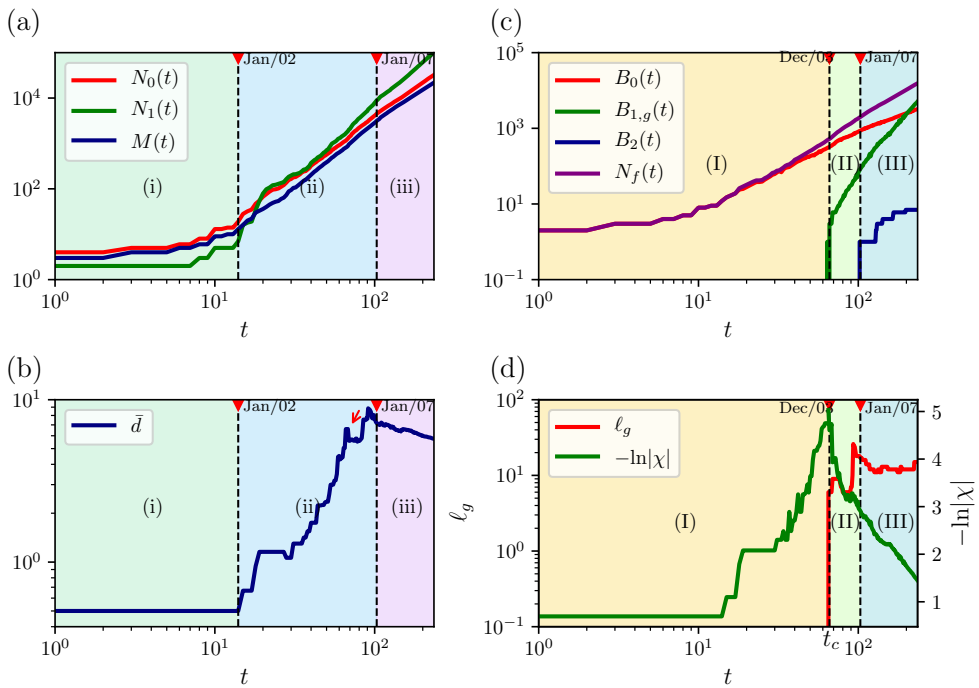

Figure 2.1: Evolution of several graph and homological quantities. (a) Plots of the number of vertices $N_0(t)$, the number of edges $N_1(t)$, and the size of the largest component $M(t)$ versus time step t in graph representation. (b) Plots of the mean separation between two vertices $\bar{d}$ as a function of t in the graph representation. (c) Plots of the zeroth Betti number B_0 (the number of components), the first Betti number $B_{1,g}$ (the number of homological one-dimensional cycles) of the largest cluster, the second Betti number B_2, and the number of facets N_f as a function of time step t. (d) Plots of the length of the longest cycle ℓ_g and the logarithm of the Euler characteristic $-\ln|\chi|$ as a function of time step t.

plicial complex representation of the coauthorship relations. A few studies using the simplicial complex have also been published recently, and here we elucidate portrays the route by which a coauthorship relations reaches a mature state.

2.1 Homological percolation transitions

The two homological percolation transitions occur successively [38] at transition points t_{c1} and t_{c2}, as shown in Figure 2.1(c). They are determined by the first and second

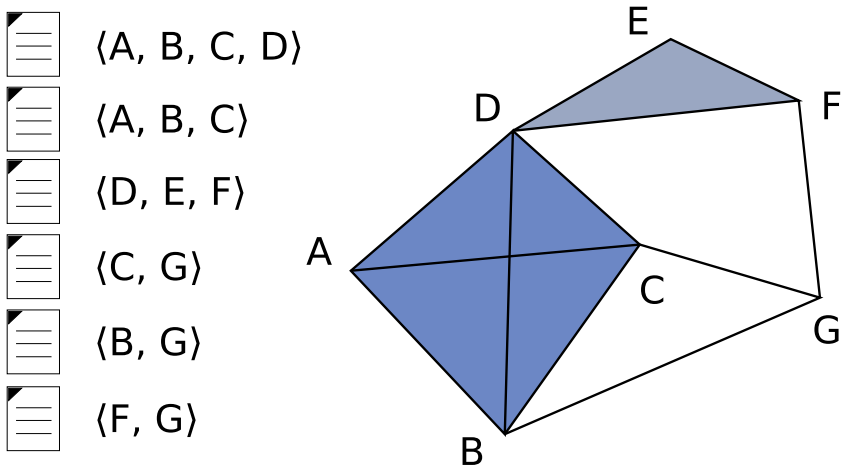

Figure 2.2: Schematic illustration of the SCR of coauthorship relationships. Each list enclosed by angle brackets in the left panel represents a paper written by the listed authors. The SC in the right panel is the coauthorship complex constructed from these six papers. The facet degree of a vertex is the number of facets in which the vertex participates. For example, the facet degree of C is 2, and that of G is 3. B-C-G-B and B-D-C-G-B are examples of homologous cycles, as their symmetric difference, B-C-D-B, is the boundary of the 2-simplex [B, C, D]. The B-A-D-C-G-B cycle is also homologous to them. They all represent the same voids. The cycles C-D-F-G and C-D-E-F-G-C are not homologous to them but are homologous to each other. Any cycle homologous to B-C-D-F-G-B can be represented as the symmetric difference of a cycle homologous to B-C-G-B and a cycle homologous to C-D-F-G up to a boundary cycle. The first Betti number is 2.

Betti numbers in the giant cluster, denoted as $B_{1,g}$ and $B_{2,g}$, which represent the numbers of homological cycles and cavities in the giant cluster, respectively. The homological cycles also exist in finite clusters smaller than the giant cluster. Moreover, the giant cluster is also called an infinite cluster in percolation theory because the critical behavior of percolation transition is treated in the thermodynamic limit $N \to \infty$. Hence, the homological cycles in finite clusters can be ignored compared with those in the giant cluster. This is also confirmed by empirical data. In contrast, the second Betti number is nonzero only in the giant cluster. Thus, $B_{2,g} = B_2$. This homological classification scheme separates the regions of phases (i) and (ii) into new phases (I) and (II), as illustrated in Figure 2.1. In phase (I), both Betti numbers are zero; in phase (II), a gi-

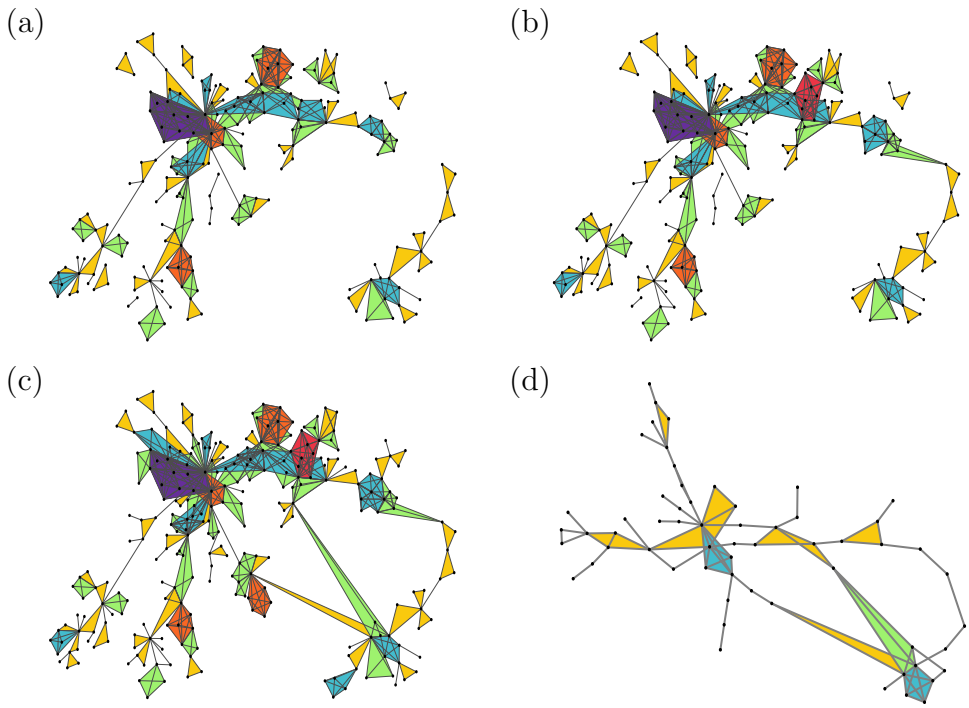

Figure 2.3: Snapshots of the coauthorship SC. (a) Snapshot of the simplicial complex at $t = 65$, where the second-largest simplicial complex has not yet merged with the giant SC. (b) Snapshot of the giant simplicial complex at $t = 66$, where the second-largest component has merged. (c) Snapshot of the simplicial complex at $t = 69$, where the long-range edges are connected. (d) Snapshot of simplicial complex after a process of homological simplification [37] of (c).

ant one-dimensional homological cycle appears, that is, $B_{1,g} > 0$, but B_2 is still zero. In phase (III), B_2 is also finite. The point t_{c2} coincides with the previous point [36], which was determined intuitively. In addition, the homological properties of coauthorship complexes, such as simplicial contraction, facet size distribution, and persistent homology, have been explored in various coauthorship datasets [**?**, 40]; however, these datasets were collected at specific times. Thus, the homological percolation transitions arising in evolutionary processes have not thus far been identified in real-world complexes. Two important phenomena underlie the evolution of coauthorship networks: divergence and internal entanglement. When a student graduates from a university,

she/he moves to a postdoctoral position in another group. This transfer enables both parties to broaden their experience and is thus beneficial to them. When the former student publishes a paper with her/his new colleagues, long-range connections are made between the old and new groups. These intergroup edges result in the formation of a long-distance homological loop. In particular, when the length of this loop is macroscopic, this giant loop results in an homological percolation transition in simplicial complex representation (see the snapshots in Figure 2.3). In addition, the intragroup edges are also reinforced as the group members publish more papers together. This internal edge entanglement results in the formation of two-dimensional voids. Thus, another type of homological percolation transition occurs, in which the second Betti number becomes nonzero. The phenomena of divergence and internal entanglement correspond to the central factors in the evolution of biological networks, divergence, and mutation during reproduction [41].

Here, we specifically considered an homological percolation transition of the coauthorship complex $S(t)$. We traced the first Betti number of the largest cluster as a function of time step t, which is denoted as $B_{1,g}(t)$. We found that $B_{1,g}(t)$ first becomes nonzero at time step $t_{c1} = 67$. It apparently exhibits a power-law increase as $B_{1,g}(t) - B_{1,g}(t_{c1}) \sim (t - t_{c1})^{2.1}$. We also measured the length of the longest homological cycle $\ell_g(t)$ as a function of t, as shown in Figure 2.1(d). We find that ℓ_g suddenly increases at t_{c1}, at which the giant cluster acquires an interbranch edge, and a macroscopic-scale long cycle is formed, as shown in Figure 2.3(d). We regarded this point as the transition point of the first homological percolation transition. In retrospect, this point was identified in the graph representation, in terms of the mean separation $\bar{d}$, where $\bar{d}$ decreases noticeably, as indicated by the arrow in Figure 2.1(b). It was reported previously that the length of a homological cycle is positively associated with the number of linked communities [**?**]. Thus, the formation of a long cycle indicates the formation of global collaborations.

We also identified the transition point t_{c1} using the Euler characteristic [38]. It was

proposed that the Euler characteristic of the giant cluster, which is defined as $\chi \equiv \sum_k (-1)^k B_{k,g}$, becomes zero near the transition point of the homological percolation transition. Here, we measured $\chi = B_{0,g} - B_{1,g} + B_{2,g}$, because we obtained $B_{k,g} = 0$ for $k \geq 3$ and plot $-\ln|\chi|$ as a function of t. It was found to diverge at t_{c1}.

We separated the region beyond t_{c1} into two regimes, (II) and (III), using the second Betti number B_2. In regime (II), the first Betti number, $B_{1,g}(t)$, increases continuously with time. In contrast, ℓ_g increases abruptly and then decreases slowly and reaches a steady state in which ℓ_g is constant overall, with some fluctuations, whereas $\bar{d}$ decreases continuously. In this late regime, the simplicial complex becomes increasingly entangled as more papers are published within each group. We measured the second Betti number $B_2(t)$ to check for the formation of cavities enclosed by simplexes. There exists a nonzero second Betti number at a transition point t_{c2}, as shown in Figure 2.1(c), beyond which $B_2(t)$ remains nonzero. We found that these cavities were formed in the giant cluster.

In Figure 2.1(c), the first Betti number $B_{1,g}(t)$ increases continuously even after the second Betti number $B_2(t)$ appears and then increases. This behavior differs from that in the Kahle localization, wherein the first Betti number decays rapidly to zero for the static Erdős–Rényi (ER)-type random complex model [26] as the second Betti number appears. This difference results from the fact that the coauthorship complex is growing, and isolated complexes are thus continuously generated and accumulate over time. Some of them merge with a giant complex and contribute to the formation of new homological cycles, and the first Betti number $B_1(t)$ increases. Therefore, the number of isolated clusters, $B_0(t)$, may be expected to decrease. However, this rate of decrease was lower than the rate of increase of $B_0(t)$ resulting from the creation of new complexes. Thus, both $B_0(t)$ and $B_1(t)$ increase. The first and second Betti numbers, $B_1(t)$ and $B_2(t)$, exhibit similar behaviors; they also increase together. This issue is discussed in detail in more subsequent sections.

2.2 Facet degree distribution

In graph representation, the degree k_i of vertex i is the number of edges connected to vertex i. Here, this degree is referred to as the graph degree to distinguish it from the facet degree proposed below. We measured the graph degree of each vertex in the giant cluster and obtained the graph degree distribution, denoted as $P_{d,g}(k)$. The graph degree distribution exhibits power-law decay, $P_{d,g}(k) \sim k^{-\lambda_g}$, where $\lambda_g \approx 2.89 \pm 0.06$. In simplicial complex representation, facets are the maximal faces of an SC. The facet degree m_i of vertex i is the number of facets to which the vertex i belongs. The facet degrees in a giant cluster have a facet degree distribution $P_{d,f}(m)$, which is also called the simplicial degree distribution [**?**]. We obtained $P_{d,f}(m) \sim m^{-\lambda_f}$, where $\lambda_f \approx 2.72 \pm 0.11$, as shown in Figure 2.4(a). Thus, the exponents of the two degree distributions have slightly different values.

To examine the correlation between the two degrees, we plotted the average facet degree $\langle m(k) \rangle$ of the vertices with graph degree k in Figure 2.4(b) and the average graph degree $\langle k(m) \rangle$ of the vertices with facet degree m in Figure 2.4(c). The vertices with a large (small) graph degree tend to have a large (small) facet degree, on average. However, fluctuations are unusual; when k and m are large, both the fluctuations of the facet degree for a given k and those of the graph degree for a given m are relatively small. Thus, the asymptotic behavior of the average quantities $\langle m(k) \rangle \sim k^{1.05 \pm 0.06}$ and $\langle k(m) \rangle \sim m^{0.91 \pm 0.04}$ are reciprocal. However, when $\langle k \rangle$ and $\langle m \rangle$ are small, the fluctuations of both are relatively large. This is because the field of network science includes interdisciplinary research subjects, such as mathematics, theoretical physics, and biology, where the number of authors per paper varies widely from one to more than 10 people. Moreover, a few review papers have large graph degrees but small facet degrees. In contrast, when the dimensions of the complexes are homogeneous, the two degree distributions have the same degree exponents, as we show later for a simple model.

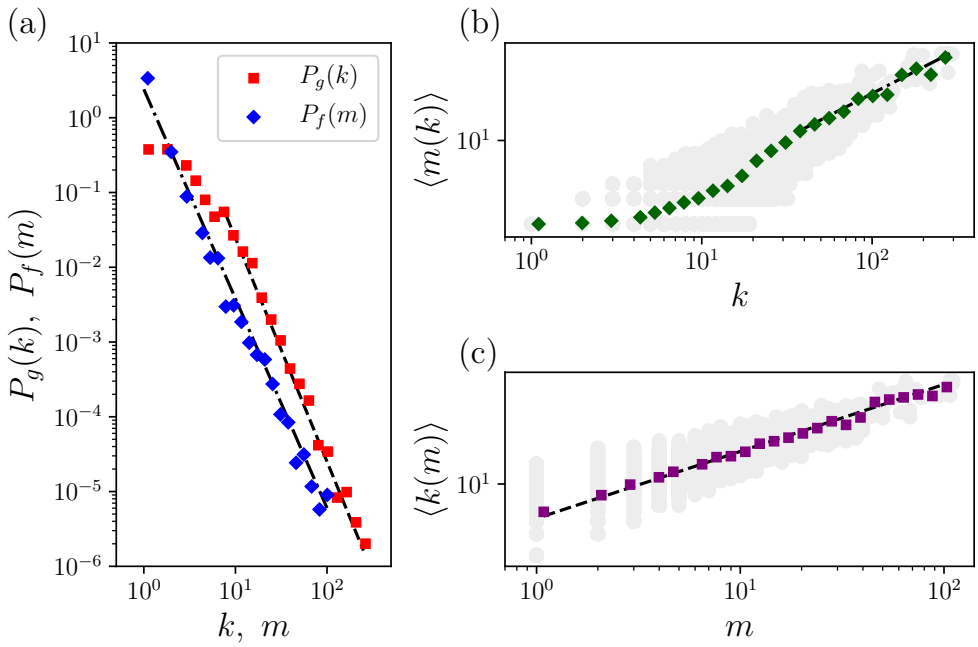

Figure 2.4: Graph and facet degree distributions. (a) Plots of the graph degree distribution $P_{d,g}(k)$ and facet degree distribution $P_{d,f}(m)$ as functions of k and m, respectively. (b) Plot of the mean facet degree $\langle m(k) \rangle$ of each vertex with graph degree k. The guide line (dotted) has a slope of 1.05 ± 0.06. (c) Plot of the mean graph degree $\langle k(m) \rangle$ of each vertex with facet degree m. The guide line (dashed) has a slope of 0.91 ± 0.04.

2.3 Minimal model

We propose a minimal model of the homological percolation transition that occurs in a growing simplicial complex. At each time step, a new vertex is added to the system; then, three vertices are selected with probability proportional to $m_i + a$, where m_i is the facet degree of node i, and a is a constant. The vertices are connected with probability p. This triangle is regarded as a two-dimensional simplex in the simplicial complex representation. This process is repeated t times. This model is an extension of the previous model of a randomly growing graph [42] in which two randomly selected vertices are connected with probability p. It differs from the previous model in that a

2-simplex rather than a 1-simplex is added, and the three nodes are selected according to their facet degrees rather than randomly.

This growing simplicial complex model exhibits an infinite-order percolation transition in graph representation at a transition point p_{c0}. The cluster size distribution for $p < p_{c0}$ exhibits power-law decay, where the exponent depends on p and a. However, the cluster size distribution of finite clusters for $p > p_{c0}$ decays exponentially. The transition point approaches zero as $a \to 0$. The giant cluster size $G(p,t)$ increases significantly with time as $G(p,t) \approx G(p)t$ asymptotically. In the steady state, $G(p)$ exhibits an essential singular behavior: $G(p) \sim \exp[-\alpha_0(p - p_{c0})^{-\beta_0}]$, where α_0 is a nonuniversal constant. The transition point, $p_{c0} \approx 0.0031$, and exponent, $\beta_0 \approx 0.44$, are obtained for $a = 0.1$. For comparison, the exponent $\beta = 1/2$ for the growing random network model. Analytical treatment for these arguments is displayed in Chapter 3.

We considered the graph degree distribution and obtain analytically $P_{d,g}(k) \sim k^{-\lambda_g}$ with $\lambda_g = 2 + a/(3p)$. However, a pair of 2-simplexes are more likely to be connected by sharing a vertex than by sharing an edge in large systems because the first case occurs with probability $O(1/N)$, whereas the second case occurs with probability $O(1/N^2)$. Hence, the graph and facet degrees of each vertex depend linearly on each other. The facet degree distribution exhibits power-law decay with the same exponent value, that is, $\lambda_f = \lambda_g$, as $P_f(m) \sim P_g(k)$. We confirmed this result using numerical simulations.

We counted the first Betti number, that is, the number of homological cycles, numerically as a function of t; it shows extensive behavior: $B_1(p) \approx b_1(p)t$ asymptotically. The first Betti number in the steady state, $b_1(p)$, exhibits a transition. The transition point p_{c1} is consistent with that for the percolation transition p_{c0} such that $b_1(p)$ is zero for $p \leq p_{c1}$ and finite for $p > p_{c1}$. To specify p_{c1}, we perform numerical analysis as follows. First, we measure the probability, $P(p)$, that a Monte Carlo sample contains at least one finite loop in the largest cluster for given p. This quantity

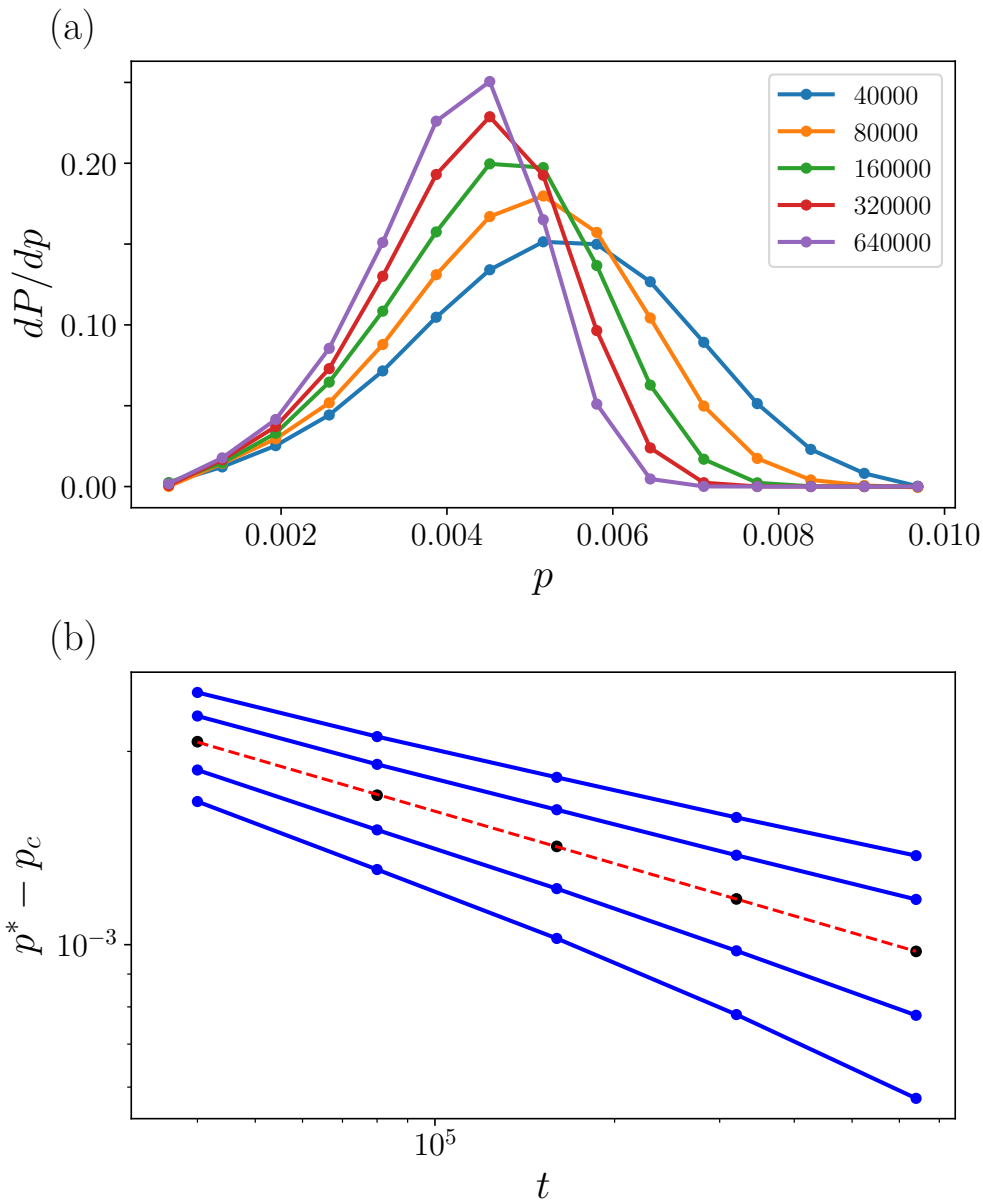

Figure 2.5: Determination of the transition point p_c for b_1, i.e., p_{c1}. In (a), plot of dP/dp versus p, and determine peak positions for each t. Legend indicates different t values. In (b), plot of $p^*(t) - p_c$ versus t for different trials of p_c, and find p_c that exhibits power-law decay. The slope of the power-law behavior determines $1/\bar{\nu}^*$.

is similar to the probability that a sample contains a spanning cluster for a given occupation probability p in ordinary percolation. We examine the slope $dP(p)/dp$ for a given p and then find p^* at which the slope becomes maximum . This value, p^*, can be regarded as the transition point of the homological percolation transition of the first Betti number. Next, using the finite-size scaling concept, we determine the transition point, p_{c1}, in the thermodynamic limit $t \to \infty$. That is, p_{c1} satisfies the power-law relation $p^* - p_{c1} \sim t^{-1/\bar{\nu}^*}$. Then, using the estimated p_{c1}, we numerically confirm that the first Betti number has the essentially singular form near the transition point, $b_1 \sim \exp(-\alpha_1(p - p_{c1})^{-\beta_1})$, where α_1 is a nonuniversal constant, and the exponent, $\beta_1 \approx 0.44$, is the same as that for the percolation transition for $a = 0.1$ (Figure 2.6(a)). This result is reminiscent of the result for a growing random graph, in which the exponents $\beta_0 = \beta_1$ [43] and $b_1(p) \sim G^2(p)$.

The second Betti number $B_2(t)$ behaves nonextensively with respect to the number of 0-simplexes t, but is proportional to $t^{0.7}$ asymptotically. Thus, $B_2(t)$ is written as $B_2(t) \approx b_2(p)t^{0.70}$ asymptotically. Simulations and finite-size scaling analysis show that $p_{c2} \approx 0.053(3)$ for $a = 0.1$. This transition point differs from $p_{c1} \approx 0.0031$ for $B_1(p)$ for the same value, $a = 0.1$. $b_2(p)$ also exhibits the essential singular form $b_2(p) \sim \exp[-\alpha_2(p - p_{c2})^{-\beta_2}]$, where α_2 is a nonuniversal constant, and $\beta_2 \approx 0.99$ for $a = 0.1$ (Figure 2.6(b)).

2.4 Kahle localization

We reconsidered the localization of the Betti numbers in the minimal model [26]. To reproduce the evolution of the Betti numbers shown in Figure 2.1(c), we numerically simulated the minimal model with a fixed $p > p_{c2}$ because the second Betti number is not generated otherwise. The three Betti numbers $B_0(t)$, $B_1(t)$, and $B_2(t)$ were obtained as a function of t. As shown in Figure 2.7(a), the three Betti numbers appear successively, and they all increase with time. The first and second Betti numbers behave similarly to those we obtained from the coauthorship complex dataset. The Kahle

localization does not occur in the minimal growing model.

To investigate the key factor affecting the localization, we considered a static model in which $N = 100$ nodes exist continuously from the beginning. At each time step, three nodes were selected randomly and connected by a 2-simplex. This process was repeated $N_\triangle = n_\triangle N$ times. Thus, the parameter p is absent. The three Betti numbers are calculated as a function of $n_\triangle$ and are presented in Figure 2.7(b). We confirmed that the Kahle localization indeed occurs. Next, the static model was modified so that three nodes are selected with a probability proportional to their facet degree m_i ($i = 1, 2, 3$) in the form of $m_i + a$. As shown in Figure 2.7(c), the first Betti number immediately increases dramatically and then decreases slowly, whereas the second Betti number increases slowly. Therefore, the first and second Betti numbers coexist for a long time. After the first Betti number vanishes, the second Betti number continues to increase. Next, we considered the case of a growing complex. Initially, we set $N_{m0} = 25$ nodes. At each time step, a node is added to the system, and three nodes are selected randomly (Figure 2.7(d)) or according to the degree-dependent rule in Figure 2.7(e). In Figure 2.7(d), there exists a finite transition point for the second Betti number; however, the first Betti number increases immediately while remaining finite but decreases thereafter. At the transition point of the second Betti number, the decreasing rate of $B_1(t)$ is changed. In Figure 2.7(e), the first and second Betti numbers exhibit behavior similar to that shown in Figure 2.7(c). This result demonstrates that the localization behavior occurs only for the static random case in Figure 2.7(b).

2.5 Remark

We investigated the homological percolation transitions of growing simplicial complexes using the empirical data of coauthorship simplicial complexes and a model study. Homological percolation transitions were identified by the Betti numbers. We revealed that the first three Betti numbers B_k ($k = 0, 1$ and 2) are nonzero and the others are zero in the empirical dataset. This implies that papers with three authors

play important role in the formation of simplicial complexes. Thus, we propose a minimal model composed of 2-simplexes. The model was designed to include the growth and preferential attachment rules, which commonly appear in various complex systems. Owing to these factors, the first Betti number continues to increase in time even after the second Betti number appears. This implies that the coauthorship simplicial complexes are still developing, at least above p_{c2} (see Figure 2.1(c) and Figure 2.7(a)). To check whether the behaviors of three Betti numbers are universal or model-dependent, we modified an existing protein-interaction network model in graph representation [41] into an simplicial complex scheme. This protein-interaction simplicial complex model has two processes: duplication and divergence processes, and evolves in the following steps: i) At each time step, an existing node (representing protein, and denoted as A) is chosen. Each facet of node A is duplicated with probability $1 - \eta$. A mutant of A is denoted as B, which corresponds to a new node in a growing simplicial complex. ii) Two distinct nodes are randomly selected and make a triangle with node B. This process occurs with probability ζ. Processes i) and ii) mimic duplication and mutation, and divergence processes, respectively. We find that the first three Betti numbers (Figure 2.7(b)) increase with time similarly to the previous ones (Figure 2.7(a)). However, their behaviors are different from the localization pattern for the static ER-like random simplicial complex model [26] (Figure 2.7(c)). For the localization and delocalization of the Betti numbers as a function of the number of triangles $n_{\triangle}$, we uncovered more detailed properties using the minimal model (see Figure 2.7(c)- 2.7(f)). Finally, we revealed that the homological percolation transitions in growing simplicial complexes are of infinite order, which is an intrinsic characteristic of growing graphs [42] and simplicial complexes.

The formation of a long-range cycle or loop is a significant factor for understanding properties of diverse problems in physical and complex systems, for instance, phase transitions in equilibrium and nonequilibrium physical systems, and information spread in complex systems. Mean-field solutions for phase transitions of percolation

and spin models are equivalent to the solutions on the Bethe lattice (tree structure) [10]. However, in lower dimensions, the mean-field solution is not correct because the effect of loop structure is significant. Thus, it is necessary to estimate when loop is formed, what loop size scales to system size, etc. For the ER model in graph representation, it was revealed that a macroscopic-scale loop is formed at a percolation threshold and the loop size is scaled as $\sim N^{1/3}$ with system size N [44]. Using this scaling, one can estimate the so-called golden time [45, 46] in an epidemic problem and others. In simplicial complex representation, however, such important and challenging problems have not been solved thus far, even though there exists an elegant mathematical tools such as algebraic topology. This study was intended as a first step toward such a novel approach.

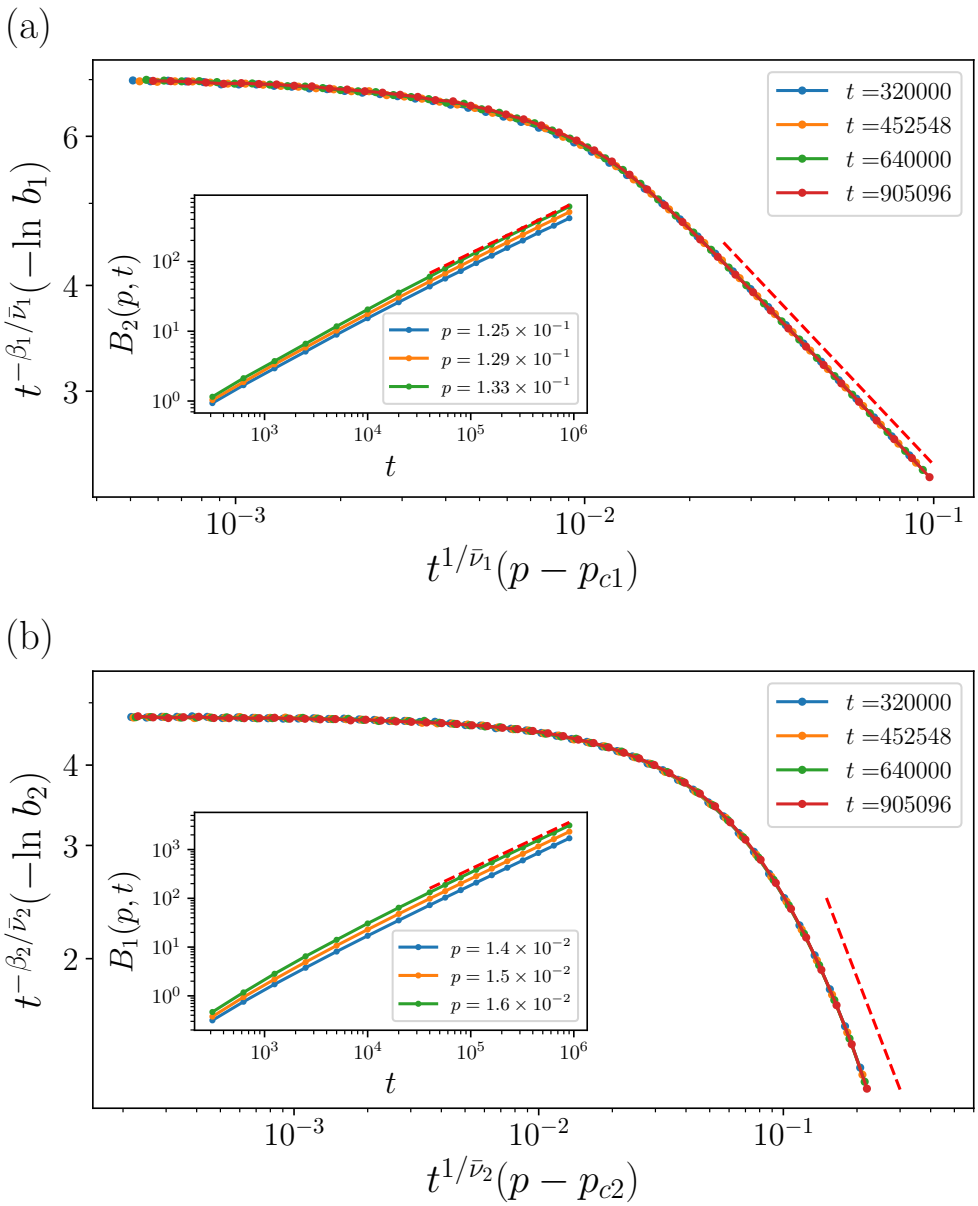

Figure 2.6: Scaling plots of the normalized first and second Betti numbers. To test the essential singular behaviors of $b_1(p)$ and $b_2(p)$, we plot $t^{-\beta_k/\bar{\nu_k}}(-\ln\ b_k)$ versus $t^{1/\bar{\nu_k}}(p - p_{ck})$, where $k = 1$ for (a) and $k = 2$ for (b). Dashed lines are guidelines with slopes $-\beta_1$ for (a) and $-\beta_2$ for (b) given in Table S2. Insets: plots of $B_1(p,t)$ (a) and $B_2(p,t)$ (b) versus t for different p values in double-logarithmic scales. They show power-law behaviors $B_1 \sim t$ and $B_2 \sim t^{0.70}$.

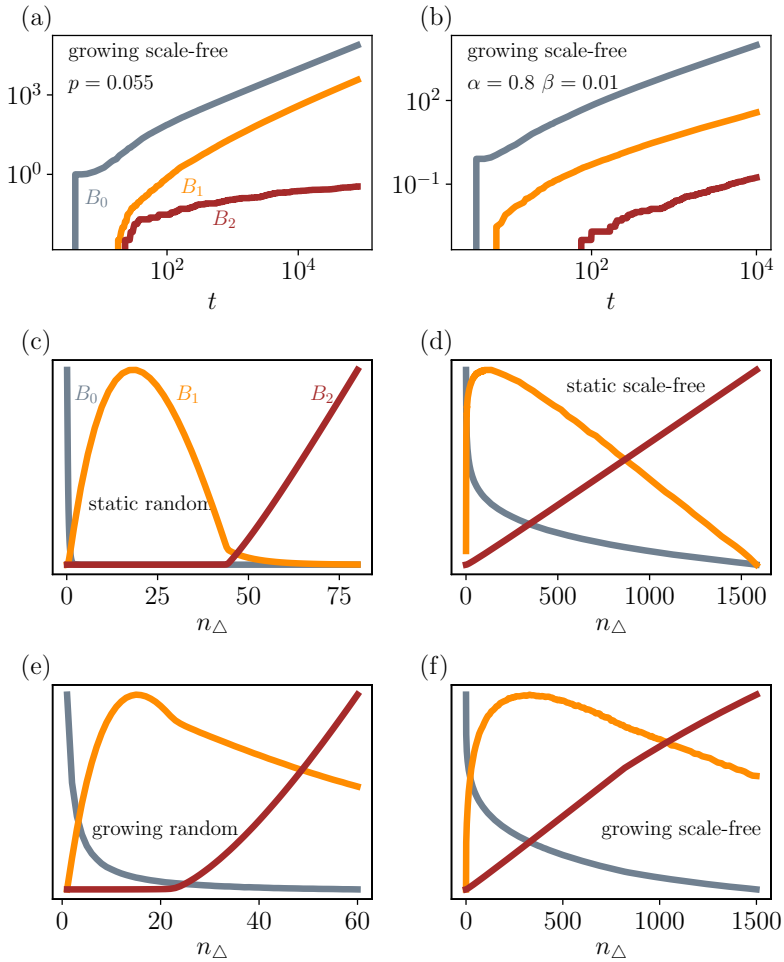

Figure 2.7: Comparison of the first three Betti numbers of a static random simplicial complex and growing scale-free SC. Plot of the Betti numbers versus time t for (a) the minimal model of growing scale-free simplicial complex at $p = 0.055$, just above $p_{c2} \approx 0.053$ and for (b) the protein-interaction simplicial complex model at the model parameter values $\alpha = 0.8$ and $\beta = 0.01$. (c) Plot of the Betti numbers versus the number of triangles per system size for the static random simplicial complex model with system size $N = 100$. For easier viewing, we adjusted each Betti number (the scale of the vertical axis) appropriately. (d) Similar to (c), but for the static scale-free simplicial complex model. (e and f) Similar to (c) and (d), but for the growing simplicial complex model. For (d) and (f), the localization of the Betti numbers does not occur. In other words, for (c) and (e), the second Betti number begins to increase only after the first Betti number reaches its maximum.

Chapter 3

Percolation of simplicial complex models

Percolation phase transition characterized by the emergence of the giant component is well studied for both static and growing complex networks. For those various types of models, we can naturally generalize to corresponding higher-order structure, simplicial complex. In this chapter, we introduce such models and corroborate that percolation phase transition also exists.

3.1 Percolation of static simplicial complex

Static random pure d-dimensional simplicial complex (SC), pure d-SC hereafter, is a higher-order version of Erdős–Rényi random graph model in which a d-face where there are $d+1$ nodes. A d-SC is pure if every face in d-SC is a subset of a d-face. We can make use of a d-SC process to understand how the higher-order interaction affects percolation properties.

3.1.1 Model description

Random graph process is a stochastic process where we have initially N isolated nodes, and at each step we add a new edge between two uniformly chosen nodes [44]. Similarly, in random d-SC process, where there are initially N isolated nodes, 0-faces, a d-face is added with probability p and downward closure among those $d+1$ of randomly selected nodes one at a time till the final time, N. For a term downward closure, it means a simultaneous occupation of all the subsets of the d-face. At the end of the

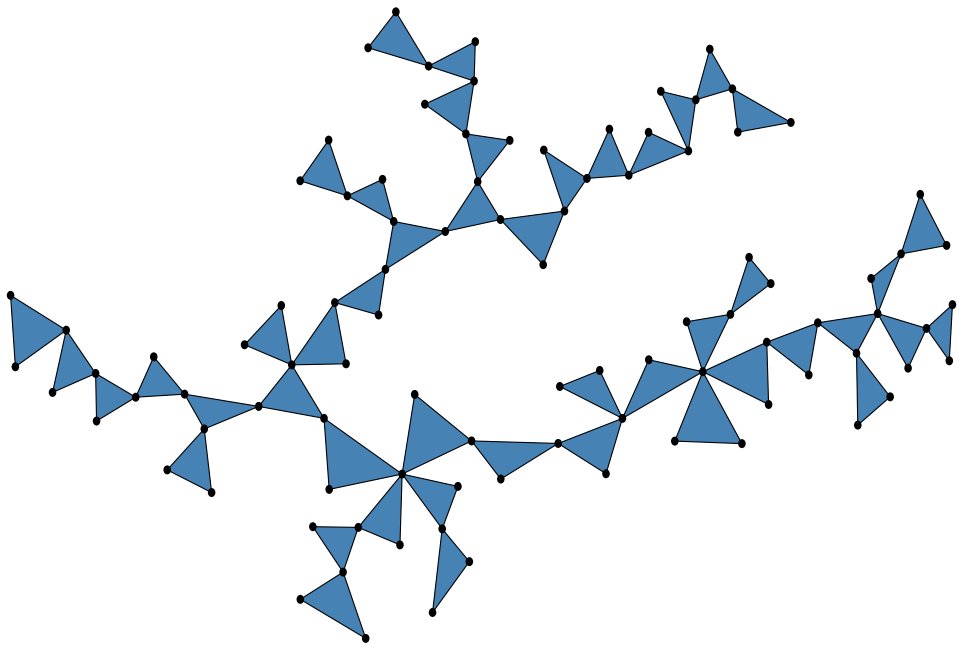

Figure 3.1: A sample of the largest cluster in pure 2-SC, with $N = 1000$, near the transition point. Every d-face is connected to one another through only one node, which forms a tree-like structure.

process, there are totally F of d-faces which equals to pN. It is of such a big importance to track of the evolution of the cluster size distribution during the process, which enables us to understand percolation properties of the system. Here we define a cluster as a set of nodes connected through d-faces. To understand this mathematically, we can build the rate equation of the cluster size as follows.

$$\frac{dN_s}{dt} = p\Big[\sum_{i+j+\cdots=s} \frac{iN_i}{N}\frac{jN_j}{N}\cdots - (d+1)\frac{sN_s}{N}\Big], \tag{3.1}$$

where N_s stands for the number of clusters of size s. (3.1) is built under the assumption that every pair of adjacent d-faces shares only one node. This assumption is quite acceptable in a sense that we only deal with percolation problem which is well de-

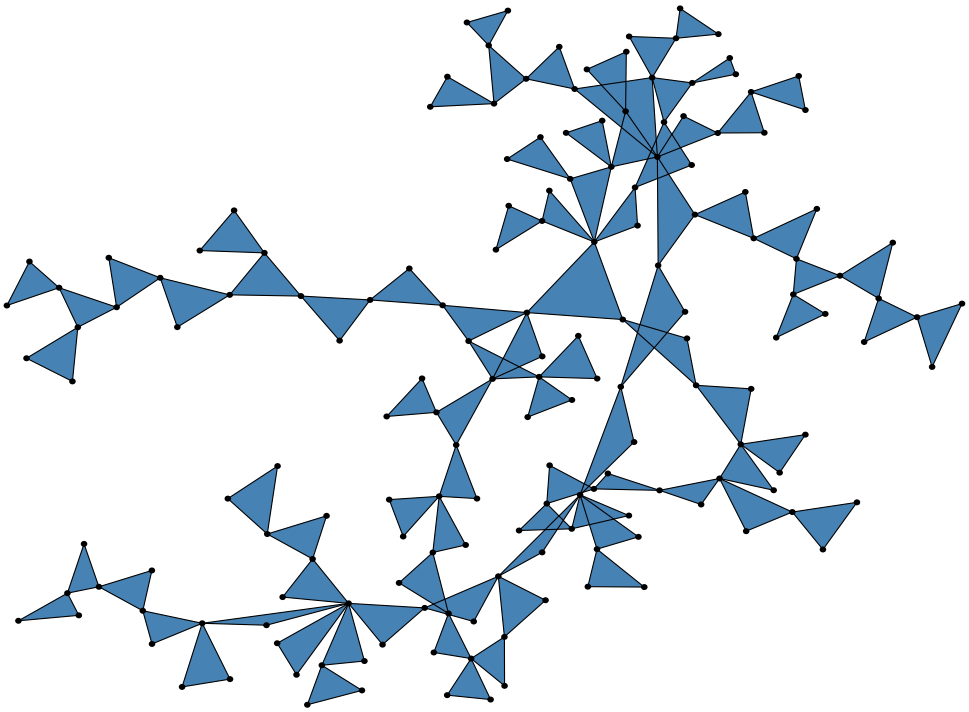

Figure 3.2: A sample of the giant cluster in pure 2-SC, with $N = 1000$, above the transition point. Complex configuration of loops made of line boundaries of 2-faces is present.

fined in the regime of the d-face density of order $O(N^{-1})$. It is too sparse to make any configuration in which d-faces join multiple nodes in common. Thus, there are finite trees only, see Fig. 3.1, until the time of imminent emergence of giant component with heterogeneous loop structures as ilustrated in Fig. 3.2. The emergence of the giant component is highly related to the emergence of heterogeneous loop structures, or 1-homology in topological language. So the percolation phase transition, somehow, can be interpreted in the language of homology, namly homological percolation transition [38]. On one hand, there has been many works done concerning various types of topological quantities including homology in various kind of SC processes [26,27,47].

3.1.2 Percolation threshold

We built a rate equation for the cluster number above, and now let us rewrite (3.1) as

$$\frac{dn_s}{dt} = \frac{p}{N}\Big[\sum_{i+j+\cdots=s} in_i\, jn_j \cdots - s(d+1)\, n_s\Big], \tag{3.2}$$

where we define cluster density as $n_s = N_s/N$. The strategy is to induce the most general solusion of any s. First, for $s = 1$ we have

$$\frac{dn_1}{dt} = -\frac{p}{N}(d+1)\, n_1. \tag{3.3}$$

Initially we have $n_1(t = 0) = 1$, so the solution is of the form,

$$n_1(p, t) = \exp(-p(d+1)t/N). \tag{3.4}$$

Plugging (3.4) into (3.2), we have a rate equation for $s = d + 1$. The rate equation for $s = d + 1$ is

$$\frac{dn_{d+1}}{dt} = \frac{p}{N}\Big[n_1^{d+1} - (d+1)(d+1)\, n_{d+1}\Big], \tag{3.5}$$

and we obtain

$$n_{d+1}(p, t) = C_{d+1}\Big(\frac{t}{N}\Big)\exp(-p(d+1)^2 t/N). \tag{3.6}$$

We can generalize the solutions for any s as follows,

$$n_s(p, t) = C_s\Big(\frac{t}{N}\Big)^{\frac{s-1}{d}} \exp(-p(d+1)st/N), \tag{3.7}$$

where $C_s's$ are coefficients independent on time t, which is utilized for generating functions,

$$f(x) = \sum_s sC_s x^s, \tag{3.8}$$

$$g(x) = \sum_s C_s x^s. \tag{3.9}$$

In fact, all the p-dependent terms are in the coefficients C_s as the remaining p-dependent portion of the exponential term is vanished later on. With (3.8) and (3.9), we can reexpress (3.2) as

$$\Big(\frac{1}{td} - \frac{p(d+1)}{N}\Big) f - \frac{1}{td} g = \frac{p}{t} f^{d+1} - (d+1)\frac{p}{N} f. \tag{3.10}$$

Taking $x\frac{d}{dx}$ on both side of (3.10) at $t = N$, we have

$$\frac{df}{dx} = \frac{f}{x(1 - pd(d+1)f^d)}. \tag{3.11}$$

For non-percolating phase, all clusters are finite, so $f(1) = \sum_s s n_s = 1$, by which (3.11) reduces to

$$f'(1) = \langle s \rangle = \frac{1}{1 - pd(d+1)}. \tag{3.12}$$

This explicitly tells us that the mean cluster size, $\langle s \rangle = 1$ at $p = 0$, same as the initial state, and $\langle s \rangle \to \infty$ as $p \to \frac{1}{d(d+1)}$, which means the percolation threshold, $p_c = \frac{1}{d(d+1)}$ where the mean cluster size diverges. This result is consistent with the result discussed in [34].

3.1.3 Cluster size distribution

It can be easily shown that the critical exponent, τ, for the cluster size distribution of a pure d-SC at $p = p_c$ is the same as that of Erdős–Rényi random graph model. (3.11) can be rewritten in integral form as

$$\int_{f(x_0)}^{f(x)} \frac{df}{f} \left(1 - pd(d+1)f^d\right) = \int_{x_0}^{x} dx\, x, \tag{3.13}$$

where the lower bound can be neglected later on. Thus we simply have

$$\exp(x^2/2) = f \exp(-p(d+1)f^d). \tag{3.14}$$

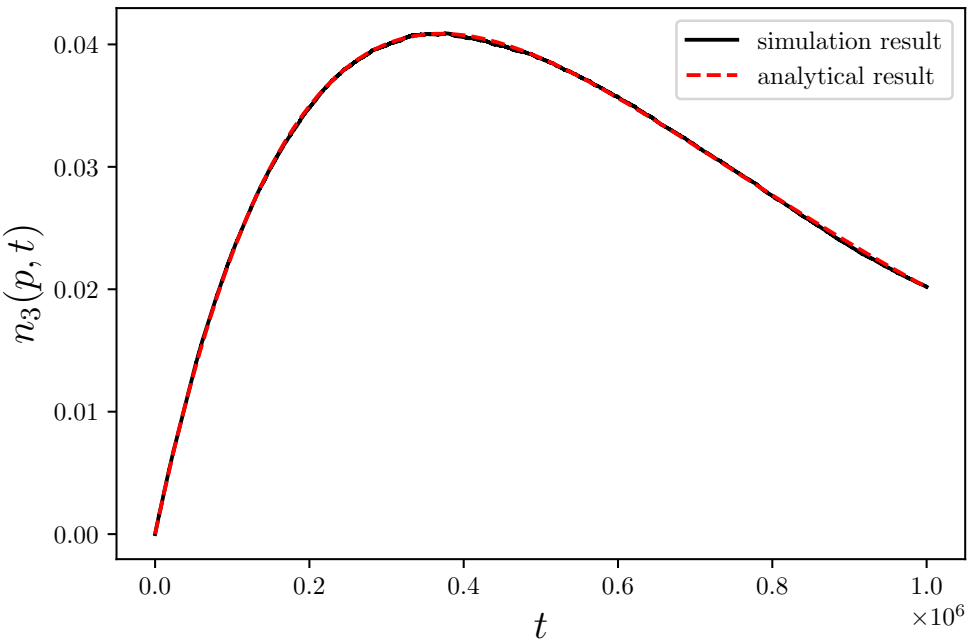

Figure 3.3: Evolution of $n_3(p,t)$ for $d = 2$ and $N = 10^6$. Though the simulation result (solid line) is from single sample only, it is in good agreement with the analytical result (dashed line).

Now the coefficient for any s in $f(x)$, sC_s, can be evaluated by using Lagrange inversion formula,

$$\begin{aligned} sC_s &= \frac{1}{2\pi i}\oint dz \frac{f}{z^{s+1}} \\ &= \frac{p(d+1)[ps(d+1)]^{\frac{s-1}{d}-1}}{(\frac{s-1}{d})!}. \end{aligned} \tag{3.15}$$

We can check how much the result is consistent with the simulation result by seeing Fig. 3.3. When it comes to the critical behavior of the cluster size distribution for sufficiently large s, $s \gg 1$,

$$C_s \simeq \frac{1}{\sqrt{2\pi d}} s^{-5/2}[pd(d+1)]^{\frac{s-1}{d}} \exp(s/d). \tag{3.16}$$

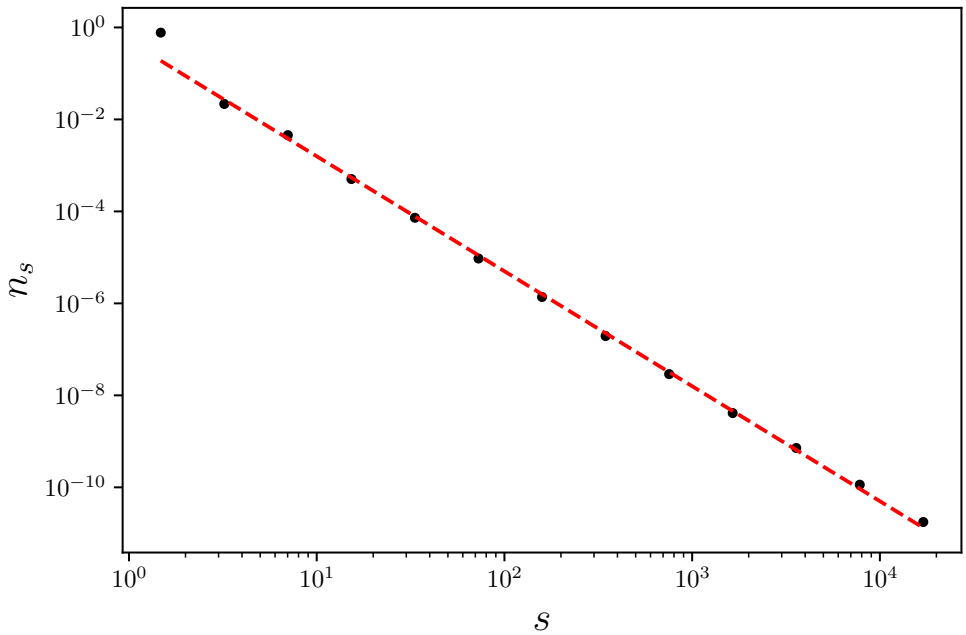

Figure 3.4: Plot of cluster density, n_s, for $N = 10^6$ at $p = p_c$. Symbols are placed by the simulation data where the number of samples is 10^3. The slope of the guide line (dashed line) is $-5/2$.

Then, we have

$$n_s(p, t = N) \simeq \frac{1}{\sqrt{2\pi d}} s^{-5/2} [pd(d+1)]^{\frac{s-1}{d}} \exp\Big(\frac{s}{d}(1 - pd(d+1))\Big), \tag{3.17}$$

where we obtain that at $p = p_c (= \frac{1}{d(d+1)})$

$$n_s \sim s^{-5/2}, \tag{3.18}$$

which is displayed in Fig. 3.4 for the case of $d = 2$. As a matter of fact, the critical exponent τ is not changed in any d.

In this section, we proposed a model for static simplicial complex where the number of nodes are fixed, N. The novel approach that we made for the static simplicial complex enalbes to obtain the analytic results for both the threshold and the cluster

size distribution that are consistent with the simulation results. We specify the exact threshold, p_c, where the giant component emerges and the critical exponent, τ for any d. One can easily find that when $d = 1$, the results converge to those of Erdős–Rényi model.

Meanwhile, a scale-free pure d-SC is also be introduced in [29], generalizing a static scale-free network. Scale-free d-SC process is the same as random d-SC process except for choosing each node, i, with the probability, p_i,

$$p_i \sim i^{-\alpha}, \tag{3.19}$$

where i is an index of each node, $i \in [1, N]$. The resulting d-SC reveals scaling behavior in facet degree distribution defined in Chapter 2, as follows.

$$P_f(m) \sim m^{-\gamma_f}, \tag{3.20}$$

with the exponent

$$\gamma_f = \frac{1+\alpha}{\alpha}. \tag{3.21}$$

Though the macroscopic behaviors of higher-order versions of complex networks reveal not much change, behaviors of higher-order version of dynamical processes defined on such structures change. These are thoroughly examined in Chapter 4.

3.2 Percolation of growing simplicial complex

All the real systems do not always leave their sizes, N, the same, but keep changing their sizes in time. Elements are newly added into the systems at some moment, or maybe removed from the systems naturally. So the static structures have limitation, to some extent, to play a role of references to describe such systems by tuning their sizes in a synthetic fashion. Here, the need for growing reference arises.

3.2.1 Model description

A pure d-dimensional growing simplicial complex, d-GSC, is a higher-order version of a growing network which have been representative framework for such systems. The most minimal picture for GSC process is define as follows. i) A new d'-face is added into the system, generally $d' = 0$. ii) With probability p, a new d-face is occupied among those existing nodes with downward closure. For $d = 1$ this reduces to the growing networks introduced in [42]. This also have percolation phase transition, but with different type of transition.

$$G \sim \exp(-\alpha(p - p_c)^{-\beta}), \tag{3.22}$$

which we call percolation phase transition of infinite-order. As for the case of static one, we can manually impose scale-free property on a GSC by selecting those existing nodes preferentially [43]. So the rate equation of the cluster size of the model that covers them all reads,

$$\frac{dN_s}{dt} = p\Big[\sum_{i+j+\cdots=s} Q_i N_i Q_j N_j \ldots\Big] - (d+1)Q_s N_s + \delta_{1s}, \tag{3.23}$$

where Q_s stands for the probability for selecting any node in cluster of size s.

$$Q_s = \sum_{n=1}^{s} p_n = \sum_{n=1}^{s} \frac{m_n + a}{\sum_{n'=1}^{N} m_{n'} + a} = \frac{(d+1)(s-1)/d + sa}{(d+1)pt + Na}, \tag{3.24}$$

where we require that p_n is proportional to facet degree, m, with initial attractiveness, a. Facets of a SC is a minimal set of maximal faces of an SC. In this model, facet degree of a node is nothing but the number of d-faces by which it is joined.

3.2.2 Percolation threshold

We can specify the percolation threshold, p_c, of d-dimensional GSG for any d with the help of generating function approach. From the fact that $N = t$, we can rewrite (3.23) as,

$$n_s = p\Big[\sum_{i+j+\cdots=s} q_i n_i q_j n_j \ldots\Big] - (d+1)q_s n_s + \delta_{1s}, \tag{3.25}$$

where $n_s = N_s/N$ is a density of cluster of size s, and $q_s = NQ_s = \frac{s(d+1+ad)-(d+1)}{d(d+1)p+ad}$. Now let us define two generating functions, $f(x) = \sum_s s n_s x^s$ and $g(x) = \sum_s n_s x^s$. In a non percolating phase all the clusters are finite, so $f(1) = \sum_s s n_s = 1$, whereas, in a percolating phase, $f(1) = 1 - G$. With these two functions, we can express (3.25). To do so, it is convenient when we introduce a generating function, $h(x)$, in a composite form of those two functions, $f(x)$ and $g(x)$.

$$h(x) = \frac{(d+1)+da}{d(d+1)p+da}\Big(f(x) - \frac{d+1}{(d+1)+da}g(x)\Big), \tag{3.26}$$

which is nothing but the generating function, $\sum_s q_s n_s x^s$. Thus, in a non percolating phase, $h(1) = 1$. Now we can express (3.25) in an integrated form as

$$\begin{aligned} f(x) &= x - p(d+1)x\frac{dh(x)}{dx} + px\frac{dh^{d+1}(x)}{dx} \\ &= x + p(d+1)xh'(x)(h^d(x) - 1). \end{aligned} \tag{3.27}$$

$g(x)$ is now rewritten as

$$\begin{aligned} g(x) &= \int_0^x dx' \frac{f(x')}{x'} \\ &= x - p(d+1)h(x) + ph^{d+1}(x). \end{aligned} \tag{3.28}$$

Plugging (3.27) and (3.28) into (3.26), we can get a non-trivial equation for $h(x)$ and $h'(x)$ as follows.

$$\begin{aligned} h(x) =& \frac{(d+1)+da}{d(d+1)p+da}\Big[x + p(d+1)xh'(x)(h^d(x)-1) \\ &- \frac{(d+1)}{(d+1)+da}(x - p(d+1)h(x) + ph^{d+1}(x))\Big]. \end{aligned} \tag{3.29}$$

Rearrange (3.29) by placing $h'(x)$ on the left hand side.

$$h'(x) = \frac{(da - p(d+1))h(x) - dax + p(d+1)h^{d+1}(x)}{p(d+1)((d+1)) + da)x(h^d(x)-1)} \tag{3.30}$$

In a non percolating phase, for $0 < p < p_c$, (3.30) should hold at least for $x = 1$. By using $h(1) = 1$ and L'Hőpital's theorem as $x \to 1$, we can get an equation for $h'(x)$ as

$$h'(1) = \frac{(da - p(d+1))h'(1) - da + p(d+1)^2 h'(1)}{pd(d+1)((d+1)+da)h'(1)} \tag{3.31}$$

Solving (3.31), we can obtain

$$h'(1) = \frac{(da + pd(d+1)) \pm \sqrt{(da + pd(d+1))^2 - 4pd(d+1)((d+1)+da)da}}{2pd(d+1)((d+1)+da)} \tag{3.32}$$

The discriminant in (3.32), $D = (da + pd(d+1))^2 - 4pd(d+1)((d+1)+da)da$, should be positive for a non percolating phase, otherwise $D < 0$ for a percolating phase, which implicate that solutions for $D = 0$ gives the percolation transition point, p_c.

$$p_c = \frac{(-a + 2a(d+1) + 2a^2 d) \pm \sqrt{(-a + 2a(d+1) + 2a^2 d)^2 - a^2}}{d+1} \tag{3.33}$$

To test validity of the solution for p_c, we can compare the result for $d = 1$ and $a \to \infty$ with that of growing random network [42]. The solution with minus sign is relevant as only it can reduce to the well know value, $p_c = 1/8$.

Meanwhile, in a percolating phase, $p > p_c$, there is the component which is no

longer finite, and is of $O(N)$. As a recap, this is quantified by generating function, f, which is $G = 1 - f(1)$. Plugging (3.28) for $n(x)$ into (3.26) gives the equation for $f(x)$, and when $x + 1$, we have

$$f(x) = \frac{d(d+1)p + da}{(d+1) + da} h(x) + \frac{d+1}{(d+1) + da}(x - p(d+1)h(x) + ph^{d+1}(x)). \quad (3.34)$$

And by taking derivative of $f(x)$ with respect to x, we obtain

$$\begin{aligned} f'(x) = & \frac{d(d+1)p + da}{(d+1) + da} h'(x) \\ & + \frac{d+1}{(d+1) + da}(1 - p(d+1)h'(x) + p(d+1)h'(x)h^d(x)). \end{aligned} \quad (3.35)$$

Thus, the expression for both G and $\langle s \rangle$ reads

$$G = \begin{cases} 0 & \text{for } p < p_c, \\ 1 - \frac{d(d+1)p+da}{(d+1)+da} h(1) - \frac{d+1}{(d+1)+da}(1 - p(d+1)h(1) + ph^{d+1}(1)) & \text{for } p > p_c, \end{cases} \quad (3.36)$$

$$\langle s \rangle = \begin{cases} \frac{d(d+1)p+da}{(d+1)+da}\left(\frac{(a+p(d+1)) - \sqrt{(a+p(d+1))^2 - 4pa(d+1)((d+1)+da)}}{2p(d+1)((d+1)+a)} + \frac{d+1}{d(d+1)p+da}\right) & \text{for } p < p_c, \\ \frac{d(d+1)p+da}{(d+1)+da} h'(1) + \frac{d+1}{(d+1)+da}(1 - p(d+1)h'(1) + p(d+1)h'(1)h^d(1)) & \text{for } p > p_c, \end{cases} \quad (3.37)$$

and we can evaluate $h(1)$ and $h'(1)$ for $p > p_c$ from (3.30).

3.2.3 Percolation phase transition

In this subsection, we derive the explicit form of G in terms of p near the critical point. First we redefine $h(x)$ as $1 - h(x)$. Then, around $x = 1$ and $p = p_c$, Eq. (3.29) become

$$\varphi'(y)\varphi(y) - \varphi(y) \simeq \frac{a/((d+1)p)}{(1 + a/((d+1)p))^2}(y^{1-(d+1+ad)} - y), \quad (3.38)$$

where $y \equiv x^{-1/(d+1+ad)}$ and $\varphi(y)/y \equiv h(x)/(1 + a/((d+1)p))$. This approximation is valid only around $x = 1$ and $p = p_c$ for small G. When we set $y = 1$, one can get

$\varphi(1) = 0$ for the normal phase, while $\varphi(1) \neq 1$ and $\varphi'(1) = 0$ for the percolation phase. Moreover, $f(x)$ in (3.27)

$$\begin{aligned} f(x) &= x + (d+1)px\frac{dh(x)}{dx}(1-(1-h(x))^d) \\ &\simeq x + d(d+1)pxh'(x)h(x), \end{aligned} \tag{3.39}$$

around $x = 1$ and $p = p_c$. In this regime, the giant cluster size G, defined as $G = 1 - f(1)$, is written as

$$G = 1 - f(1) = \frac{d(d+1)p}{d+1+ad}\Big(1 + \frac{a}{(d+1)p}\Big)^2(1-\varphi(1))\varphi(1) \tag{3.40}$$

Now, let us solve the Eq. (3.38) to find $\varphi(1)$. Near $y = 1$ and $p = p_c$, this equation is reduced to

$$\varphi'(y)\varphi(y) - \varphi(y) \simeq -(\frac{1}{4} + \alpha)(y-1), \tag{3.41}$$

where α is defined as $\alpha \equiv (a/((d+1)p))(d+1+ad)/(1+a/((d+1)p))^2 - 1/4$. The critical point $p_c(d,a)$ lies on the (d,a)-plane satisfying the condition of $\alpha = 0$. Substituting $(y-1)\psi$ for φ, Eq. (3.41) become

$$(y-1)\psi\frac{d\psi}{dy} = -\Big[\Big(\psi - \frac{1}{2}\Big)^2 + \alpha\Big], \tag{3.42}$$

and the solution is written as

$$\ln\left(C(y-1)\right) = -\int \frac{\psi d\psi}{(\psi - 1/2)^2 + \alpha}, \tag{3.43}$$

where C is a integration constant. For $\alpha > 0$, the solution of Eq. (3.43) becomes

$$\ln\left(C(y-1)\right) = -\frac{1}{2}\ln\Big(\Big(\frac{\varphi}{y-1}-\frac{1}{2}\Big)^2+\alpha\Big) - \frac{1}{2\sqrt{\alpha}}\Big[\frac{\pi}{2} + \arctan\Big(\frac{1}{\sqrt{\alpha}}\Big(\frac{\varphi}{y-1}-\frac{1}{2}\Big)\Big)\Big], \tag{3.44}$$

thus,

$$C(y-1) = \Big(\Big(\frac{\varphi}{y-1}-\frac{1}{2}\Big)^2+\alpha\Big)^{-1/2} \times \exp\Big[-\frac{1}{2\sqrt{\alpha}}\Big[\frac{\pi}{2}+\arctan\Big(\frac{1}{\sqrt{\alpha}}\Big(\frac{\varphi}{y-1}-\frac{1}{2}\Big)\Big)\Big]\Big]. \tag{3.45}$$

As $y \to 1$ and $\alpha \to 0$, satisfying $1 \gg y-1 \gg \exp\left[-\pi/(2\sqrt{\alpha})\right]$, the Eq. (3.45) is reduced to

$$\varphi(1) = \frac{1}{C}\exp\Big(-\frac{\pi}{2\sqrt{\alpha}}\Big). \tag{3.46}$$

Substituting this into Eq. (3.40), one finally arrives at

$$\begin{aligned} G &\simeq \frac{d(d+1)p}{d+1+ad}\Big(1+\frac{a}{(d+1)p}\Big)^2\frac{1}{C}\exp\Big(-\frac{\pi}{2\sqrt{\alpha}}\Big), \\ &= \frac{4ad}{C}\exp\Big(-\frac{\pi}{2\sqrt{\alpha}}\Big), \\ &= \frac{4ad}{C}\exp\Big[-\frac{\pi}{2}\Big[\frac{a(d+1+ad)}{(d+1)p}\Big(1+\frac{a}{(d+1)p}\Big)^{-2}-\frac{1}{4}\Big]^{-1/2}\Big], \end{aligned} \tag{3.47}$$

for $p > p_c$ around $p = p_c$ in the percolation phase.

For $\alpha = 0$, the solution of Eq. (3.43) satisfies

$$4\Big[\ln\Big(2+\frac{4\varphi}{1-y}\Big)+\frac{2}{2+\frac{4\varphi}{1-y}}\Big] = C - 4\ln(y-1), \tag{3.48}$$

where C is a integral constant. In other form, this equation becomes

$$\ln\Big(\frac{1}{2+\frac{4\varphi}{1-y}}\Big)-\frac{2}{2+\frac{4\varphi}{1-y}}=\ln\left[C'(y-1)\right], \tag{3.49}$$

where C' is a new constant. Thus, one can get

$$\varphi(y)=\frac{y-1}{2}\Big(1+\frac{1}{W[-C''(y-1)]}\Big), \tag{3.50}$$

where C'' is a new constant and $W(z)$ is the Lambert function satisfying $W(z)\exp\left[W(z)\right]=z$. Using the asymptotic form $W(-z)\simeq\ln z$ for $|z|\ll 1$, this solution around $y=1$ is reduced to

$$\varphi(y)\simeq\frac{y-1}{2}\Big(1+\frac{1}{\ln\left[C''(y-1)\right]}\Big). \tag{3.51}$$

Thus, when $y=1$, one get $\varphi(1)=0$ and the giant cluster size G becomes zero at the critical point $p=p_c$. This is consistent with the fact that the value of Eq. (3.47) for $p>p_c$ becomes zero as p goes to p_c.

For $\alpha<0$, the solution of Eq. (3.43) becomes

$$\begin{aligned}\ln\left(C(y-1)\right)=&\Big(\frac{1}{4\sqrt{-\alpha}}-\frac{1}{2}\Big)\ln\Big|\psi-\frac{1}{2}+\sqrt{-\alpha}\Big|\\&+\Big(\frac{-1}{4\sqrt{-\alpha}}-\frac{1}{2}\Big)\ln\Big|\psi-\frac{1}{2}-\sqrt{-\alpha}\Big|,\end{aligned} \tag{3.52}$$

where C is a constant. By considering the case of the normal phase for $p<p_c$, The value of $\varphi(1)$ should be zero at $y=1$, because giant cluster is absent. In this case, a valid solution is written as

$$\begin{aligned}&C(y-1)\\&=\Big(\frac{1}{2}-\sqrt{-\alpha}-\frac{\varphi}{y-1}\Big)^{\frac{1}{4\sqrt{-\alpha}}-\frac{1}{2}}\Big(\frac{1}{2}+\sqrt{-\alpha}-\frac{\varphi}{y-1}\Big)^{\frac{-1}{4\sqrt{-\alpha}}-\frac{1}{2}},\end{aligned} \tag{3.53}$$

for $\varphi/(y-1) < 1/2 - \sqrt{-\alpha}$. This equation can be rewritten as

$$\begin{aligned}
&C'(y-1)^{\frac{4\sqrt{-\alpha}}{1-2\sqrt{-\alpha}}} \\
&= \Big(\frac{1}{2} - \sqrt{-\alpha} - \frac{\varphi}{y-1}\Big)\Big(1 - \frac{2}{2\sqrt{-\alpha}+1}\frac{\varphi}{y-1}\Big)^{\frac{-1-2\sqrt{-\alpha}}{1-2\sqrt{-\alpha}}} \\
&\simeq \frac{1}{2} - \sqrt{-\alpha} - \frac{2\varphi^2}{(y-1)^2(1-2\sqrt{-\alpha})},
\end{aligned} \tag{3.54}$$

where C' is a new constant. Around $y = 1$, one can get

$$\frac{\varphi^2}{(y-1)^2} = \Big(\frac{1}{2} - \sqrt{-\alpha}\Big)\Big(\frac{1}{2} - \sqrt{-\alpha} - C'(y-1)^{\frac{4\sqrt{-\alpha}}{1-2\sqrt{-\alpha}}}\Big). \tag{3.55}$$

Thus,

$$\varphi(y) = \pm(y-1)\sqrt{\Big(\frac{1}{2} - \sqrt{-\alpha}\Big)\Big(\frac{1}{2} - \sqrt{-\alpha} - C'(y-1)^{\frac{4\sqrt{-\alpha}}{1-2\sqrt{-\alpha}}}\Big)}. \tag{3.56}$$

The only plus sign of Eq. (3.56) is valid because the value of φ should be always positive. Finally one get,

$$\varphi(y) \simeq (y-1)\Big(\frac{1}{2} - \sqrt{-\alpha} + C''(y-1)^{\frac{4\sqrt{-\alpha}}{1-2\sqrt{-\alpha}}}\Big), \tag{3.57}$$

where C'' is a new constant. It confirm that $\varphi(1) = 0$ when $y = 1$, and then the corresponding value of the giant cluster size G becomes zero in the normal phase for $p < p_c$.

In summary, the explicit form of the giant cluster size G, around $p = p_c$, is written as

$$G = \begin{cases} 0 & \text{for} \quad p < p_c, \\ \frac{4ad}{C}\exp\Big[-\frac{\pi}{2}\Big[\frac{a(d+1+ad)}{(d+1)p}\Big(1 + \frac{a}{(d+1)p}\Big)^{-2} - \frac{1}{4}\Big]^{-1/2}\Big] & \text{for} \quad p \geq p_c, \end{cases} \tag{3.58}$$

. where p_c is the critical point satisfying $\alpha = 0$.

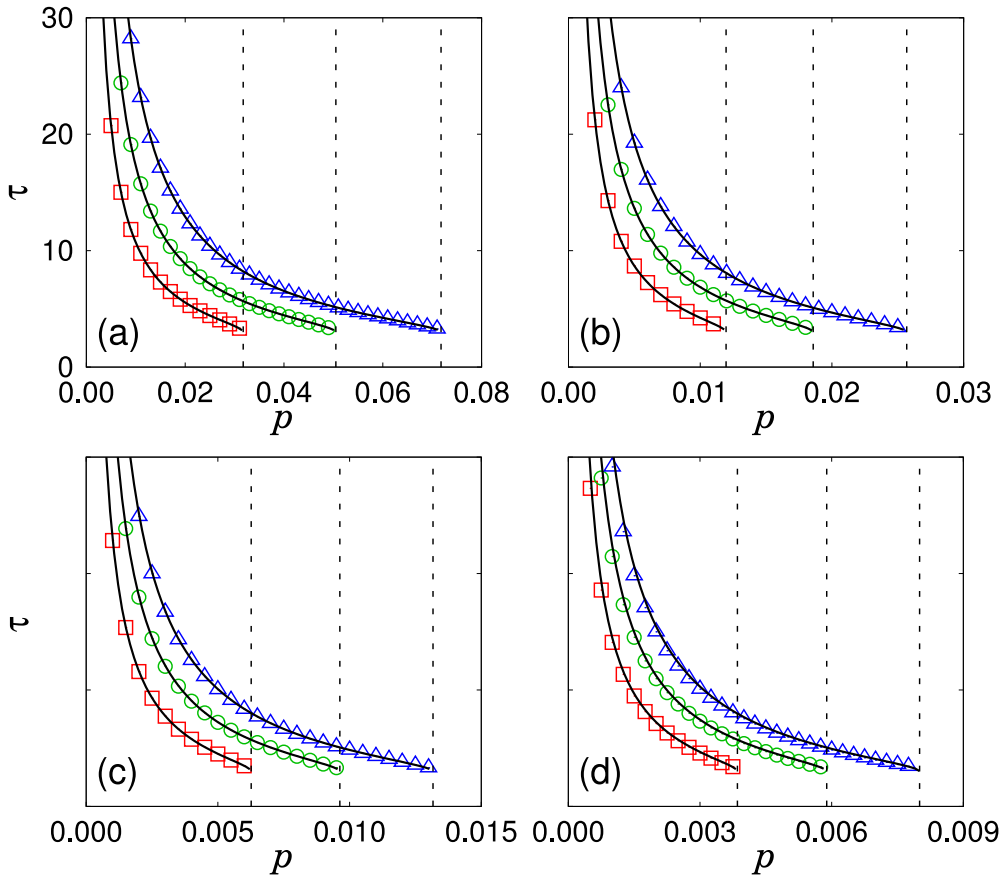

Figure 3.5: Plots of τ versus p in growing scale-free simplicial complexes for (a) $d = 1$ (link), (b) 2 (triangle), (c) 3 (tetrahedron), and (d) 4 (5-cell). Red ($a = 0.5$), green ($a = 1.0$), and blue ($a = 2.0$) symbols represent the results obtained from measures by solving numnerically the rate equation of cluster size distribution. Each solid line is the analytic solution $\tau = 3 + 4\sqrt{-\alpha}/(1 - 2\sqrt{-\alpha})$. For each plot, dotted lines from the left represent the critical points for $a = 0.5$, 1.0, and 2.0.

3.2.4 Degree distributions

In this subsection, we show that the graph and facet degree distributions of d-GSC are in power-law with characteristic exponents, γ_g and γ_f. Given a fixed facet density, p, we can construct a rate eqaution for the probability, $q(m, t', t)$, for a node added at time t' to have facet degree, m, at time t, where t' can be interpreted as a label of each node. At the moment when a new d-face is occupied with probability p, the probability

for a node to join r new d-faces is

$$u_r = \Big((d+1)\frac{m+a}{pt(d+1)+aN(t)}\Big)^r \Big(1-(d+1)\frac{m+a}{pt(d+1)+aN(t)}\Big)^{1-r}, \quad (3.59)$$

where we have $r = 0$ or 1 in our model. With this, we can write the evolution of $q(m, t', t)$ as

$$\begin{aligned} q(m,t',t+1) = p\Big[(d+1)\Big(\frac{m-1+a}{pt(d+1)+aN(t)}\Big)q(m-1,t',t) \\ + \Big(1-(d+1)\Big(\frac{m+a}{pt(d+1)+aN(t)}\Big)\Big)\Big] + (1-p)q(m,t',t) \end{aligned} \quad (3.60)$$

Summing over all nodes, $P_f(m,t) = \sum_{t'} q(m,t',t)/t$, we have

$$\begin{aligned} &N(t+1)P_f(m,t+1) - q(m,t+1,t+1) \\ &= p\Big[\Big(\frac{m-1+a}{pt/N(t)+a/(d+1)}\Big)P_f(m-1,t) + \Big(N(t) - \frac{m+a}{pt/N(t)+a/(d+1)}\Big) \\ &\times P_f(m,t)\Big] + (1-p)N(t)P_f(m,t) + O(\frac{P}{N}). \end{aligned} \quad (3.61)$$

In the limit, $t \to \infty$, (3.61) is rewritten as

$$\begin{aligned} &\frac{d(tP_f(m,t))}{dt} \\ &= \Big(\frac{m-1+a}{1+a/(p(d+1))}\Big)P_f(m-1,t) - \Big(\frac{m+a}{1+a/(p(d+1))}\Big)P_f(m,t) + \delta_{0m}, \end{aligned} \quad (3.62)$$

where $\delta_{0m} = q(m, t+1, t+1)$ because a node added at $t+1$ has zero facet degree at $t+1$. Seeking for a seady state solution, $dP/dt = 0$, we then have

$$\Big(1+\frac{a}{p(d+1)}\Big)P_f(m) + (m+a)P_f(m) - (m-1+a)P_f(m-1) = \Big(a+\frac{a}{p(d+1)}\Big). \quad (3.63)$$

Now we introduce a generating function, $Q(z)$, of facet degree distribution,

$$Q(z) = \sum_{m=0}^{\infty} P_f(m) z^m. \tag{3.64}$$

Thus (3.63) is now expressed as

$$z(1-z)\frac{dQ}{dz} + a(1-z)Q + \Big(1 + \frac{a}{p(d+1)}\Big)Q = \Big(1 + \frac{a}{p(d+1)}\Big). \tag{3.65}$$

The solution, around $z = 0$, of the differential (3.65) is the hypergeometric function,

$$Q(z) = \frac{1 + a/(p(d+1))}{1 + a + a/(p(d+1))} {}_2F_1(1, a; 2 + a + \frac{a}{p(d+1)}; z), \tag{3.66}$$

where the hypergeometric fuction is

$${}_2F_1(a, b; c; z) = \sum_{m=0}^{\infty} \frac{1}{m!} \frac{\Gamma(m+a)}{\Gamma(a)} \frac{\Gamma(m+b)}{\Gamma(b)} \frac{\Gamma(c)}{\Gamma(m+c)}. \tag{3.67}$$

So (3.66) is then

$$\begin{aligned} Q(z) = &\sum_{m=0}^{\infty} \Big(1 + \frac{a}{p(d+1)}\Big) \\ &\times \frac{\Gamma(1 + a + a/(p(d+1))}{\Gamma(a)} \frac{\Gamma(m+a)}{\Gamma(2 + m + a + a/(p(d+1))} z^m, \end{aligned} \tag{3.68}$$

where the summand is facet degree distribution. For sufficiently large m, $P_f(m)$ can be approximated as a simple form,

$$P_f(m) \simeq \Big(1 + \frac{a}{p(d+1)}\Big) \frac{\Gamma(1 + a + a/(p(d+1))}{\Gamma(a)} (m+a)^{-(2+a/(p(d+1)))}, \tag{3.69}$$

which means that the power-law exponent is obtained as $\gamma_f = 2 + a/(p(d+1))$. Similarly, for graph degree distribution, $P_g(k)$, we can write the evolutionary equation

by simply modifying (3.60),

$$q(k,t',t+1) = p\Big[(d+1)\Big(\frac{k-d+a}{pt(d+1)+aN(t)}\Big)q(k-d,t',t) \\ + \Big(1-(d+1)\Big(\frac{k+a}{pt(d+1)+aN(t)}\Big)\Big)\Big] + (1-p)q(k,t',t), \tag{3.70}$$

which indicate that when a d-face is newly occupied with probability p, each selected node gets additive degree of d. Thus,

$$P_g(k) = \Big(1+\frac{a}{p(d+1)}\Big)\frac{\Gamma(1+a+a/(p(d+1))}{\Gamma(a)}\frac{\Gamma(k/d+a)}{\Gamma(2+k/d+a+a/(p(d+1))}. \tag{3.71}$$

In large k limit,

$$P_g(k) = \Big(1+\frac{a}{p(d+1)}\Big)\frac{\Gamma(1+a+a/(p(d+1))}{\Gamma(a)}(k/d+a)^{-(2+a/(p(d+1)))}, \tag{3.72}$$

which reveals the same sacling form of graph degree distribution, $P_g(k) \sim k^{-\gamma_g}$, where $\gamma_g = 2 + a/(p(d+1))$.

3.2.5 Cluster size distribution

As we derived the cluster size distribution for d-SSC, we can do the same prodedure for d-GSC as well. Using the Lagrange inversion formula, we have

$$sn_s = \frac{1}{2\pi i}\oint dz\frac{f}{z^{s+1}} = \tag{3.73}$$

where the contour c is a unit circle and counterclockwise closed path encircling the point $z = 0$. Substituting Eq. (3.39) into Eq. (3.73), Eq. (3.73) becomes then

$$n_s = \delta_{1s} + \frac{d(d+1)p}{2}\oint_c \frac{dz}{2\pi i}h^2(z)z^{-k-1}. \tag{3.74}$$

Thus we obtain

$$n_s = \delta_{1s} - \frac{d(d+1)p}{2}(d+1+ad)\Big(1+\frac{a}{(d+1)p}\Big)^2 \times \int_{c'} \frac{dy}{2\pi i}\varphi^2 y^{s(d+1+ad)-3}, \tag{3.75}$$

where c' is the new integration contour and $y \equiv z^{-/(d+1+ad)}$ and $\varphi(y)/y \equiv h(z)/(1+a/((d+1)p))$. Because there is a singularity at $y = 1$, we change the integration variable y into $1+u$ for small u. For large s, Eq. (3.75) becomes

$$n_s = \frac{d(d+1)p}{2}(d+1+ad)\Big(1+\frac{a}{(d+1)p}\Big)^2 \times \int_{c''} \frac{du}{2\pi i}\varphi^2(1+u)e^{s(d+1+ad))u}, \tag{3.76}$$

where c'' is the new integral contour.

When $p = p_c$, by using Eq. (3.51), one get the cluster size distribution

$$n_s \simeq \frac{d^2(d+1)p(1+a/((d+1)p))^2}{4(d+1+ad)^2}\frac{1}{s^3\ln^2 s} = \frac{ad^2}{d+1+ad}\frac{1}{s^3\ln^2 s}, \tag{3.77}$$

for large s at $p = p_c$. The coefficient changes depending on the values of d and a, however, the corresponding critical exponent τ is always 3 at the critical point.

In the same way, when $p < p_c$, by using Eq. (3.57), one get

$$n_s \sim s^{-3-4\sqrt{-\alpha}/(1-2\sqrt{-\alpha})}, \tag{3.78}$$

where α is defined as $\alpha \equiv (a/((d+1)p))(d+1+ad)/(1+a/((d+1)p))^2 - 1/4$. Thus, the critical exponent τ is $\tau = 3 + 4\sqrt{-\alpha}/(1-2\sqrt{-\alpha})$ for $p < p_c$.

3.3 Homological percolation of simplicial complex models

There are several quantities which share the same notion of global order that the giant component of the system is supposed to depict, such as the mean distance, loop statistics, and so on. In many cases, there are difficulties to understand such global orders of the real systems with just the giant component. In one hand, it is much more easier to understand the orders of the real systems when we are in short of well refined samples, but we have tools to calculate several topological features. For instance, the number of loops is more obvious for quantification of the global order rather than the size of the largest component which we can hardly determine if it is $O(N)$. It is not only easy to count, but also highly related to the size of the giant component as is that the maximal tree can not grow as a tree beyond the very edge of the system, which leads to intra-cluster linkages to form many loops. We call this the first Betti number, and this is denoted as B_1 in the frame of homology. In this chapter, we mainly focus on both analytic and numerical analysis for the emergence of the first Betti number both in d-dimensional static and growing simplicial complex, d-SSC and d-GSC respectively.

3.3.1 The first Betti number of d-GSC

First, we consider the total facet degree of the system.

$$M(t) = (d+1)F(t) = \sum_{i=1}^{N(t)} m_i(t) \tag{3.79}$$

where $F(t)$ is the total number of d-faces in the system. In GSC process, we occupy every d-face in preferential attachment scheme, $p_i \sim \frac{m_i+a}{\sum_j m_j+a}$, where a is an initial attractiveness. Thus, the probability, $p_{\vec{n}}$, for a set of $d+1$ nodes to be connected is written as

$$p_{\vec{n}} = \frac{\prod_i^{d+1}(m_{n_i}(t)+a)}{(M(t)+aN(t))^{d+1}}. \tag{3.80}$$

Let us now define a generating function, f, as

$$f(N,M;x,t) = \frac{1}{N}\Big\langle \delta(N(t)-N)\delta(M(t)-M)\sum_{i=1}^{N} x^{s_i(t)}\Big\rangle, \tag{3.81}$$

where s_i is the size of the cluster which i belongs to. This evolves in time as

$$\begin{aligned}
f(N,M;x,t+dt) &= (1-dt-pdt)f(N,M;x,t) + \frac{dt}{N}\Big\langle \delta(N(t)+1-N) \\
&\times \delta(M(t)-M)\sum_{i=1}^{N} x^{s_i(t)}\Big\rangle + \frac{pdt}{N}\Big\langle \delta(N(t)-N)\delta(M(t)+(d+1)-M) \\
&\times \sum_{\vec{n}} \frac{\prod_{i=1}^{d+1}(m_{n_i}(t)+a)}{(M(t)+aN(t))^{d+1}}\Big\{ \sum_{i=1}^{N} x^{s_i(t)} - \Big[\sum_{m=1}^{N} S_{mn_1}(1-S_{mn_2})\dots(1-S_{mn_{d+1}}) \\
&\times \Big(x^{s_{n_1}(t)} - x^{s_{n_1}(t)+s_{n_2}(t)+\dots+s_{n_{d+1}}(t)}\Big) + \sum_{m=1}^{N}(1-S_{mn_1})S_{mn_2}\dots(1-S_{mn_{d+1}}) \\
&\times \Big(x^{s_{n_2}(t)} - x^{s_{n_1}(t)+s_{n_2}(t)+\dots+s_{n_{d+1}}(t)}\Big) + \dots + \sum_{m=1}^{N}(1-S_{mn_1})(1-S_{mn_2})\dots S_{mn_{d+1}} \\
&\times \Big(x^{s_{n_{d+1}}(t)} - x^{s_{n_1}(t)+s_{n_2}(t)+\dots+s_{n_{d+1}}(t)}\Big)\Big]\Big\}\Big\rangle,
\end{aligned} \tag{3.82}$$

where S_{ij} stands for a connectivity matrix,

$$S_{ij} = \begin{cases} 1 & \text{if } i \text{ and } j \text{ are in the same cluster ,} \\ 0 & \text{otherwise.} \end{cases} \tag{3.83}$$

As is the case that we only consider tree-like SCs, all the factors, $(1-S)$, in (3.82) is negligible in the thermodynamic limit. Then,

$$
\begin{aligned}
f(N,M;x,t+dt) &= (1-dt-pdt)f(N,M;x,t) + (1-\frac{1}{N})\frac{dt}{N-1} \\
&\times \Big\langle \delta(N(t)+1-N)\delta(M(t)-M)\sum_{i=2}^{N} x^{s_i(t)} \Big\rangle \\
&+ \frac{dt}{N}\Big\langle \delta(N(t)+1-N)\delta(M(t)-M)\Big\rangle x \\
&+ pdtf(N,M-(d+1);x,t) - \frac{p(d+1)dt}{N(M-(d+1)+aN)} \\
&\times \Big\langle \delta(N(t)-N)\delta(M(t)+(d+1)-M)\sum_{j=1}^{N}(m_j+a)s_j(t)x^{s_j(t)} \Big\rangle \\
&+ \frac{p(d+1)dt}{N(M-(d+1)+aN)^{d+1}}\Big\langle \delta(N(t)-N)\delta(M(t)+(d+1)-M) \\
&\times \Big(\sum_{j=1}^{N}(m_j+a)s_j(t)x^{s_j(t)}\Big)\Big(\sum_{j=1}^{N}(m_j+a)x^{s_j(t)}\Big)^{d}\Big\rangle.
\end{aligned}
\tag{3.84}
$$

Using the relations,

$$
\sum_{i=1}^{N(t)} m_i(t)s_i(t)x^{s_i(t)} = \frac{d+1}{d}\sum_{j=1}^{N(t)}(s_j(t)-1)x^{s_j(t)} \tag{3.85}
$$

$$
\sum_{i=1}^{N(t)} m_i(t)x^{s_i(t)} = \frac{d+1}{d}\sum_{j=1}^{N(t)}\Big(1-\frac{1}{s_j(t)}\Big)x^{s_j(t)} \tag{3.86}
$$

we can rewrite (3.86) as

$$
\begin{aligned}
f(N,M;x,t+dt) &= (1-dt-pdt)f(N,M;x,t)+dt(1-\frac{1}{N})f(N-1,M;x,t)\\
&+\frac{1}{N}f(N,M;1,t)x+pdtf(N,M-(d+1);x,t)\\
&-\frac{p(d+1)dt}{N(M-(d+1)+aN)}\Big\langle\delta(N(t)-N)\delta(M(t)+(d+1)-M)\\
&\times\sum_{j=1}^{N}\Big(\Big(\frac{d+1}{d}+a\Big)s_j(t)-\frac{d+1}{d}\Big)x^{s_j(t)}\Big\rangle+\frac{p(d+1)dt}{N(M-(d+1)+aN)^{d+1}}\\
&\times\Big\langle\delta(N(t)-N)\delta(M(t)+(d+1)-M)\\
&\times\Big(\sum_{j=1}^{N}\Big(\Big(\frac{d+1}{d}+a\Big)s_j(t)-\frac{d+1}{d}\Big)x^{s_j(t)}\Big)\\
&\times\Big(\sum_{j=1}^{N}\Big(\Big(\frac{d+1}{d}+a\Big)-\frac{d+1}{ds_j(t)}\Big)x^{s_j(t)}\Big)^{d}\Big\rangle.
\end{aligned}
\tag{3.87}
$$

$$
\begin{aligned}
&t\frac{\partial f}{\partial t}+f+\frac{p(d+1)}{p(d+1)+a}\Big(\Big(\frac{d+1}{d}+a\Big)x\frac{\partial f}{\partial x}-\frac{d+1}{d}f\Big)-\frac{p(d+1)}{(p(d+1)+a)^{d+1}}\\
&\times\Big(\Big(\frac{d+1}{d}+a\Big)x\frac{\partial f}{\partial x}-\frac{d+1}{d}f\Big)\Big(\Big(\frac{d+1}{d}+a\Big)f-\frac{d+1}{d}g\Big)^{d}=x
\end{aligned}
\tag{3.88}
$$

where $g(x,t)=\int_0^x dyf(y,t)/y$. Now (3.88) can be written as

$$
\begin{aligned}
&t\frac{\partial g}{\partial t}+g+\frac{p(d+1)}{p(d+1)+a}\Big(\Big(\frac{d+1}{d}+a\Big)f-\frac{d+1}{d}g\Big)\\
&\quad-\frac{p(d+1)}{(p(d+1)+a)^{d+1}}\Big(\Big(\frac{d+1}{d}+a\Big)f-\frac{d+1}{d}g\Big)^{d+1}=x
\end{aligned}
\tag{3.89}
$$

From the fact that there are no loops in finite clusters, we need to count the number of loops in giant component only. Using the Euler characteristic which is an alternating sum of any finite topological quantities, we can obtain the number of loops, the first

Betti number.

$$\chi = F_0 - F_1 + \cdots = B_0 - B_1 + \ldots. \tag{3.90}$$

Though the relation (3.90) is simple enough, it is still annoying to consider all the faces of dimension $1 < k < d$. So we can effectively map a SC to a cell complex of which constituents are 0-, 1-, and 2-cells. Now let us rewrite (3.90) as

$$\chi = C_0 - C_1 + C_2 = B_0 - B_1, \tag{3.91}$$

where C_0, C_1, C_2 are the number of nodes, edges, $(d+1)$-polygons. This map is valid since we only have tree-like SCs, and can be interpreted as that there are loops only made of line boundary of $(d+1)$-polygons. Now we get

$$C_0 = t(1 - f(1)), \tag{3.92}$$

$$C_1 = t(d+1)(p - \frac{1}{d}f(1) + \frac{1}{d}g(1)), \tag{3.93}$$

$$C_2 = t(p - \frac{1}{d}f(1) + \frac{1}{d}g(1)). \tag{3.94}$$

Thus, the first Betti number reads

$$B_1/t = b_1 \simeq g(1) - (1 - pd), \tag{3.95}$$

in the limit of $t \to \infty$. Rearranging (3.95) with respecto $g(1)$, and pluging it into (3.89) at $x = 1$, we get

$$\begin{aligned} b_1 + (1-pd) + \frac{p(d+1)}{p(d+1)+a}\Big(\Big(\frac{d+1}{d} + a\Big)(1-G) - \frac{d+1}{d}(b_1 + (1-pd))\Big) \\ - \frac{p(d+1)}{(p(d+1)+a)^{d+1}}\Big(\Big(\frac{d+1}{d} + a\Big)(1-G) - \frac{d+1}{d}(b_1 + (1-pd))\Big)^{d+1} = 1, \end{aligned} \tag{3.96}$$

and

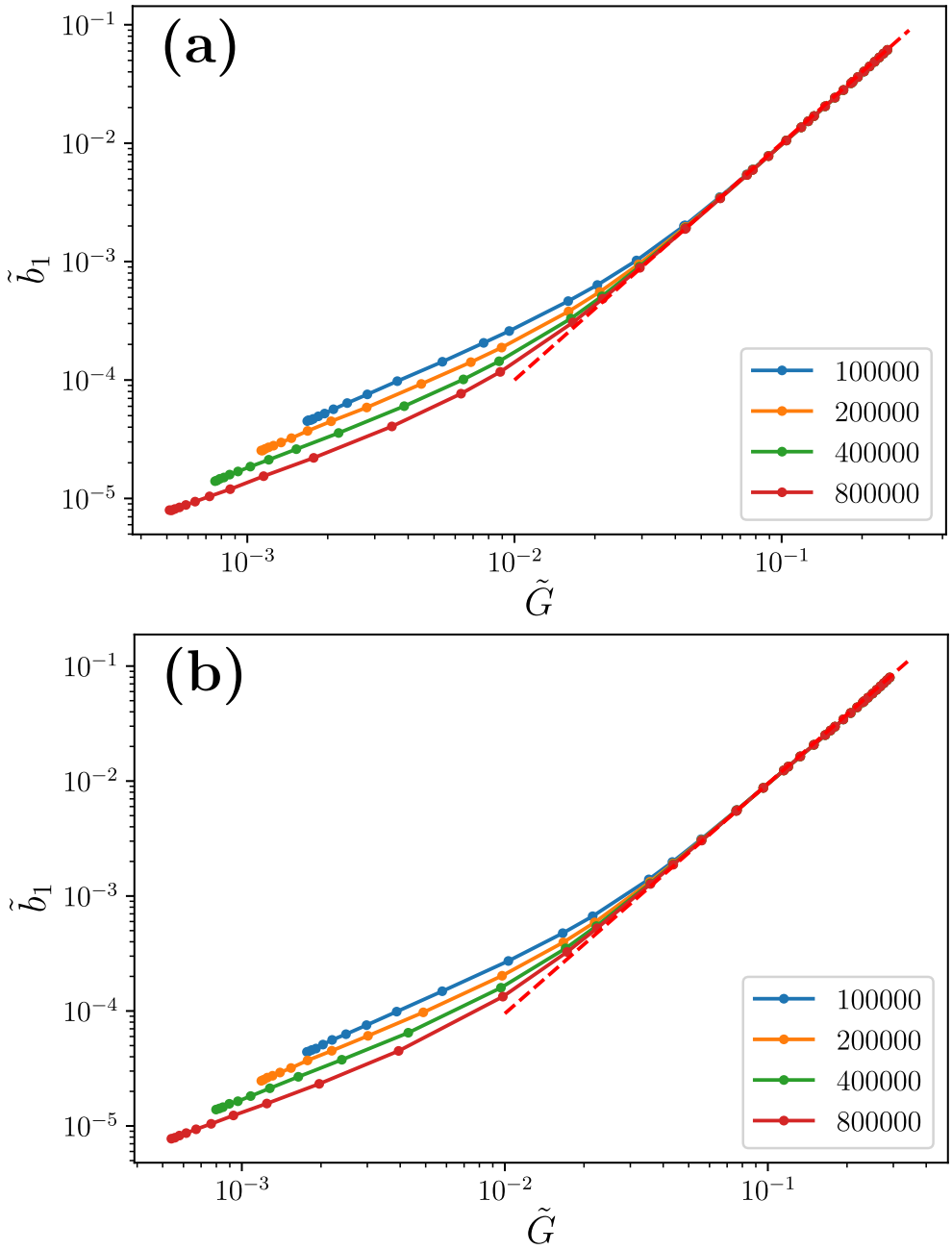

Figure 3.6: Plot of $\tilde{b}_1$ versus the $\tilde{G}$ for (a) $d = 3$, and (b) $d = 4$. The slopes of the guidelins both in (a) and (b) are the same, $\tilde{b}_1 \sim \tilde{G}^2$.

$$
\begin{aligned}
b_1 - pd + p(d+1)\Big[1 - \frac{G((d+1)+da) + b_1(d+1)}{pd(d+1)+da}\Big] \\
- p\Big[1 - \frac{G((d+1)+da) + b_1(d+1)}{pd(d+1)+da}\Big]^{d+1} = 0.
\end{aligned}
\tag{3.97}
$$

We finally get

$$
b_1 \simeq \frac{pd(d+1)}{2}\Big(\frac{(d+1)+da}{pd(d+1)+da}G\Big)^2 \tag{3.98}
$$

in the vicinity of percolation phase transition. This is in good agreement with the result of numerical simulation, see Fig. 3.6. This equation shows that the first Betti number is not just of the same functional form with G, and this can serve the percolation phase transition of the system as well. We call this a homological percolation transition of the first Betti number,

$$
b_1 \sim \exp(-\alpha_1(p - p_c)^{\beta_1}). \tag{3.99}
$$

3.3.2 The first Betti number of d-SSC

In the previous chapter, we derived the relation between f and g, from the rate equation for d-SSCs that we built earlier. Let us invoke

$$
f - g = pd\, f^{d+1}, \tag{3.100}
$$

which can be used to obtain the number of loops. To count the number of loops made of very edges of d-faces, we should count the number of nodes, C_0, the number of edges, C_1, and the number of d-faces, C_2. Everything is the same as that of d-GSC, so all we need to do is just plugging $g(1)$ of (3.95) into (3.100) at $x = 1$. So we have

$$
\begin{aligned}
b_1 &= pd(1 - (1 - G^{d+1})) - G \\
&\equiv \xi(G) \\
&\simeq (pd(d+1) - 1)G,
\end{aligned}
\tag{3.101}
$$

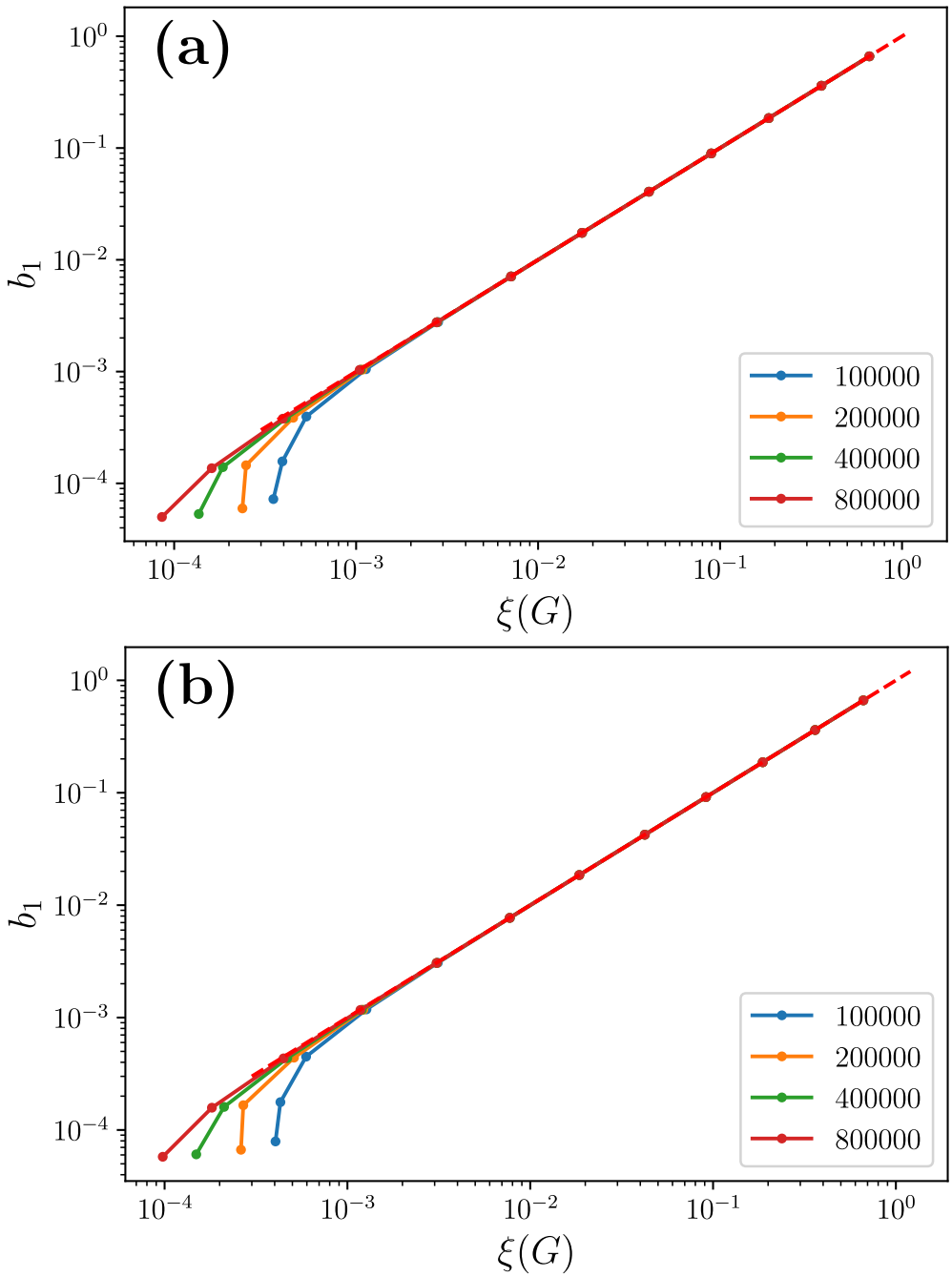

Figure 3.7: Plot of b_1 versus the $\xi(G)$ for (a) $d = 2$, and (b) $d = 3$. The slopes of the guidelins both in (a) and (b) are the same, which are one.

which is numerically verified in Fig. 3.7. Now let $p = p_c + \delta p$, then we have

$$b_1 \sim \delta p^{\beta+1}, \tag{3.102}$$

where β is the critical exponent for the ginat component. A homological percolation transition of the first Betti number is also found in static simplicial complexes, but with different exponet.

3.4 Remark

We study the models for both static and growing simplicial complexes. In particular, we investigate percolation transitions in such models and confirm that the critical behaviors are the same in any d. This means that the simultaneous group formation has no effect on long-wavelength behavior of the percolation system no matter what the size of the group is. It is only to do with the threshold of the system, which is the larger the size of the group is, the lower the threshold becomes. Furthermore, we obtain analytic results of the first Betti number in both static and growing models, which is consistent with the numerical simulation results. In particular, we show that this quantity serves the critical behavior the giant component reveals.

Chapter 4

Higher-order interacting oscillators

Kuramoto model is naturally generalized to the model of which constituents are many-body interacting oscillators on higher-order networks. In this chapter, we show how the type of synchronization transition changes under such higher-order interaction specifically on uniform hypergraphs.

4.1 Globally coupled higher-order interaction

Consider a rate equation for the phase of each oscillator with a general form of interaction,

$$\dot{\theta}_j = \omega_j + K/N^{d-1} \sum_{j_1,\cdots,j_{d-1}} G(\theta_j, \theta_{j_1}, \ldots, \theta_{j_{d-1}}), \tag{4.1}$$

which is extended from the kuramoto equation. Note that the subscripts, k's, of j_k indicate that each of them is a k-th neighbor in a certain hyperedge. Since each oscillator has $(N-1)(N-2)(\simeq N^2)$ hyperedges considering the order of neighboring oscillators, the interaction strength, K, has to be rescaled by N^2 to avoid the divergence of interaction trem as $N \to \infty$. Compared to the kuramoto dynamics, each oscillator interacts with the chunks of neighboring oscillators through hyperedges of size d.

4.1.1 Model of bistable synchronization

Consider a model with an interaction of the form,

$$G(\theta_j, \theta_{j_1}, \ldots, \theta_{j_{d-1}}) = \sin(\theta_{j_1} + \cdots + \theta_{j_{d-1}} - \theta_j), \tag{4.2}$$

Then, the equation of motion can be written as

$$\dot{\theta}_j = \omega_j + K/N^{d-1} \sum_{j_1,\dots,j_{d-1}} \sin(\theta_{j_1} + \cdots + \theta_{j_{d-1}} - \theta_j). \tag{4.3}$$

The complex valued order parameter is

$$R = 1/N \sum_j e^{i\theta_j} = re^{i\psi}, \tag{4.4}$$

which is utilized to reexpress the Eq. 4.3 as

$$\begin{aligned} \dot{\theta}_j &= \omega_j + K\mathrm{Im}(R^{d-1}e^{-i\theta_j}), \\ &= \omega_j + Kr^{d-1}\sin((d-1)\psi - \theta_j). \end{aligned} \tag{4.5}$$

We set $\psi = 0$ without loss of generality. To further investigate, consider a phase space distribution, $f(\omega, \theta)$, which satisfies the continuity equation,

$$\frac{\partial}{\partial t} f + \frac{\partial}{\partial t}(\dot{\theta} f) = 0. \tag{4.6}$$

Because the variable θ is bounded in the range $[0, 2\pi)$, $f(\omega, \theta)$ can be expanded by the Fourier modes.

$$f(\omega, \theta, t) = \frac{g(\omega)}{2\pi}\Big[1 + \sum_{n=1}^{\infty} f_n(\omega, t)e^{in\theta} + \text{c.c.}\Big], \tag{4.7}$$

where c.c. stands for complex conjugate of the second term in the bracket. If we fully understand the dynamical behaviors of each coefficient, $f_n(\omega, t)$, we have the entire evolutionary behavior of the $f(\theta, \omega, t)$. Specifically, if we know the evolution of $f_1^*(\omega, t)$, this gives the evolution of the order parameter by the fact that

$$\int f(\omega, \theta, t)e^{i\theta} d\omega d\theta = \langle e^{i\theta} \rangle = R. \tag{4.8}$$

Therefore, the only interest of ours is just the dynamical behavior of the first coefficient, $f_1(\omega, t)$, as follows,

$$\frac{\partial}{\partial t} f_1 + i\omega f_1 + \frac{K r^{d-1}}{2}(f_2 - 1) = 0. \tag{4.9}$$

Here comes the ansatz that was originally introduced by Ott and Antonsen to be more tractable.

$$f_1 = a(\omega, t), \tag{4.10}$$

$$f_n = (a(\omega, t))^n. \tag{4.11}$$

Furthermore, if the distribution of intricsic frequency is of Cauchy,

$$g(\omega) = \frac{\Delta/\pi}{\Delta^2 + \omega^2}, \tag{4.12}$$

the order parameter is obtained as

$$R^*(t) = a(\omega = -i\Delta, t). \tag{4.13}$$

The rate equation of the order parameter is then,

$$\frac{\partial}{\partial t} r + \Delta r + \frac{K r^{d-1}}{2}(r^2 - 1) = 0. \tag{4.14}$$

This is in a good agreement with the simulation result, see Fig. 4.1 and Fig. 4.2. Compared to the supercritical behavior, as displayed in Fig. 4.2, the subcritical behavior shows a clue that there might be a meta-stable state, which means there can be exist an abrupt change of the order paramete with respect to the coupling strength, K. To see this, let the time derivative of the order parameter be zero to obtain the steady state solution of it,

$$\Delta r + \frac{K r^{d-1}}{2}(r^2 - 1) = rF(r, K) = 0. \tag{4.15}$$

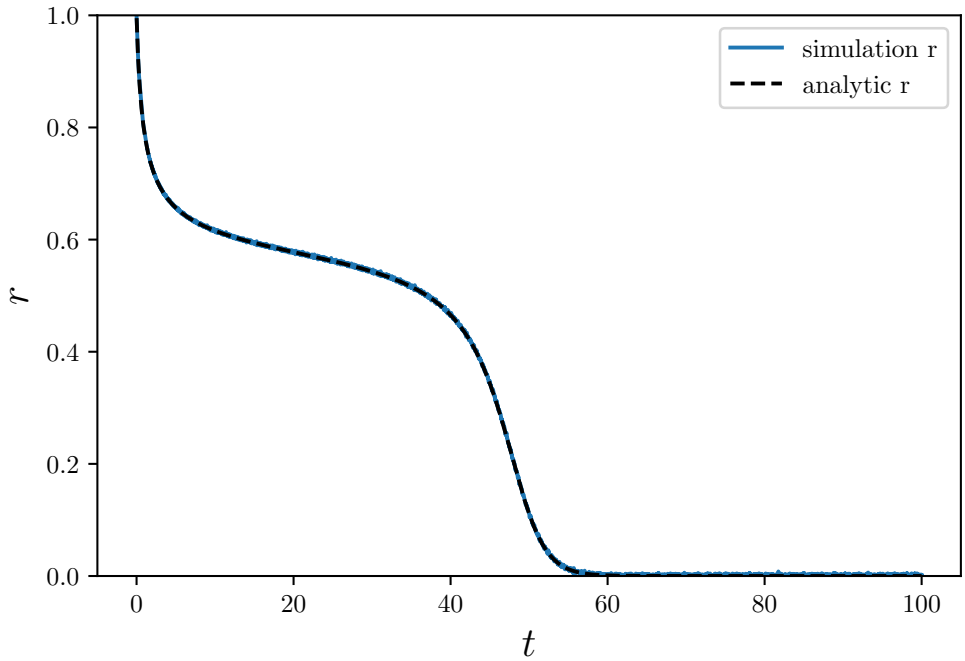

Figure 4.1: Simulation and analytic results for subcritical dynamics of order parameter on an all-to-all hypgergraph. The size of the system, N, is 10^4 with $d = 3$, $\Delta = 0.5$, and $K = 2.57$. Simulation is performed for the oscillators with intrinsic frequencies regularly sampled from the distribution.

The roots of the Eq. 4.15 are the steady state solutions of the system, each of which is either unstable or stable. Especially, the roots of $F(r, K)$ cover the entire non-zero solutions. We can obtain critical points, where synchronization transition occurs, and jump sizes for any d. Knowing the fact that the non-zero roots for $F(r, K) = 0$ exist only if $K \geq K_c$, it is obvious that $\frac{\partial}{\partial r} F(r, K) = 0$, which gives the jump size as

$$r_c = \sqrt{\frac{d-2}{d}}. \tag{4.16}$$

Plugging the obtained r_c into $F(r, K)$, we can obtain the critical point as follows,

$$K_c = \frac{1}{(\frac{d-2}{d})^{\frac{d-2}{2}} - (\frac{d-2}{d})^{\frac{d}{2}}}, \tag{4.17}$$

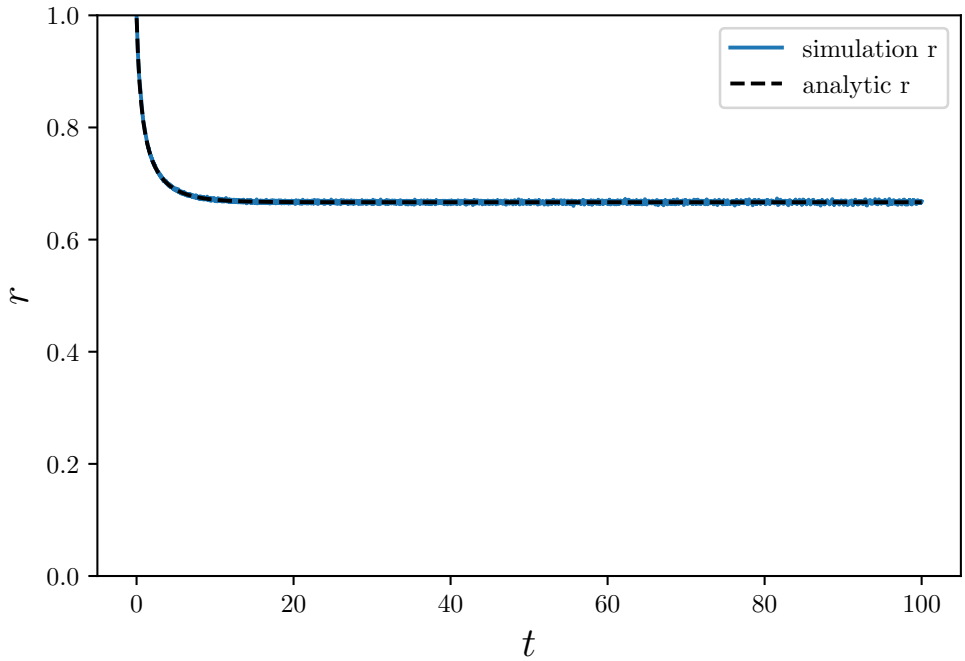

Figure 4.2: Simulation and analytic results for suprecritical dynamics of order parameter on an all-to-all hypgergraph. The size of the system, N, is 10^4 with $d = 3$, $\Delta = 0.5$, and $K = 2.7$. Simulation is performed for the oscillators with intrinsic frequencies regularly sampled from the distribution.

which directly shows the critical point for $d = 3$ as $K_c \simeq 2.598$ given the jump size $r_c \simeq 0.577$. The critical point where the finite global order emerges is understood as the point at which a saddle node bifurcation occurs. As K exceeds K_c, both stable and unstable solutions which are non-zero apppear, which leads to the bistability for $K > K_c$. That is why we calculate the solution r of $\frac{\partial}{\partial r}F(r, K) = 0$ to obtain the critial values of the coupling strength and the order parameter. In the viewpoint of critical phenomena, we confirm that there exists a hybrid synchronization transition, which reveals critical behavior right above the explosive change of the global order

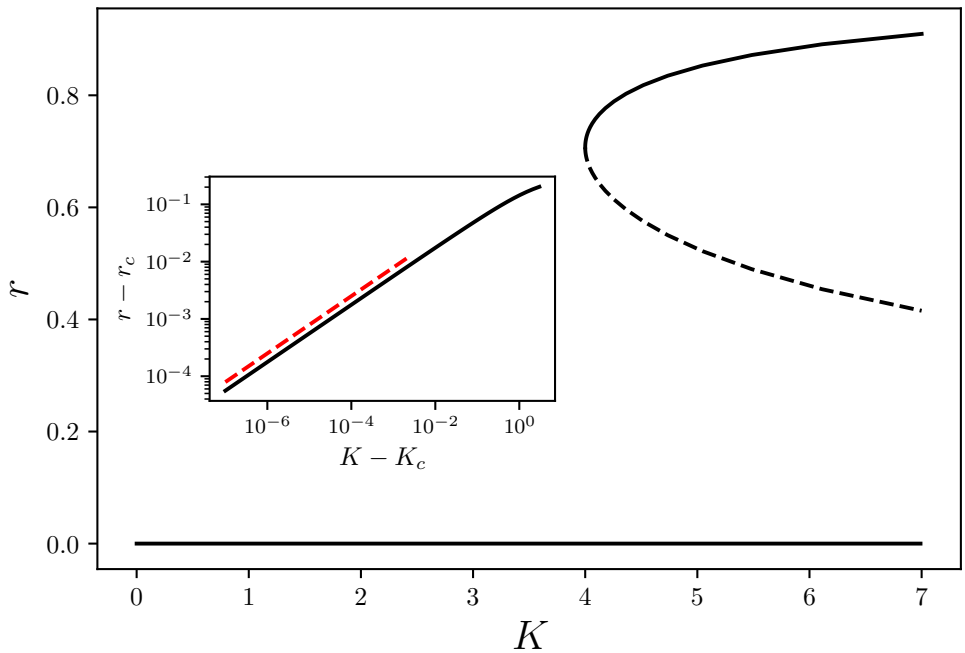

Figure 4.3: Plot of the order parameter, r, with respect to the coupling strength, K, for $d = 4$ and $\Delta = 0.5$. The solid lines are the collection of stable fixed points, whereas the dashed line is made of unstable fixed points. Bistability holds for $K > K_c$. Inset plot indicates that $r - r_c \simeq (K - K_c)^{1/2}$.

parameter, $\delta r = r_c$, such that

$$r = \begin{cases} r_c + C(K - K_c)^{\beta} & \text{if } K \geq K_c, \\ 0 & \text{otherwise,} \end{cases} \tag{4.18}$$

where β stands for the critical exponent for the order parameter. We can see this by expanding $F(r, K)$ around $r = r_c$ and $K = K_c$,

$$\begin{aligned} F(r, K) &= F(r_c, K_c) + \frac{\partial}{\partial r} F(r, K)|_{r_c, K_c}(r - r_c) \\ &+ \frac{\partial}{\partial K} F(r, K)|_{r_c, K_c}(K - K_c) + \frac{\partial^2}{\partial r^2} F(r, K)|_{r_c, K_c}(r - r_c)^2 + \dots . \end{aligned} \tag{4.19}$$

Since $F(r_c, K_c) = 0$ and $\frac{\partial}{\partial r}F(r,K)|_{r_c,K_c} = 0$, considering the first two leading terms in the vicinity of the critical point, we get

$$0 = F(r,K) = \frac{\partial}{\partial K}F(r,K)|_{r_c,K_c}(K-K_c) + \frac{\partial^2}{\partial r^2}F(r,K)|_{r_c,K_c}(r-r_c)^2, \quad (4.20)$$

which leads to

$$(r - r_c) \simeq (K - K_c)^{1/2}. \quad (4.21)$$

Therefore, the value of critical exponent for order parameter, $\beta = 1/2$, is universal for any d larger than two. When it comes to the other critical exponent such as λ for susceptibility, we can see it as well by introducing the external field,

$$\dot{\theta}_j = \omega_j + K/N^{d-1} \sum_{j_1,\ldots,j_{d-1}} \sin(\theta_{j_1} + \cdots + \theta_{j_{d-1}} - \theta_j) + h_i \sin(\phi_i - \theta_i). \quad (4.22)$$

where h_i plays a role of local field exerting on the oscillator i to force it being parallel to the field. Let us consider a uniform external field,

$$h_i = h \quad (4.23)$$

$$\phi_i = \phi = \psi, \quad (4.24)$$

where we let the angular velocity, ϕ, to be same with ψ for simplicity. Thus, we have in the rotating frame,

$$\dot{\theta}_j = \omega_j - (Kr^{d-1} + h)\sin(\theta_j), \quad (4.25)$$

which leads to

$$\frac{\partial}{\partial t}r + \Delta r + \frac{Kr^{d-1} + h}{2}(r^2 - 1) = 0. \quad (4.26)$$

The steady state solution reads

$$\Delta r + \frac{Kr^{d-1} + h}{2}(r^2 - 1) = rF(r, K, h) = 0. \quad (4.27)$$

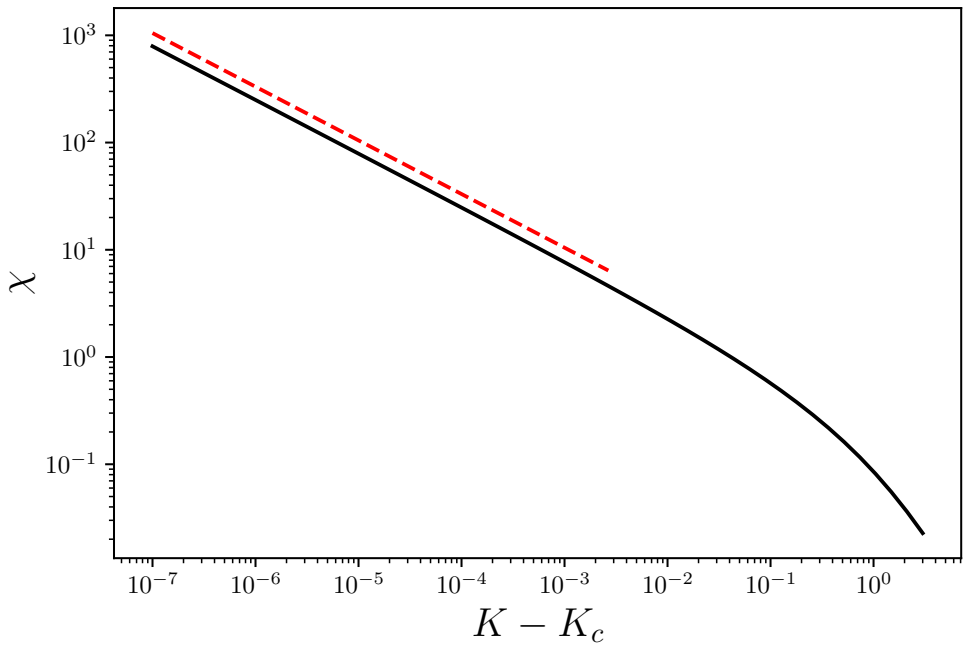

Figure 4.4: Plot of the susceptibility, χ, with respect to the coupling strength, K, for $d = 4$ and $\Delta = 0.5$. The susceptibility diverges as $K \to K_c^+$.. The slope of the red dashed line is -1/2, which means that $\chi \sim (K - K_c)^{-1/2}$.

Now, the susceptibility is defined as

$$\chi \equiv \frac{\partial r}{\partial h}\Big|_{h\to 0}, \tag{4.28}$$

which can be easily calculated by taking derivative of $f(r, K, h)$ with respect to h.

$$\begin{aligned} \frac{\partial r}{\partial h}\Big|_{h\to 0} &= \frac{r(1-r^2)}{Kr^{d-1}(1+r^2-(d-1)(1-r^2))}, \\ &\sim (K-K_c)^{1/2}. \end{aligned} \tag{4.29}$$

The critical exponent for susceptibility is obtained as $\gamma = 1/2$, which leads to $\bar{\nu} = 3/2$.

There is another approach to obtain (4.15), which is a kind of static method. From

(4.5), the phase of each oscillator can be obtained as

$$\theta^* = \sin^{-1}\Big[\frac{\omega}{Kr^{d-1}}\Big] \tag{4.30}$$

which is from the fact that all the locked oscillator have their phase velocities as $\dot{\theta} = 0$ in the rotating frame. The intrinsic frequencies of the locked oscillators are bounded in $[-Kr^{d-1}, Kr^{d-1}]$. Despite we take the full spectrum of a phase space distribution, $f(\omega, \theta)$, we consider a distribution of locked oscillators, $f_{\text{locked}}(\omega, \theta)$. Since the locked oscillators are in state of $\theta^*(\omega)$, $f_{\text{locked}}(\omega, \theta)$ can be written as

$$f_{\text{locked}}(\omega, \theta) = g(\omega)\delta(\theta - \theta^*(\omega)), \tag{4.31}$$

where $\delta(\cdots)$ stands for the dirac-delta function. Now from (4.8) we have

$$\begin{aligned} r &= \int d\omega d\theta g(\omega)\delta(\theta - \theta^*(\omega)) \\ &= \frac{Kr^{d-1}\Delta}{\pi}\int_{-\frac{\pi}{2}}^{\frac{\pi}{2}} d\theta \frac{\cos^2(\theta)}{(Kr^{d-1}\sin(\theta))^2 + \Delta^2} \\ &= \frac{\sqrt{(Kr^{d-1})^2 + \gamma^2} - \gamma}{Kr^{d-1}} \end{aligned} \tag{4.32}$$

Thus, the self-consistency function reads

$$H(r, K) = \frac{\sqrt{(Kr^{d-1})^2 + \gamma^2} - \gamma}{Kr^{d-1}} - r, \tag{4.33}$$

which is consistent with the result obtained in (4.15).

4.1.2 Model of multistable synchronization

Another model of our concern is of an interacting function of the form,

$$G(\theta_j, \theta_{j_1}, \ldots, \theta_{j_{d-1}}) = \sin(\theta_{j_1} + \cdots + \theta_{j_{d-1}} - (d-1)\theta_j), \tag{4.34}$$

where the arguments in the sine function are diffusive. Then, the equation of motion is written as

$$\dot{\theta}_j = \omega_j + K/N^{d-1} \sum_{j_1,\ldots,j_{d-1}} \sin(\theta_{j_1} + \cdots + \theta_{j_{d-1}} - (d-1)\theta_j). \tag{4.35}$$

Thus, the mean-field equation reads,

$$\dot{\theta}_j = \omega_j + Kr^{d-1}\sin((d-1)\psi - (d-1)\theta_j), \tag{4.36}$$

where we use the order parameter same with that of the former. The only difference with the former is $(d-1)$ factor of θ_j, which directly causes the multistability of the system. For being locked into the synchronized state, each oscillator j has to be in one of the fixed states,

$$\begin{aligned}
\theta_1^* =& \frac{1}{d-1}\sin^{-1}\left[\frac{\omega}{Kr^{d-1}}\right] + 2\pi\frac{1}{d-1}, \\
\theta_2^* =& \frac{1}{d-1}\sin^{-1}\left[\frac{\omega}{Kr^{d-1}}\right] + 2\pi\frac{2}{d-1}, \\
& \ldots, \\
\theta_{d-1}^* =& \frac{1}{d-1}\sin^{-1}\left[\frac{\omega}{Kr^{d-1}}\right],
\end{aligned} \tag{4.37}$$

which are the solutions of

$$\omega_j = Kr^{d-1}\sin((d-1)\theta_j) \tag{4.38}$$

in the rotating frame such that $\psi = 0$. Since there are $(d-1)$ fixed states, the phase space distribution, $f(\theta, \omega)$, in the steady state is

$$f_{\text{locked}}(\omega, \theta) = g(\omega) \sum_{j=1}^{d-1} \eta_j \delta(\theta - \theta_j^*), \tag{4.39}$$

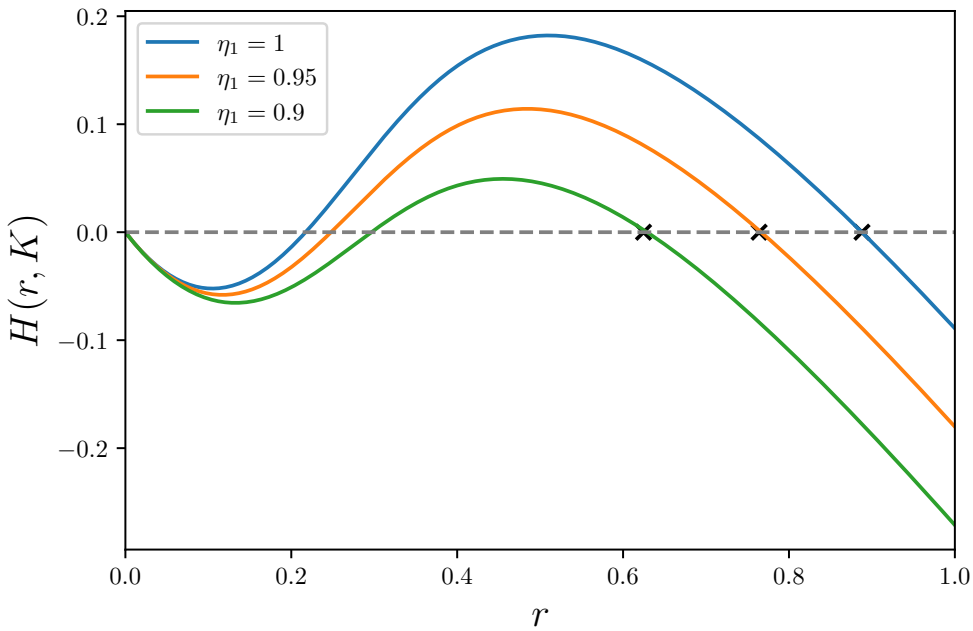

Figure 4.5: The self-consistency function, $H(r, K)$, versus r in different η_1 for $d = 3$, $\Delta = 0.5$, $K = 4$. Black markers represent the simluation results performed for $N = 10^4$. In simulation, each oscillator is initially placed in either $\theta = 0$ state with probability η_1 or $\theta = \pi$ state with probability $1 - \eta_1$.

where η_j stands for the density of the oscillators in θ_j^* state such that $\sum_{j=1}^{d-1} \eta_j = 1$. Multistability originate from η, and this is captured via the order parameter, r. The

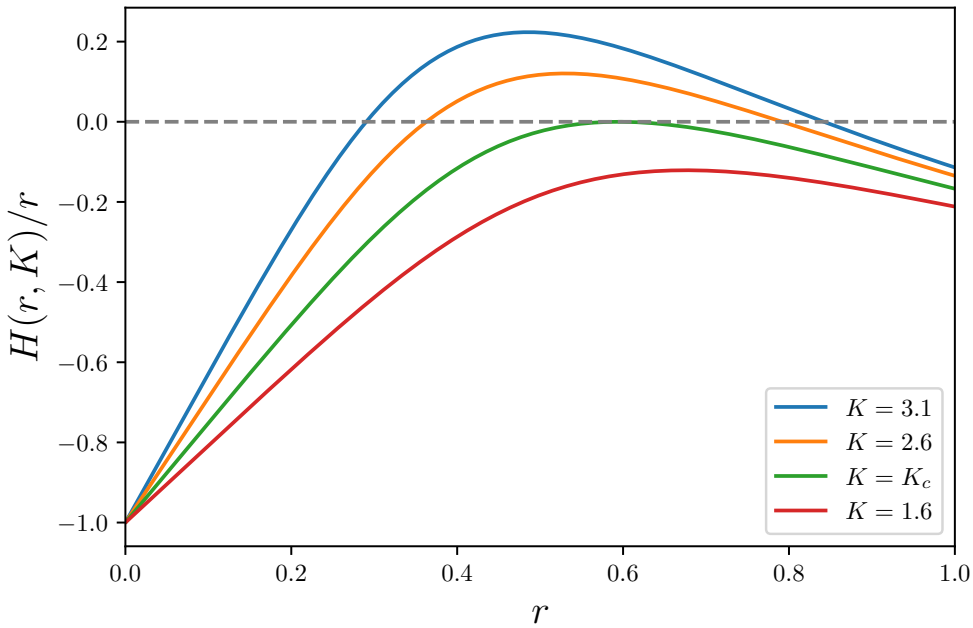

Figure 4.6: The Plot of $H(r, K)/r$ versus r in different K for $d = 3$, $\Delta = 0.5$. η_1 is fixed as one because it gives the upper bound of multistable region, which apppear along with the unstable point as K exceeds K_c.

self-consistency function for r reads

$$
\begin{aligned}
r &= \int f_{\text{locked}}\, e^{i\theta} d\omega d\theta, \\
&= \sum_{j=1}^{d-1} \eta_j \int_{-Kr^{d-1}}^{Kr^{d-1}} e^{i\theta_j^*(\omega)} g(\omega)\, d\omega, \\
&= \sum_{j=1}^{d-1} \eta_j \int_{-Kr^{d-1}}^{Kr^{d-1}} \cos(\theta_j^*(\omega)) g(\omega)\, d\omega, \\
&= \sum_{j=1}^{d-1} \eta_j (d-1) K r^{d-1} \\
&\quad \times \int_{-\frac{\pi}{2(d-1)}}^{\frac{\pi}{2(d-1)}} \cos\theta \cos((d-1)\theta) g(Kr^{d-1} \sin((d-1)\theta))\, d\theta,
\end{aligned}
\tag{4.40}
$$

where the drifting oscillators have no contribution to the order parameter.

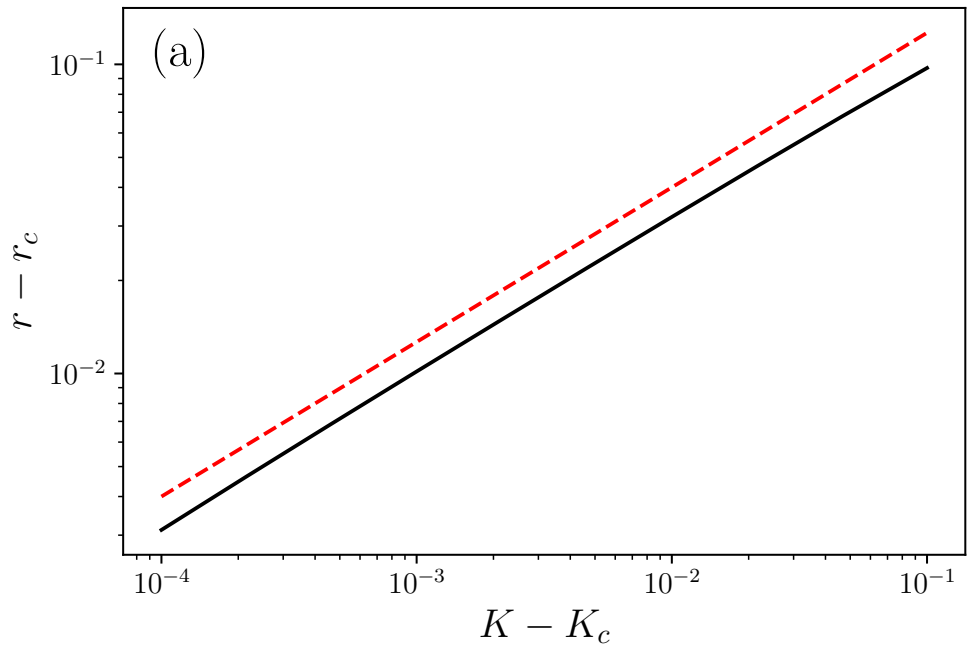

Figure 4.7: The Plot of $r - r_c$ versus $K - K_c$ for $d = 3$, $\Delta = 0.5$ and $\eta_1 = 1$. Slope, β, of the guide line is $1/2$, meaning that $r - r_c \sim (K - K_c)^{1/2}$.

Now we turn to the particular case of $d = 3$, in which all the oscillators are fully connected by all the possible three dimensional hyperedges. The self-consistency relation for $d = 3$ is

$$\begin{aligned} r =& 2Kr^2(2\eta_1 - 1)\int_{-\frac{\pi}{4}}^{\frac{\pi}{4}} \cos\theta\,\cos(2\theta) g(Kr^2\sin(2\theta))\,d\theta, \\ =& 2Kr^2(2\eta_1 - 1)\int_{-\frac{\pi}{4}}^{\frac{\pi}{4}} \cos\theta\,\cos(2\theta)\frac{\Delta/\pi}{(Kr^2\sin(2\theta))^2 + \Delta^2}\,d\theta, \\ =& \frac{(2\eta_1 - 1)}{\pi}\sqrt{\frac{2\Delta^2}{Kr^2}}\left[\frac{\tan^{-1}\left(\sqrt{\frac{Kr^2}{\sqrt{(Kr^2)^2+\Delta^2}-Kr^2}}\right)}{\sqrt{\sqrt{(Kr^2)^2+\Delta^2}-Kr^2}}\right. \\ & \left. - \frac{\tanh^{-1}\left(\sqrt{\frac{Kr^2}{\sqrt{(Kr^2)^2+\Delta^2}+Kr^2}}\right)}{\sqrt{\sqrt{(Kr^2)^2+\Delta^2}+Kr^2}}\right], \end{aligned} \tag{4.41}$$

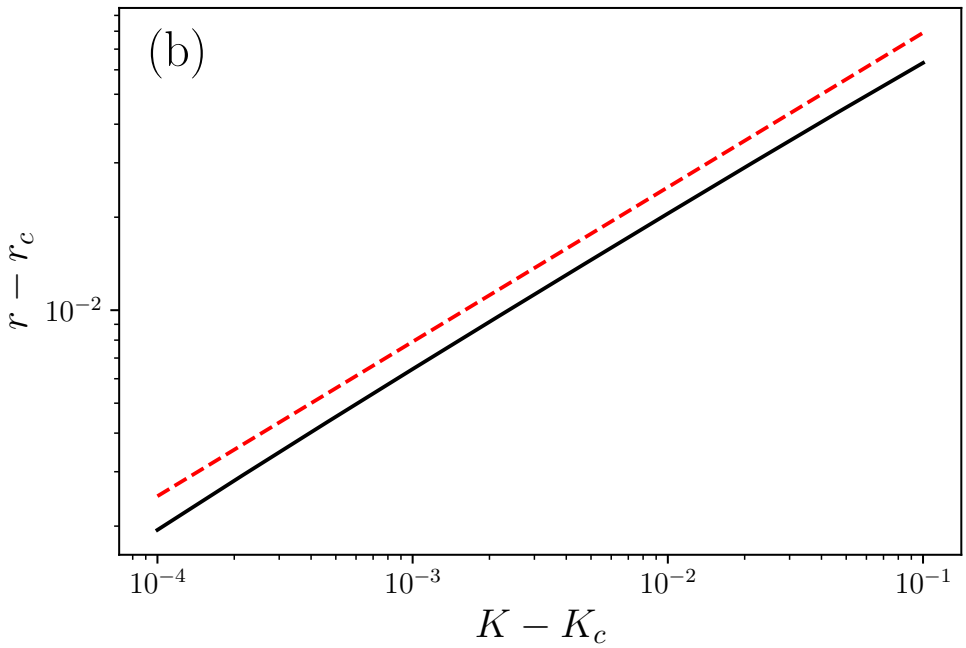

Figure 4.8: The Plot of $r - r_c$ versus $K - K_c$ for $d = 3$, $\Delta = 0.5$ and $\eta_1 = 0.9$. Slope, β, of the guide line is $1/2$, meaning that $r - r_c \sim (K - K_c)^{1/2}$.

with $g(\omega)$ as Cauchy distribution. Then the self-consistency function is obtained as

$$H(r, K) = -r + \frac{(2\eta_1 - 1)}{\pi}\sqrt{\frac{2\Delta^2}{Kr^2}}\left[\frac{\tan^{-1}\left(\sqrt{\frac{Kr^2}{\sqrt{(Kr^2)^2+\Delta^2}-Kr^2}}\right)}{\sqrt{\sqrt{(Kr^2)^2+\Delta^2}-Kr^2}} - \frac{\tanh^{-1}\left(\sqrt{\frac{Kr^2}{\sqrt{(Kr^2)^2+\Delta^2}+Kr^2}}\right)}{\sqrt{\sqrt{(Kr^2)^2+\Delta^2}+Kr^2}}\right]. \tag{4.42}$$

The closed form of the self-consistency function is in good agreement with the simulation results as displayed in Fig. 4.5. Though we have the systems with the same K, there are infinitely many realizations conditioned on η_1 in supercritical regime. The origin of multistability is nothing but the population configuration of oscillators in phase space. From the fact that η_1 plays a role of competing strength between two

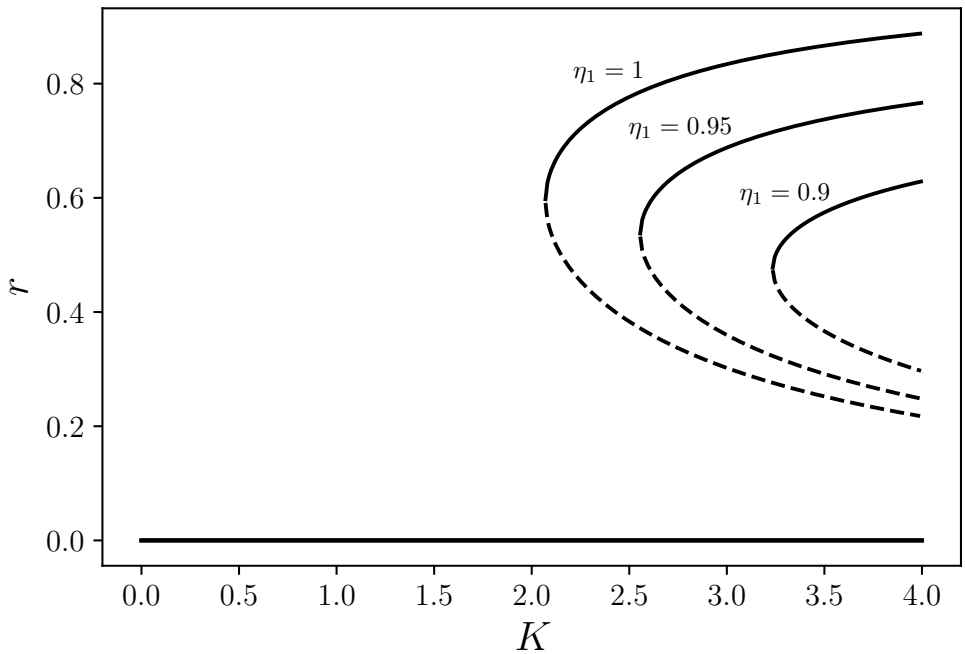

Figure 4.9: The Plot of r versus K for $d = 3$ and $\eta_1 = 0.9,\ 0.95,\ 1$. They show the same transitional behaviors, but with different thresholds, K_c and r_c.

fixed points, it is, to some extent, similar to the case of competing oscillators introduced in [48]. The suprecritical state is characterized by the critical coupling strength, K_c. The critical values of K and r can be obtained as we did in the former case,

$$\frac{\partial}{\partial r}\Big(\frac{H(r,K)}{r}\Big) = 0, \tag{4.43}$$

which explicitly gives the critical values for $\eta_1 = 1$ as, see Fig. 4.6,

$$\begin{aligned} r_c &\simeq 0.5944725985679503, \\ K_c &\simeq 2.070487838627744, \end{aligned} \tag{4.44}$$

and for $\eta_1 = 0.9$,

$$
\begin{aligned}
r_c &\simeq 0.4756101905301064, \\
K_c &\simeq 3.235137448285337.
\end{aligned}
\tag{4.45}
$$

The critical coupling strength, K_c, gets larger as η_1 gets smaller. Separated oscillators can hardly be synchronized to one another. It is remarkable that the systems with different η_1 reveal the same critical behavior through the order parameter, which helps us to induce that this holds for any η_1. Moreover, the critical behavior of the order parameter is universal for both bistable and multistable models,

$$
r - r_c \sim (K - K_c)^{1/2}. \tag{4.46}
$$

This means that the additional factor $(d-1)$ of θ_j in (4.34) has no effect on the critical behavior of higher-order system. The only relevant factor for the hybrid synchronization transition is the higher-order interactions. One can ask if all the higher-order system for synchronization show abrupt synchronization transition with critical behavior or not. The answer is no. If we take into account heterogeneity in higher-order system, the existence of hub gives rise to a different scenario. This is thoroughly dealt with in the following section.

4.2 Heterogeneous higher-order interaction

One of candidates of platforms which enables that three or more elements interact simultaneously is the hypergrphs. Given a set of hyperedge degrees of size N nodes, $\{k_1, \ldots, k_N s\}$, sampled from arbitrary hyperedge degree distribution, a number of hypergraphs can be realized [49]. Each hypergraph is realized preserving detailed structure by an adjacency tensor which directly informs the higher-order connectivity.

$$
A_{j_1,\ldots,j_d} = \begin{cases} 1 & \text{if } j_1, \ldots, j_d \text{ are connected} \\ 0 & \text{otherwise} \end{cases} \tag{4.47}
$$

One typical model of heterogeneous hypergraph is scale-free hypergraph introduced in [29], which follows power-law degree distribution,

$$P(k) \sim k^{-\lambda}. \tag{4.48}$$

The exponent λ represents the amount of intrinsic heterogeneity the system has. The scale-free uniform hypergraph of dimension d is realized as follows.

i) Each node, j, has a weight, $j^{-\alpha}$, which is normalized being the probability for selection,

$$p_j = \frac{j^{-\alpha}}{\sum_{l=1}^{N} l^{-\alpha}}. \tag{4.49}$$

ii) At each time step, a hyperedge is occupied among d nodes each of which is selected via probability (4.49).

iii) Repeat ii) till the number of hyperedges reaches to M.

This results in a hypergraph composed of N noeds and M hyperedge, wherein each node, j, has its hyperedge degree proportional to $j^{-\alpha}$. In other words, the hypergraph follows power-law distribution with degree exponent $\lambda = 1 + 1/\alpha$.

We suggest a specific model which is a way to generalize the Kuramoto model defined on complex networks,

$$\dot{\theta}_{j_1} = \omega_{j_1} + K \sum_{j_2,\ldots,j_d} A_{j_1,\ldots,j_d} \sin(\theta_{j_2} + \cdots + \theta_{j_d} - \theta_{j_1}), \tag{4.50}$$

where the distribution of ω, $g(\omega)$, is of Lorentzian, a representative of unimodal distribution, with zero mean for the sake of simplicity,

$$g(\omega) = \frac{\Delta/\pi}{\Delta^2 + \omega^2}. \tag{4.51}$$

For an uncorrelated d-dimensional hypergraph in which each hyperedge contains dis-

tinct d nodes, an adjacency tensor is approximately expressed as

$$A_{j_1,\ldots,j_d} \simeq \frac{k_{j_1}\ldots k_{j_d}}{(N\langle k\rangle)^{d-1}}, \tag{4.52}$$

where $\langle k\rangle$ is the mean hyperedge degree of the hypergraph [50]. The local field exerting on an oscillator, j_1, is defined as

$$\begin{aligned} h_{j_1}e^{i\phi_{j_1}} &= \frac{1}{(d-1)!}\sum_{j_2,\ldots,j_d} A_{j_1,\ldots,j_d}(e^{i\theta_{j_2}}+\cdots+e^{i\theta_{j_d}}) \\ &= \frac{k_{j_1}}{N}\sum_l \frac{k_l e^{i\theta_l}}{\langle k\rangle}. \end{aligned} \tag{4.53}$$

Now the global order parameter is written as

$$re^{i\psi} = \frac{\sum_j h_j e^{i\phi_j}}{\sum_j k_j} = \frac{1}{N}\sum_j \frac{k_j e^{i\theta_j}}{\langle k\rangle}. \tag{4.54}$$

Thus, the Eq. 4.50 can be written in terms of mean-field exerting on each node,

$$\dot{\theta}_j = \omega_j + Kk_j\, r^{d-1}\sin((d-1)\psi-\theta_j). \tag{4.55}$$

4.2.1 Heterogeneous mean-field theory

To further analyze, consider a probability density function, $f_m(\theta,\omega,t)$, for oscillators with k hyperedge degree, spanning θ, ω space. This function satisfies the continuity equation since the population of oscillators are fixed,

$$\dot{f}_k + \frac{\partial}{\partial\theta}(\dot{\theta}f_k) = 0, \tag{4.56}$$

and f_k can be expanded with Fourier modes as follows.

$$f_k(\theta,\omega,t) = \frac{g(\omega)}{2\pi}\Big[1+\sum_{n=1} f_{k,n}(\omega,t)e^{in\theta} + \text{c.c.}\Big], \tag{4.57}$$

where we have $f_{k,n}$ as an amplitude of the n-th mode in f_k. We have each amplitude of n-th mode satisfying $f_{k,n}(\omega, t) = (\alpha_k(\omega, t))^n$, which originate from the so called Ott-Antonsen (OA) ansatz [51]. Now we obtain the rate equation for $n = 1$ as

$$\dot{\alpha}_k + i\omega\alpha_k + \frac{Kk}{2} r^{d-1}(\alpha_k^2 - 1) = 0, \tag{4.58}$$

Since $(r_k e^{i\psi_k})^* = \alpha_k(\omega = -i\Delta, t) = r_k e^{-i\psi_k}$ in the rotating frame such that $\psi_k = 0$. Now the Eq. 4.58 is rewritten as

$$\dot{r}_k + \Delta r_k + \frac{Kk}{2} r^{d-1}(r_k^2 - 1) = 0. \tag{4.59}$$

By integrating the Eq. 4.59 with respect to time, we obtain the exact dynamical trajectory of the order parameter for oscillators with hyperedge degree k. In the steady state, $\dot{r}_k = 0$, solving Eq. 4.59, we obtain

$$r_k = \frac{-\Delta \pm \sqrt{\Delta^2 + (Kr^{d-1}k)^2}}{Kr^{d-1}k}, \tag{4.60}$$

where the only $+$ sign is relevant since r_k has to be non-negative. So, the self-consistency equation is

$$\begin{aligned} r &= \int_{k_m}^{\infty} dk \, \frac{kP(k)r_k}{\langle k \rangle} \\ &= -\frac{A(r)}{\langle k \rangle} + \int_{k_m}^{\infty} dk \, kP(k)\sqrt{1 + A^2(r)/k^2}, \end{aligned} \tag{4.61}$$

where we define

$$A(r) = \frac{\Delta}{Kr^{d-1}} \tag{4.62}$$

and denote k_m as minimum hyperedge degree of the system.

$$\begin{aligned}&\frac{1}{\langle k\rangle}\int_{k_m}^{\infty} dk\ kP(k)\sqrt{1+A^2(r)/k^2}\\&=(\lambda-2)\int_{k_m}^{\infty} dk\ k_m^{\lambda-2}k^{-\lambda+1}\sqrt{1+A^2(r)/k^2},\end{aligned}\tag{4.63}$$

Therefore, given K, the self-consistency function is

$$H(r)=-\frac{A(r)}{\langle k\rangle}+\frac{1}{\langle k\rangle}\int_{k_m}^{\infty} dk\ kP(k)\sqrt{1+A^2(r)/k^2}-r\tag{4.64}$$

By using the fact

$$\begin{aligned}\langle k\rangle&=\frac{\lambda-1}{\lambda-2}k_m\\P(k)&=(\lambda-1)k_m^{\lambda-1}k^{-\lambda},\end{aligned}\tag{4.65}$$

and letting $x\equiv(k_m/k)^2$, we have an alternative expression of the Eq. 4.64 as

$$H(r)=-\frac{(\lambda-2)A(r)}{(\lambda-1)k_m}+\frac{\lambda-2}{2}\int_0^1 dx\ x^{\frac{\lambda}{2}-2}\Big(1+\frac{A^2(r)}{k_m^2}x\Big)^{1/2}-r.\tag{4.66}$$

The second term on the right hand side of Eq. 4.66 is expressed as hypergeometric function [52, Ch. 15], ${}_2F_1(a,b;c;z)$,

$${}_2F_1(a,b;c;z)=\frac{\Gamma(c)}{\Gamma(b)\Gamma(c-b)}\int_0^1 x^{b-1}(1-x)^{c-b-1}(1-zx)^{-a}dx.\tag{4.67}$$

Thus, we have

$$H(r)=-\frac{(\lambda-2)A(r)}{(\lambda-1)k_m}+{}_2F_1\Big(-\frac{1}{2},\frac{\lambda}{2}-1;\frac{\lambda}{2};-\frac{A^2(r)}{k_m^2}\Big)-r,\tag{4.68}$$

which can be alternatively expressed in terms of $\langle k\rangle$ rather than k_m as

$$H(r)=-\frac{A(r)}{\langle k\rangle}+{}_2F_1\Big(-\frac{1}{2},\frac{\lambda}{2}-1;\frac{\lambda}{2};-\Big(\frac{\lambda-1}{\lambda-2}\frac{A(r)}{\langle k\rangle}\Big)^2\Big)-r,\tag{4.69}$$

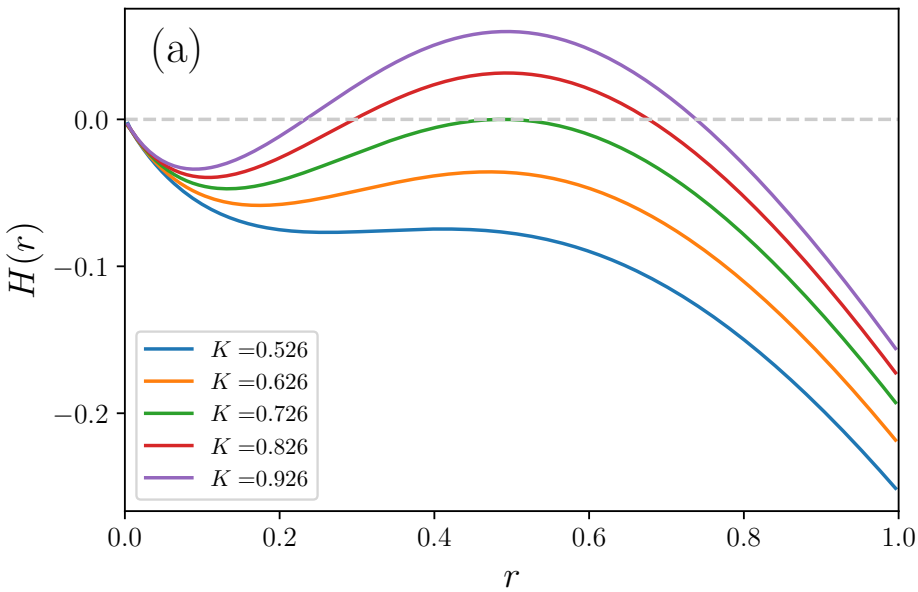

Figure 4.10: Plot of self-consistency function, $H(r)$, for $\lambda = 3(> \lambda_c)$ in the case of $d = 3$ with mean degree $\langle k \rangle = 3$. Non-zero solutions appear (saddle node bifurcation) at $r_c(\simeq 0.487935)$ if K exceeds $K_c(\simeq 0.726385)$, wherein there are two stable fixed point and one unstable fixed point.

and $H'(r)$ reads

$$\begin{aligned} H'(r) = &- \frac{d-1}{r}\frac{A(r)}{\langle k \rangle} + {}_2F_1\Big(\frac{1}{2}, \frac{\lambda}{2}; \frac{\lambda}{2}+1; -\Big(\frac{(\lambda-1)A(r)}{(\lambda-2)\langle k \rangle}\Big)^2\Big) \\ &\times \frac{(\lambda-1)^2}{\lambda(\lambda-2)}\frac{(d-1)A^2(r)}{r\langle k \rangle^2} - 1. \end{aligned} \tag{4.70}$$

To see the asymptotic behavior of Eq. 4.70 as $r \to 0$, we make use of

$$\begin{aligned} &{}_2F_1(a, b; c; -z) = \\ &\quad z^{-a}\frac{\Gamma(c)\Gamma(b-a)}{\Gamma(b)\Gamma(c-a)}{}_2F_1\Big(a, 1-c+a, 1-b+a, -\frac{1}{z}\Big) \\ &\quad + z^{-b}\frac{\Gamma(c)\Gamma(a-b)}{\Gamma(a)\Gamma(c-b)}{}_2F_1\Big(b, 1-c+b, 1-a+b, -\frac{1}{z}\Big). \end{aligned} \tag{4.71}$$

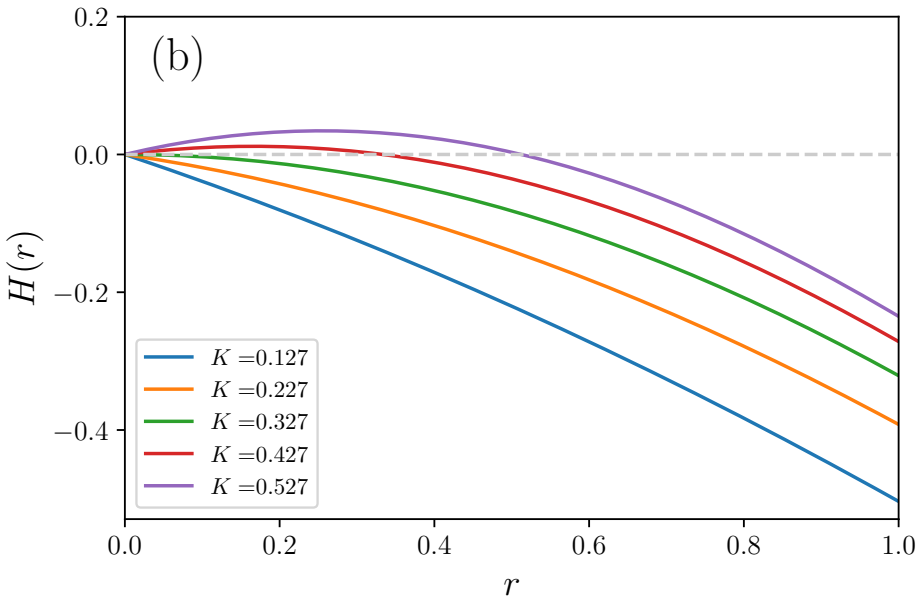

Figure 4.11: Plot of self-consistency function, $H(r)$, for $\lambda = 2.5(= \lambda_c)$ in the case of $d = 3$ with mean degree $\langle k \rangle = 3$. Non-zero solution appears only if K exceeds $K_c(\simeq 0.327263)$.

So $H'(r \to 0)$ is expressed as

$$\begin{aligned} H'(r \to 0) + 1 &= \left(\frac{(\lambda-1)A(r)}{(\lambda-2)\langle k \rangle}\right)^{2-\lambda} \frac{\Gamma(\frac{\lambda}{2}+1)\Gamma(\frac{1-\lambda}{2})}{\Gamma(\frac{1}{2})\Gamma(1)} \frac{(2-\lambda)(d-1)}{r\lambda} \\ &\sim \left(\frac{1}{r}\right)^{(d-1)(2-\lambda)+1}. \end{aligned} \tag{4.72}$$

Thus we have

$$H'(r \to 0) = \begin{cases} \infty & \text{if } \lambda < 2 + \frac{1}{d-1} \\ -1 & \text{if } \lambda > 2 + \frac{1}{d-1}, \end{cases} \tag{4.73}$$

which means there is a characteristic value of λ, namely $\lambda_c = 2 + 1/(d-1)$, that determines the type of synchronization transition. In other words, this model reveals three different types of synchronization transition each of which is determined by a

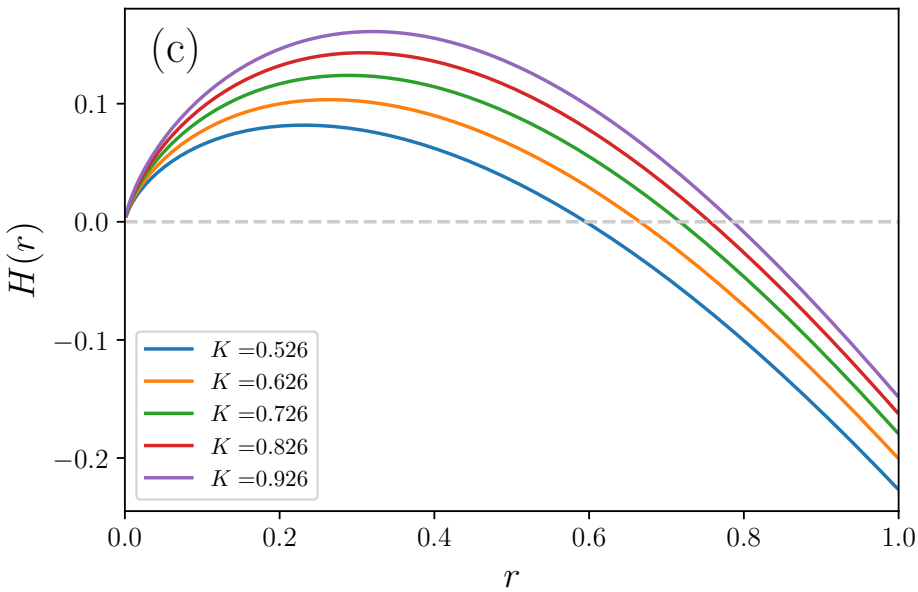

Figure 4.12: Plot of self-consistency function, $H(r)$ for $\lambda = 2.4(< \lambda_c)$ in the case of $d = 3$ with mean degree $\langle k \rangle = 3$. There always exists a non-zero solution, meaning that unconditional synchronization occurs.

critical value of λ,

$$\lambda_c = 2 + 1/(d-1). \tag{4.74}$$

4.2.2 Critical behavior

Expanding $H(r)$ around $r = 0$ and taking the first two leading orders, we have

$$\begin{aligned} H(r) \simeq & -r - \left(\frac{\Delta(\lambda-1)}{Kr^{d-1}(\lambda-2)\langle k\rangle}\right)^{2-\lambda} \frac{\Gamma(\frac{1-\lambda}{2})\Gamma(\frac{\lambda}{2})}{2\sqrt{\pi}} \\ & + \frac{Kr^{d-1}(\lambda-2)^2\langle k\rangle}{2(\lambda-1)(\lambda-3)\Delta}. \end{aligned} \tag{4.75}$$

i) For $\lambda < \lambda_c$, $H'(r \to 0) = \infty$ for all K, which means there is no finite transition point, K_c. Considering the first two terms in the right hand side of Eq. 4.75, we obtain

$$r \sim K^{(\lambda-2)/(1-(d-1)(\lambda-2))}, \tag{4.76}$$

which means that the system is unconditionally in synchronized state. The synchronized state is the only stable fixed point for any K.

ii) For $\lambda = \lambda_c$, the sign of $H'(r \to 0)$ changes only at a certain value of K, namely, K_c. We can evaluate K_c by $H'(r \to 0) = 0$. From Eq. 4.72, we obtain

$$K_c = \Big(\frac{-2\sqrt{\pi}}{\Gamma(1+\frac{1}{2(d-1)})\Gamma(-\frac{1}{2}-\frac{1}{2(d-1)})}\Big)^{d-1}\frac{\Delta d}{\langle k\rangle}. \tag{4.77}$$

We can express the right hand side of the Eq. 4.75 with respect to K_c. Equating it to zero, we have

$$\begin{aligned} 0 &= \Big(\Big(\frac{K}{K_c}\Big)^{\frac{1}{d-1}} - 1\Big) - \frac{Kr^{d-2}\langle k\rangle}{2\Delta d(d-2)} \\ &\simeq \frac{1}{d-1}\Big(\frac{K-K_c}{K_c}\Big) - \frac{K_c r^{d-2}\langle k\rangle}{2\Delta d(d-2)} \\ r &\sim (K-K_c)^{\frac{1}{d-2}}. \end{aligned} \tag{4.78}$$

In this case, there exists a finite transition point, K_c, and the synchronization transition is of second-order, The synchronized state turn into a stable fixed point when $K > K_c$, otherwise the incoherent state being unstable.

iii) For $\lambda > \lambda_c$, $H'(r \to 0) = -1$ for all K. Therefore, there is a finite K_c along with a finite r_c, which cause a discontinuous synchronization transition. By using the fact that $H(r = r_c, K = K_c) = 0$ and $H'(r = r_c, K = K_c) = 0$, we can expand $H(r)$ around $r = r_c$ and $K = K_c$ as

$$\begin{aligned} H(r) =& \frac{1}{2}\partial_r^2 H|_{r=r_c,K=K_c}(r-r_c)^2 \\ &+ \partial_K H|_{r=r_c,K=K_c}(K-K_c) + \dots, \end{aligned} \tag{4.79}$$

which indicates that

$$r - r_c \sim (K - K_c)^{1/2}. \tag{4.80}$$

We call this a hybrid synchronization transition. The incoherent state is stable for any K. When $K > K_c$, two fixed point emerges, one of which is stable and the other is unstable. This means that K_c is the critical point at which saddle node bifurcation occurs. The mean-field behavior of the system with $\lambda > \lambda_c$ is in great agreement with the results of [30].

4.2.3 Correlation size

The hypergraphs on which the finite number of oscillators are placed has a natural cutoff in hyperedge degree, $k_c = k_m N^{\frac{1}{\lambda-1}}$. This affects the so called finite-size effect to the oscillators. To see this effect, we should specify the characteristic point for different sizes, for example the critical coupling, $K_c(N)$, associated with N oscillators, and see how $K_c(N) - K_c(\infty)$ behaves with respect to N. Consider a finite-size self-consistency function defined as

$$H_N(r) = \int_{k_m}^{k_c} dk \, \frac{kP_N(k)r_k}{\langle k \rangle_N} - r, \tag{4.81}$$

where we define

$$\begin{aligned} P_N(k) &= (\lambda - 1)k_m^{\lambda-1}(N^{1/(\lambda-1)} - 1)^{-1}k^{-\lambda}, \\ \langle k \rangle_N &= \frac{\lambda - 1}{\lambda - 2}k_m(1 - N^{-(\lambda-2)/(\lambda-1)})^{-1}. \end{aligned} \tag{4.82}$$

Thus, we have

$$
\begin{aligned}
H_N(r) &= H(r) - N^{-\frac{\lambda-2}{\lambda-1}}(\lambda-2)k_c^{\lambda-2}\int_{k_c}^{\infty} dk\, k^{-\lambda+1} r_k. \\
&\simeq H(r) - N^{-\frac{\lambda-2}{\lambda-1}}{}_2F_1\Big(-\frac{1}{2}, \frac{\lambda}{2}-1; \frac{\lambda}{2}; -\frac{A^2(r)}{k_c^2}\Big) \\
&= -\frac{A(r)}{\langle k\rangle} + \int_{k_m}^{\infty} dk\, kP(k)\sqrt{1+A^2(r)/k^2}, \\
&\simeq H(r) - N^{-\frac{\lambda-2}{\lambda-1}}.
\end{aligned}
\tag{4.83}
$$

Expanding the right hand side of Eq. 4.83 near $K_c(\infty)$, and equating it to zero, we can obtain critical coupling strength for finite N, $K_c(N)$, and the critical exponent for correlation size, $\bar{\nu}$, which are explicitly appeared in $K_c(N) - K_c(\infty) \sim N^{-1/\bar{\nu}}$.

i) For $\lambda < \lambda_c$, $K_c(\infty) = 0$, so, $K \to 0$ and for large N, Eq. 4.83 can be rewritten as

$$
H_N(r) \simeq -\Big(\frac{\Delta(\lambda-1)}{Kr^{d-1}(\lambda-2)\langle k\rangle}\Big)^{2-\lambda}\frac{\Gamma(\frac{1-\lambda}{2})\Gamma(\frac{\lambda}{2})}{2\sqrt{\pi}} - N^{-\frac{\lambda-2}{\lambda-1}}, \tag{4.84}
$$

which implies that, for fixed N, the synchronized state emerges as the maximum value of the first term on the right hand side of Eq. 4.84 exceeds $N^{-\frac{\lambda-2}{\lambda-1}}$. Thus we have

$$
K_c(N) - K_c(\infty) \sim N^{-\frac{1-(d-1)(\lambda-2)}{\lambda-1}}, \tag{4.85}
$$

where we find $\bar{\nu} = (\lambda-1)/(1-(d-1)(\lambda-2))$.

ii) For $\lambda = \lambda_c$, $K_c(\infty)$ is finite (Eq. 4.77). Similarly, by utilizing Eq. 4.75, we have

$$
H_N(r) \simeq A(K - K_c(\infty))r + Br^{d-1} - N^{-\frac{\lambda-2}{\lambda-1}}, \tag{4.86}
$$

where A (B) is positive (negative). Therefore, we have

$$
K_c(N) - K_c(\infty) \sim N^{-\frac{d-2}{d(d-1)}}, \tag{4.87}
$$

which means $\bar{\nu} = d(d-1)/(d-2)$.

iii) For $\lambda > \lambda_c$, as is the similar case for those above, we have

$$H_N(r) \simeq H(r) + \frac{\partial H}{\partial K}(K - K_c(\infty)) - N^{-\frac{\lambda-2}{\lambda-1}}. \tag{4.88}$$

So,

$$K_c(N) - K_c(\infty) \sim N^{-\frac{\lambda-2}{\lambda-1}}, \tag{4.89}$$

which indicates $\bar{\nu} = (\lambda - 1)/(\lambda - 2)$.

4.3 Numerical simulation

We perfoem numerical simulation of coupled oscillators on a scale-free hypergraph of dimension three, $d = 3$, based on the rate equation (4.55). We use Runge-Kutta method of fourth order with $dt = 0.01$ [**?**]. Due to the computational complexity, we consider an annealed hypergraph for average behabior, in which each node has degree, d_j, not an integer,

$$d_j = N\langle k\rangle \frac{j^{-\alpha}}{\sum_{l=1}^{N} l^{-\alpha}}. \tag{4.90}$$

The mean degree $\langle k\rangle$ is controllable, and we set $\langle k\rangle = 3$ for hyperedge density to be one. To eliminate sample-to-sample fluctuation induced by ramdom initialization of intrinsic frequencies, we fix a set of frequencies as described in Appendix. The only remaining fluctuation we have to deal with is induced by multiplicity of a degree-frequency pair each oscillator has. For example, in a particular sample, the hub node may come to have maximum value of intrinsic frequency, or maybe zero value. To see the average behavior of a finite population of the oscillators, we sample ten thousand realizations out of $N!$ realizations.

We numerically confirm the analytical result of $\bar{\nu}$ for $\lambda > \lambda_c$. We track a specific coupling strength, K^*, of each finite size sample, where the variance of bimodal distribution of the order parameter becomes maximum, see Fig. X. From the fact that the critical system reveals its critical behavior through any quantity in any form [34], one

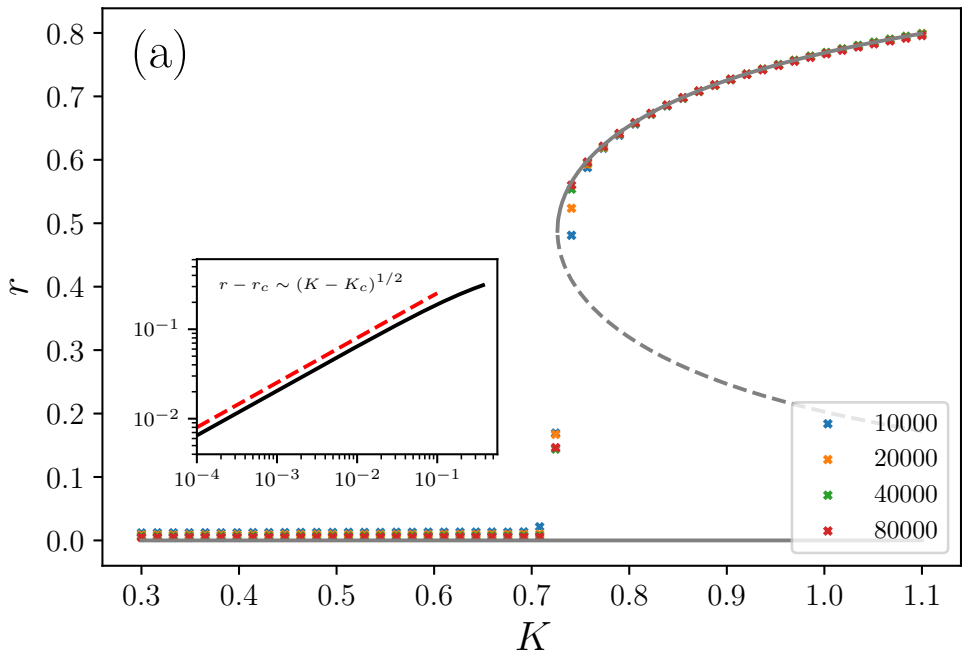

Figure 4.13: Plot of order parameter with $\lambda = 3$ and $\langle k \rangle = 3$ for the case of $d = 3$. Solid lines represent collection of stable fixed points whereas dashed line is made of unstable fixed points. Each marker is obtained by ensemble average of 10^4 numerical simulations. Initial configuration is set to be fully synchronized state, i.e., $r(t = 0) = 1$. Inset shows that the system analytically reveals a hybrid synchronization transition with the exponent $\beta = 1/2$.

can expect that $K^* - K_c$ serves critical behavior regarding the size of the system as

$$K^* - K_c \sim N^{-1/\bar{\nu}}, \tag{4.91}$$

which we call the critical decaying of the system. The only one pair of K_c and $\bar{\nu}$ shows critical decaying, which both are consistent with the analytical results obtained above.

To confirm the critical behavior which the order parameter reveals, we focus on the upper stable fixed point out of two stable fixed points at $\lambda > \lambda_c$. For obtaining the upper stable states which is not an incoherent state, the initial state is set to be $r(t = 0) = 1$. In other words, all the oscillator's phases are set to be equal to one

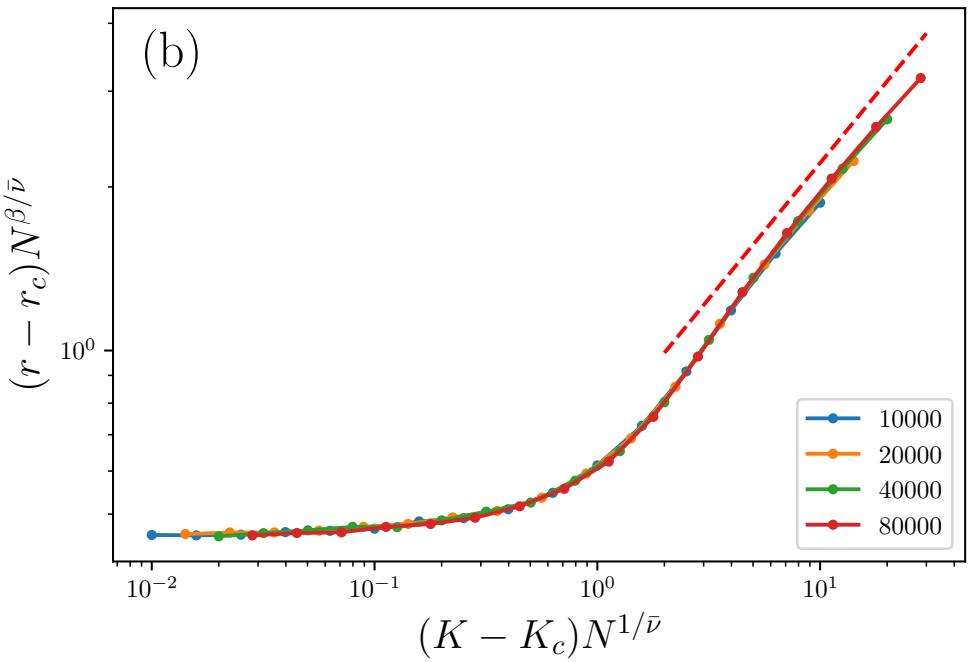

Figure 4.14: Scaling plots of order parameter for non-zero stable fixed point with $\lambda = 3$ and $\langle k \rangle = 3$ for the case of $d = 3$. Data collapse is performed using critical exponents, $\beta = 0.5$ and $\bar{\nu} = 2$, which are determined analytically.

another to reach the upper stable state as $t \to \infty$, as depicted in Fig. 4.13. By using the analytic results of critical exponents $beta$ and $\bar{\nu}$ at $\lambda = 3,\ 3.5$, the lines of upper stable states with different sizes collapse into a single line, see Fig. 4.14.

4.4 Remark

We study two models of higher-order synchronization, one with bistability and the other with multistability. For an all-to-all topology, they both show hybrid synchronization transition with the same critical exponents. The crucial factor causing abrupt synchronization transition is the higher-order interaction that three or more oscillator do.

To further study what affects to the abrupt synchronization transition, we consider

heterogeneous substrate on which dynamical units interact in higher-order manner, a scale-free uniform hypergraph of dimension d. We obtain the critical value of λ which plays a role of the strength of structural heterogeneity. We found that the existence of the hubs is critical to offset the local suppression effect come from higher-order interaction. If the hubs can not make any influences enough their neighbors to offset the strength of the local suppression, i.e., for $\lambda > \lambda_c$, each oscillator is likely to be in its local state, so the globally incoherent state becomes stable. Otherwise, if the influence of the hubs is strong enough, the globally incoherent state becomes unstable. This result is lying on the same line as that of higher-order epidemic spreading model is lying on, which implies that the systems defined in different detailed interaction actually share the universal critical behaviors.

Chapter 5

Conclusion

We finalize this dissertation summarizing what we deal with in the whole chpaters. We investigate both the structural and dynamical properties when considering higher-order interacting substrates.

For the structural property, we specifically consider coauthorship relations, the most representative example of growing complex systems wherein the higher-order structure is inherent. The quantification of topological signals is made use of the determination of evolutionary stages in growing complex systems. The first appearance of a long-range loop structure is related to the continuous growth of the complex system, and the first appearance of a higher-order cavity structure is related to the densely connected regime of the system. The successive emergence of the Betti number in each order directly indicates that the system undergoes a stage transition in time. This statement is supported by the fact that the Betti numbers in the growing higher-order model we proposed serve the global order of connectivity. Furthermore, it is confirmed that the phase transition the first Betti number reveals in the model is precisely the same as the percolation transition. This implies a possibility for the second Betti number, related to the higher-order connectivity, to show transitional behavior as well, which was confirmed in numerical simulation. However, there are still no analytical treatments for the phase transition of the second Betti number.

For the investigation of the higher-order dynamical processes, we focus on the explosively switching phenomena that the oscillatory systems exhibit. The existence of the higher-order interaction has an impact on the stability change of the incoherent

state, which naturally leads to the abrupt switching between synchronized state and incoherent state triggered by external perturbation. We specifically show that the systems with different forms of interaction essentially share the same critical behaviors, which means they reveal the same form of macroscopic behavior. To further analyze how structural heterogeneity affects macroscopic behavior, we consider the model on the scale-free higher-order network. As a result, both the homogeneous structure and the higher-order interaction must be satisfied for the incoherent state to become stable. The higher-order interaction plays a role of local suppression on the dynamical units, whereas the existence of the hub is to do with the global attraction. The exponent of the degree distribution, the extent of the heterogeneity, determines which ingredient is dominant. If the local suppression is dominant, each oscillator is astray on determination of which state to follow. On the other hand, in the case the global attraction is dominant, every oscillator is likely to be in a synchronized state.

The result on the non-linear higher-order dynamical system is the same as that of the linear higher-order dynamical system [29]. It is remarkable that the extent of diffrence in the form of interaction is allowed to the non-linearity. More investigation is needed on how further the difference in the form of interaction is allowed.

Appendices

Appendix A

Computation of the Betti numbers

Given a simplicial complex, K, we have to focus on $(k+1)$-th faces, k-th faces and $(k-1)$-th faces to compute the k-th Betti number. By definition, the k-th Betti number is the number of k-cycles which is not boundaries of higher diemnsional simplexes. As depicted in Fig. A.1, a set of k-cycles is mapped into zero under boundary operation, which means that it is the kernel of ∂_k. A set of arbitrary chains are mapped into boundaries, meaning it is the image of ∂_{k+1}. This implies that there are, in principle, cycles that are not boundaries of any higher dimensional simplex. The homology is to do with such remaining cycles where boundaries are subtracted properly.

In the group theoretical point of view, the coefficient of each simplex is isomorphic to coefficient group. For example, if the coefficient is boolean, the corresponding group

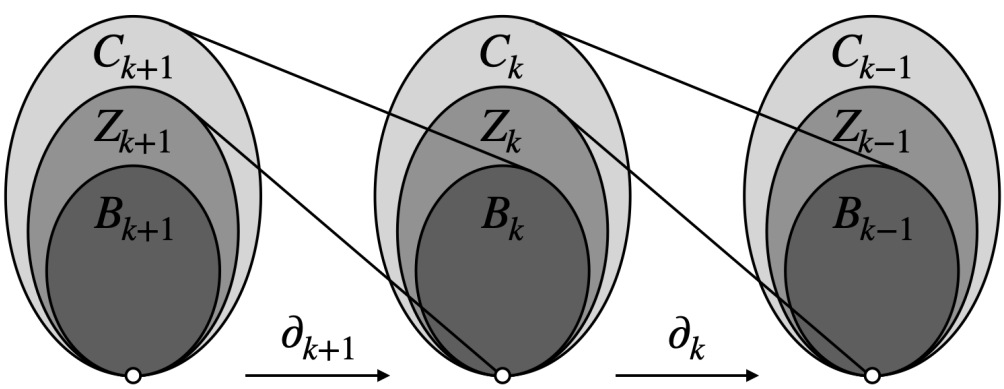

Figure A.1: Boundary operation on chain groups of each dimension. C_k, Z_k, B_k represent chain, cycle, boundary group of dimension k respectively.

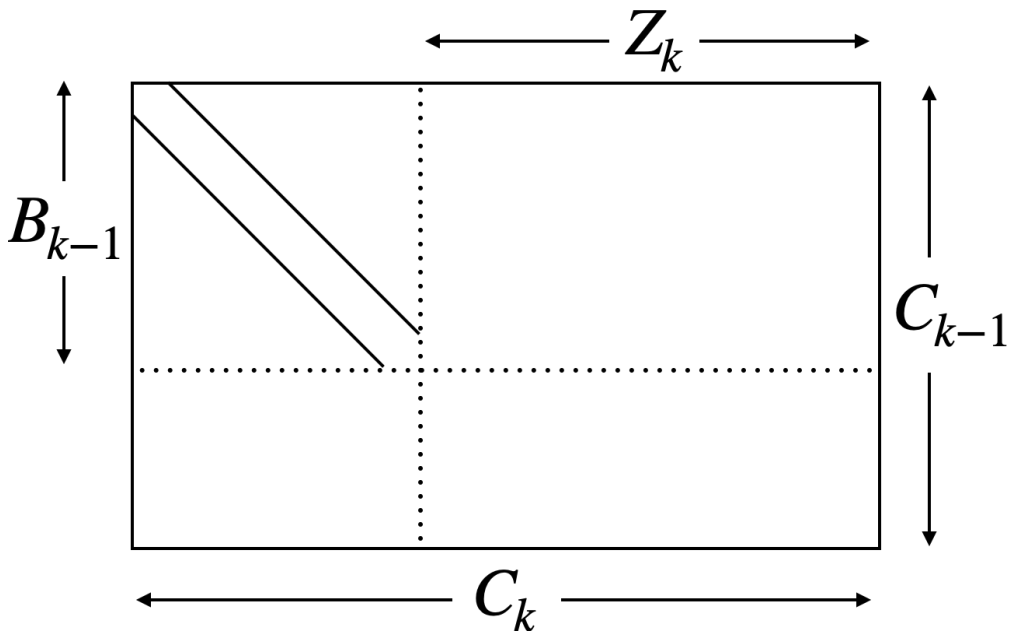

Figure A.2: Boundary operator in Smith normal form. Except for the diagonal elements in upper left block, all the elements are zero.

is the group of integer modulo two. The homology group is then written as

$$\begin{aligned} H_k(K) &= \ker(\partial_k)/\mathrm{im}(\partial_{k+1}), \\ &= Z_k(K)/B_k(K). \end{aligned} \tag{A.1}$$

This can be computed by using matrix representation of boundary operator in Smith normal form [54], which directly show the rank of each group according to rank nullity theorem [55], see Fig. A.2. Knowing ranks of groups, we can calculate rank of homology group, i.e., $\mathrm{rank}(Z_k) - \mathrm{rank}(B_k)$ [56].

Appendix B

Simplifying homology via strong collapse

An arbitrary simplicial complex can be reduced to the simplest form preserving its homological properties. Strong collapse, which is introduced in [37], can be realized as follows.

i) Represent a given simplicial complex as a bipartite network: one set is for 0-simplexes and the other set is for all faces.

ii) Remove faces if they are subsets of one of facets (maximal faces) of the simplicial complex.

iii) Conjugate the bipartite network to make nodes (faces) to be faces (nodes), and do ii) again.

iv) Conjugate the bipartite network.

v) Repeat ii)-iv) until it converges.

Doing so, we can get the most simplified form of simplicial complex which has the same Betti numbers, see Fig. B.1.

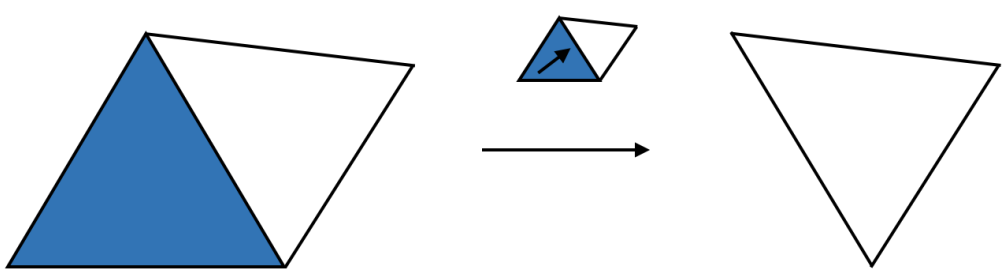

Figure B.1: An example of strong collapse. A 2-simplex is collapsed while preserving the Betti numbers, $\beta_0 = 1$ and $\beta_1 = 1$.

Appendix C

Lagrange inversion formula

Let $f(x) = \sum_s sC_s x^s$ be the generating function of the cluster size distribution, such that $f(1) = \sum_s sC_s = 1$ for non-percolating phase. The coefficient C_s can be obtained by integration in the complex z plane as

$$\begin{aligned}
sC_s &= \frac{1}{2\pi i}\oint dz \frac{f}{z^{s+1}} = \frac{1}{2\pi i}\oint dx\, x \exp(x^2/2)\frac{f}{\exp(x^2/2)^{s+1}} \\
&= \frac{1}{2\pi i}\oint \frac{df}{f}\,(1 - pd(d+1)f^d)\frac{f\exp(ps(d+1)f^d)}{f^s} \\
&= \frac{1}{2\pi i}\oint df\, \exp(ps(d+1)f^d)(1 - pd(d+1)f^d)f^{-s} \\
&= \frac{1}{2\pi i}\oint df \sum_{n=0}^{\infty}\frac{[ps(d+1)]^n}{n!}f^{nd}(f^{-s} - pd(d+1)f^{d-s}) \\
&= \frac{[ps(d+1)]^{\frac{s-1}{d}} - p(d+1)(s-1)[ps(d+1)]^{\frac{s-1}{d}-1}}{(\frac{s-1}{d})!} \\
&= \frac{p(d+1)[ps(d+1)]^{\frac{s-1}{d}-1}}{(\frac{s-1}{d})!},
\end{aligned} \tag{C.1}$$

where we utilize (3.14).

Bibliography

[1] R. Albert and A.-L. Barabási, ”Statistical mechanics of complex networks”, *Rev. Mod. Phys.* **74**, 47 (2002).

[2] S. N. Dorogovtsev and J. F. F. Mendes, ”Evolution of networks”, *Adv. Phys.* **51**, 1079 (2002).

[3] M. E. J. Newman, ”The Structure and Function of Complex Networks”, *SIAM Review* **45**, 167 (2003).

[4] S. Boccaletti, V. Latora, Y. Moreno, M. Chavez, and D. Hwang, ”Complex networks: Structure and dynamics”, *Phys. Rep.* **424**, 175 (2006).

[5] N. Araújo, P. Grassberger, B. Kahng, K. J. Schrenk, and R. M. Ziff, ”Recent advances and open challenges in percolation”, *Eur. Phys. J. Spec.* **223**, 2307 (2014).

[6] D. Lee, B. Kahng, Y. S. Cho, K.-I. Goh, and D.-S. Lee, ”Recent Advances of Percolation Theory in Complex Networks”, *J. Korean Phys. Soc.* **73**, 152 (2018).

[7] N. E. Friedkin, ”Theoretical Foundations for Centrality Measures”, *Am. J. Sociol.* **96**, 1478 (1991).

[8] L. Lű and T. Zhou, ”Link prediction in complex networks: A survey”, *Phys. A: Stat. Mech. Appl.* **390**, 1150 (2011).

[9] V. D. Blondel, J.-L. Guillaume, R. Lambiotte, and E. Lefebvre, ”Fast unfolding of communities in large networks”, *J. Stat. Mech.: Theory Exp*. P10008 (2008).

[10] S. N. Dorogovtsev, A. V. Goltsev, and J. F. F. Mendes, ”Critical phenomena in complex networks”, *Rev. Mod. Phys.* **80**, 1275 (2008).

[11] S. Boccaletti, G. Bianconi, R. Criado, C. I. del Genio, J. Gómez-Gardenes, M. Romance, I. Sendina-Nadal, Z. Wang, and M. Zanin, ”The structure and dynamics of multilayer networks”, *Phys. Rep.* **544**, 1, (2014).

[12] C. Berge and E. Minieka, *Graphs and Hypergraphs*. North-Holland Publishing Company, 1973.

[13] E. H. Spanier, *Algebraic Topology*. McGraw-Hill series in higher mathematics. Springer, 1989.

[14] P. S. Aleksandrov, *Combinatorial topology* Dover Publications, Mineola, N.Y, 1998.

[15] A. Patania, F. Vaccarino, and G. Petri, ”Topological analysis of data”, *EPJ Data Sci.* **6**, 7 (2017).

[16] S. Yu, H. Yang, H. Nakahara, G. S. Santos, D. Nikolić, and D. Plenz, ”Higher-Order Interactions Characterized in Cortical Activity”, *J. Neurosci.* **31**, 17514 (2011).

[17] A. R. Benson, D. F. Gleich, and J. Leskovec, ”Higher-order organization of complex networks”, *Science* **353**, 163 (2016).

[18] A. E. Sizemore, C. Giusti, A. Kahn, J. M. Vettel, R. F. Betzel, and D. S. Bassett, ”Cliques and cavities in the human connectome”, *J. Comput. Neurosci.* **44**, 115 (2018).

[19] J. Grilli, G. Barabás, M. J. Michalska-Smith, and S. Allesina, ”Higher-order interactions stabilize dynamics in competitive network models”, *Nature* **548**, 210 (2017).

[20] U. Alvarez-Rodriguez, F. Battiston, G. Ferraz de Arruda, Y. Moreno, M. Perc, and V. Latora, ”Evolutionary Dynamics of Higher-Order Interactions”, *Nat. Hum. Behav.* **5** 586–595 (2021).

[21] R. Lambiotte, M. Rosvall, and I. Scholtes, ”From networks to optimal higher-order models of complex systems”, *Nat. Phys.* **15**, 313 (2019).

[22] F. Battiston, G. Cencetti, I. Iacopini, V. Latora, M. Lucas, A. Patania, J.-G. Young, and G. Petri, ”Networks beyond pairwise interactions: Structure and dynamics”, *Phys. Rep.* **874**, 1 (2020).

[23] F. Battiston, E. Amico, A. Barrat, G. Bianconi, G. F. de Arruda, B. Franceschiello, I. Iacopini, S. Kéfi, V. Latora, Y. Moreno, M. M. Murray, T. P. Peixoto, F. Vaccarino, and G. Petri, ”The physics of higher-order interactions in complex systems”, *Nat. Phys.* **17**, 1093 (2021).

[24] A. R. Benson, R. Abebe, M. T. Schaub, A. Jadbabaie, and J. Kleinberg, ”Simplicial closure and higher-order link prediction”, *Proc. Natl. Acad. Sci. (U.S.A.)* **115**, 11221 (2018).

[25] G. Petri and A. Barrat, ”Simplicial Activity Driven Model”, *Phys. Rev. Lett.* **121**, 228301 (2018).

[26] M. Kahle, *Topology of random simplicial complexes: a survey* arXiv:1301.7165 2013.

[27] N. Linial and Y. Peled, ”On the phase transition in random simplicial complexes”, *Ann. Math.* **184**, 745 (2016).

[28] I. Iacopini, G. Petri, A. Barrat, and V. Latora, ”Simplicialmodels of social contagion”, *Nat. Commun.* **10**, 2485 (2019).

[29] B. Jhun, M. Jo, and B. Kahng, ”Simplicial SIS model in scale-free uniform hypergraph”, *J. Stat. Mech.: Theory Exp.* P123207 (2019).

[30] P. S. Skardal and A. Arenas, ”Higher order interactions in complex networks of phase oscillators promote abrupt synchronization switching”, *Commun. Phys.* **3**, 218 (2020).

[31] N. W. Landry and J. G. Restrepo, ”The effect of heterogeneity on hypergraph contagion models”, *Chaos* **30**, 103117 (2020).

[32] A.-L. Barabási and R. Albert, ”Emergence of Scaling in Random Net- works”, *Science* **, 286**, 509 (1999).

[33] M. Karoński and T. Łuczak, ”The phase transition in a random hyper- graph”, *J. Comput. Appl. Math.* **142**, 125 (2002).

[34] K. Christensen and N. R. Moloney, *Complexity and Criticality* (Imperial College Press, 2005).

[35] A. Arenas, A. Fernández, S. Fortunato, and S. Gómez, ”Motif-based communities in complex networks”, *J. Phys. A Math.* **41**, 224001 (2008).

[36] D. Lee, K.-I. Goh, B. Kahng, and D. Kim, ”Complete trails of coauthorship network evolution”, *Phys. Rev. E* **82**, 26112 (2010).

[37] A. C. Wilkerson, T. J. Moore, A. Swami, and H. Krim, ”Simplifying the homology of networks via strong collapses”, *Proc. - ICASSP IEEE Int. Conf. Acoust. Speech Signal Process.*, 5258 (2013).

[38] O. Bobrowski and P. Skraba, ”Homological percolation and the Euler characteristic”, *Phys. Rev. E* **101**, 32304 (2020).

[39] A. Patania, G. Petri, and F. Vaccarino, ”The shape of collaborations”, *EPJ Data Sci.* **6**, 18 (2017).

[40] C. J. Carstens and K. J. Horadam, ”Persistent Homology of Collaboration Networks”, *Math. Probl. Eng.* **2013**, 1 (2013).

[41] J. Kim, P. L. Krapivsky, B. Kahng, and S. Redner, ”Infinite-order percolation and giant fluctuations in a protein interaction network”, *Phys. Rev. E* **66**, 55101 (2002).

[42] D. S. Callaway, J. E. Hopcroft, J. M. Kleinberg, M. E. J. Newman, and S. H. Strogatz, ”Are randomly grown graphs really random?”, *Phys. Rev. E* **64**, 41902 (2001).

[43] S. N. Dorogovtsev, J. F. F. Mendes, and A. N. Samukhin, ”Anomalous percolation properties of growing networks”, *Phys. Rev. E* **64**, 66110 (2001).

[44] B. Bollobás, B. Béla, W. Fulton, A. Katok, F. Kirwan, P. Sarnak, and B. Simon, *Random Graphs*. Cambridge University Press, 2001.

[45] D. Lee, W. Choi, J. Kertész, and B. Kahng, ”Universal mechanism for hybrid percolation transitions”, *Sci. Rep.* **7**, 5723 (2017).

[46] W. Choi, D. Lee, J. Kertész, and B. Kahng, ”Two golden times in two-step contagion models: A nonlinear map approach”, *Phys. Rev. E* **98**, 12311 (2018).

[47] A. Costa and M. Farber, *Configuration Spaces*, Pages 129-153, Springer International Publishing, Cham, 2016.

[48] J. Park and B. Kahng, ”Abnormal hybrid phase transition in the passively competing Kuramoto model”, *Physica D* **399**, 186 (2019).

[49] P. S. Chodrow, ”Configuration models of random hypergraphs”, *J. Complex Netw.* **8** (2020).

[50] J. Um, H. Hong, and H. Park, ”Nature of synchronization transitions in random networks of coupled oscillators”, *Phys. Rev. E* **89**, 012810 (2014).

[51] E. Ott and T. M. Antonsen, ”Low dimensional behavior of large sys- tems of globally coupled oscillators”, *Chaos* **18**, 037113 (2008).

[52] A. B. Olde Daalhuis, *NIST Digital Library of Mathematical Functions: Chapter 15*, http://dlmf.nist.gov/, 2021

[53] W. H. Press, S. A. Teukolsky, W. T. Vetterling, and B. P. Flannery, *Numerical Recipes in C (2nd Ed.): The Art of Scientific Computing* Cambridge University Press, USA, 1992.

[54] H. J. S. Smith and J. J. Sylvester, ”XV. On systems of linear indeterminate equations and congruences”, *Philos. Trans. R. Soc. Lond.* **151**, 293 (1861).

[55] S. Axler, *Linear Algebra Done Right* Springer, USA, 2015.

[56] G. Bianconi, *Higher-Order Networks* Cambridge University Press, 2021.

초 록

복잡계는 비균질적인 구성원들이 다양한 상호작용을 주고받는 시스템이다. 네트워크는 이러한 시스템의 각 요소를 점, 그 사이의 상호작용을 선으로 표현함으로써 복잡계 구조에서 나타나는 보편적인 특성과 그 동역학적 효과를 기술하는데 널리 쓰여왔다. 하지만 네트워크는 정의로부터 기인하는 내재적인 제약을 지니고 있다. 연결선은 오직 두 요소의 관계만 표현할 수 있기에 쌍으로 상호작용(pairwise interaction)하지 않는 요소들을 표현하는 것에 어려움을 갖고있다. 고차 네트워크는 정점과 고차연결선(higher-order edge)으로 이루어져 있는 네트워크의 일반화인데, 이것은 셋 이상의 고차 연결을 고려하기에 이 제약에서 자유롭다.

첫째로 우리는 본 학위논문에서 성장하는 복잡계의 데이터 및 모형을 고차 네트워크의 관점에서 분석하여 복잡계의 단계적 구조 변화를 단체 복합체(simplicial complex) 관점으로 기술하였다. 태동의 단계를 비롯하여 연결성(connectivity)이 확립되는 단계와 강건성(robustness)이 확립되는 단계를 위상적인 양인 베티 수(Betti number)로 구분하였다. 연결성이 확립되는 단계의 특징인 거시적인 고리 형성을 첫째 베티 수로, 강건성이 확립되는 단계에서 계의 밀도가 높아짐에 따라 나타나는 국소적인 폐곡면(void) 형성을 둘째 베티 수로 정량화 할 수 있다는 것을 보였다.

시간에 대해 성장하는 고차 네트워크에서 베티 수들이 순차적으로 생기며 증가한다는 것이 일반적이라는 것을 여러 고차 네트워크 모델 공부를 통해 확인하였다. 특히 성장하는 척도없는 고차 네트워크에서 정의되는 베티 수들 또한 각각 상전이를 보인다는 것을 수치적으로 확인하였다. 또한 첫째 베티수는 네트워크와 단체 복합체 모두에서 여과 상전이와 정확히 같은 상전이 양상을 보인다는 것을 해석적으로도 보였다.

둘째로 복잡계의 고차 상호작용에서 나타나는 허브 구조가 상전이와 임계현상에 어떤 영향을 미치는지 동기화 모형의 해석적, 수치적 분석을 통해 규명하였다. 이중 안정성, 다중 안정성을 보이는 두 가지의 전역 결합(globally coupled) 모형을

다루었는데, 공통적으로 고차 상호작용이 불연속 상전이와 임계 현상을 동시에 함유하는 하이브리드 상전이를 유발한다는 것을 확인하였다.

비균질적 구조를 지닌 척도없는 고차 네트워크에서 정의되는 이중 안정 모형에서 연결선 수 분포 지수의 특정 값($\lambda_c = 2 + 1/(d-1)$)을 기준으로 동기화 해의 양상(임계현상) 이 급격하게 변한다는 사실을 수치적 및 해석적으로 도출했다. 도수분포 지수가 임계지수보다 작은 경우인 $\lambda < \lambda_c$일 때에, 즉 허브의 영향력이 큰 영역에서는 무조건적 동기화 현상이 나타나고, 그렇지 않은 경우, $\lambda = \lambda_c$ 일 때 연속 상전이가, $\lambda > \lambda_c$ 일 때 폭발적인 하이브리드 동기화 상전이(hybrid synchronization transition)가 발견된다.

주요어: 상전이, 임계현상, 여과이론, 동기화, 단체복합체, 단체호몰로지, 하이퍼그래프

학번: 2017-29476